CHAPTER 1

USING GENERALIZED SHEET TRANSITION CONDITIONS (GSTCS) IN THE ANALYSIS OF METASURFACES

Christopher L. Holloway and Edward F. Kuester

Please enter `\offprintinfo{(Title, Edition)}{(Author)}` at the beginning of your document.

CONTENTS

1 Using Generalized Sheet Transition Conditions (GSTCs) in the Analysis of Metasurfaces 1

1.1 Introduction and Definitions of Metasurfaces 4
1.2 Metasurfaces versus Frequency-Selective Surfaces 5
1.3 Characterization of Metasurfaces: Surface versus Bulk Properties 9
1.4 Generalized Sheet Transition Conditions (GSTCs) 10
1.4.1 GSTCs for a Metafilm 14
1.4.2 GSTCs for a Metascreen 14
1.4.3 GSTCs for a Metagrating 15
1.5 Reflection and Transmission Coefficients 16
1.5.1 Metafilms 16
1.5.2 Metascreens 20
1.5.3 Metagratings 23
1.6 Determining the Surface Parameters 25
1.6.1 Retrieval Expressions for Metafilms 25
1.6.2 Retrieval Expressions for Metascreens 26
1.6.3 Retrieval Expressions for Metagratings 28
1.7 Some Applications of GSTCs 29
1.7.1 Guided-waves on a Single Metasurface 29
1.7.2 Resonator Size Reduction 35
1.7.3 Waveguides 38
1.7.4 Controllable Reflections and Transmissions 39
1.8 Impedance-Type Boundary Conditions 42
1.9 Isolated Scatterers and One-Dimensional Arrays 42
1.10 Summary 43

References 45

1.1 Introduction and Definitions of Metasurfaces

In recent years, there has been a great deal of attention devoted to metastructures, which include metamaterials and metasurfaces. The prefix "meta" is a Greek preposition meaning (among other things) "beyond". In the context of metamaterials or metasurfaces, this refers to a metastructure that has some type of exotic property that normally does not occur in nature. Although in this chapter we will discuss metasurfaces and the use of generalized sheet transmission conditions (GSTCs), we begin our discussion with three-dimensional metamaterials.

Metamaterials are novel, synthetic materials engineered to achieve unique properties, i.e., materials beyond those occurring naturally. Metamaterials are often engineered by arranging a set of small scatterers (e.g., metallic rings and rods, spherical magneto-dielectric particles, or other arbitrarily shaped inclusions) in a regular array throughout a region of three-dimensional space, in order to obtain some desirable bulk behavior [1]-[10]. The term metamaterial does not refer to classical periodic structures, such as what are now called photonic bandgap (PBG) structures, or to frequency-selective surfaces (FSS). The term metamaterial refers to a material or structure with more exotic properties than artificial dielectrics, but which can still be described by bulk material parameters in the same way that natural materials can. One example is a so-called "double-negative" (DNG) material [11]-[26], also known as negative-index material (NIM), a backward-wave (BW) medium, or left-handed material (LHM). This type of material has the property that its effective permittivity and effective permeability are simultaneously negative in a given frequency band. A second example is near-zero refractive index material, with either the permittivity or permeability designed to have its real part close to zero. Materials with unique properties such as these have a wide range of potential applications in electromagnetics at frequencies ranging from the low microwaves to optical, including shielding, low-reflection materials, novel substrates, antennas, electronic switches, devices, perfect lenses, resonators, and of course cloaking, among many other possibilities.

The concept of three-dimensional metamaterials can be extended by placing the scatterers (or apertures) in a two-dimensional arrangement on a surface. This surface version of a metamaterial is called a metasurface, and includes metafilms, metascreens, and metagratings as special cases [27]-[34]. Metasurfaces are an attractive alternative to three-dimensional metamaterials because of their simplicity and relative ease of fabrication. Throughout the literature, there are several applications where metamaterials are replaced with metasurfaces. Metasurfaces have the advantage of taking up less physical space than do full 3D metamaterial structures; as a consequence they can also offer the possibility of lower losses. The application of metasurfaces at frequencies from microwave to optical has attracted great interest in recent years [27]-[84]. In addition to the applications mentioned above for metamaterials, metasurfaces allow for controllable smart surfaces, miniaturized cavity resonators, novel waveguiding structures, compact and wide-angle absorbers, impedance matching surfaces, biomedical devices, wave front tailoring, polarization conversion, antennas, and high speed switching devices, to name only a few.

In general, a metasurface is any periodic two-dimensional structure whose thickness and periodicity are small compared to a wavelength in the surrounding media. Metasurfaces should not be confused with classical frequency-selective surfaces (FSS); the important distinction between the two is discussed below. We can identify two important subclasses (metafilms and metascreens) within this general designation of metasurfaces. These two subclasses are distinguished by the type of topology that constitutes the metasurface. Metafilms (as coined in [29]) are metasurfaces that have a "cermet" topology, which refers to an array of isolated (non-touching) scatterers (see Fig. 1.1). Metascreens are metasurfaces with a "fishnet" structure (see Fig. 1.2), which are characterized by periodically spaced apertures in an otherwise relatively impenetrable surface [31]. There are other types of meta-structures that lie somewhere between a metafilm and a metascreen. For example, a grating of parallel coated wires (a metagrating, see Fig. 1.3) behaves like a metafilm to electric fields perpendicular to the wire axes and like a metascreen for electric fields parallel to the wire axes [32]. It is important to note that the individual scatterers constituting a metafilm (or apertures constituting a metascreen) are not necessarily of zero thickness (or even small compared to the lattice constants); they may be of arbitrary shape, and their dimensions are required to be small only in comparison to a wavelength in the surrounding medium, *a fortiori* because the lattice constant has been assumed small compared to a wavelength.

It has been shown that a type of boundary conditions known as generalized sheet transition conditions (GSTCs) is the most appropriate way to model metasurfaces [29]-[34]). While the functional form of the

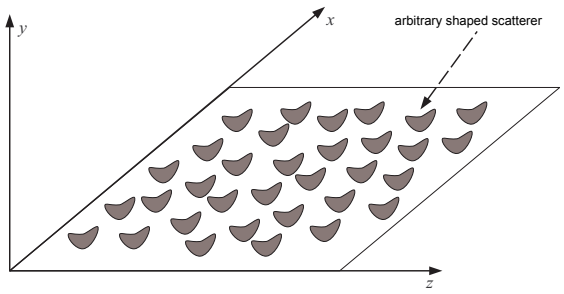

(a) array of arbitrarily shaped scatterers

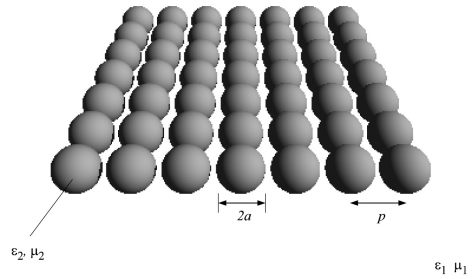

(b) metafilm: array of spherical particles

Figure 1.1 Illustration of a metafilm, which consists of an array of arbitrarily shaped scatterers placed on the xz-plane: (a) array of arbitrarily spaced scatterers and (b) array of spherical particles.

GSTCs may be different depending on the type of metasurface, the GSTC description allows the metasurface to be replaced by an interface as shown in Fig. 1.4. The interaction of the electric (E) and magnetic (H) fields on either side of the metasurface is taken care of through the GSTCs applied at that interface. In this model, all the information about the metasurface (geometry of the scatterers or apertures: shape, size, material properties, etc.) is incorporated into the effective surface parameters that appear explicitly in the GSTCs. These surface parameters (effective electrical and magnetic surface susceptibilities and surface porosities) that appear explicitly in the GSTCs are uniquely defined, and as such serve as the physical quantities that most appropriately characterize the metascreen. The effective surface parameters for any given metasurface together with the GSTCs are all that are required to model its interaction with an EM field at the macroscopic level.

In this chapter, we present the GSTCs needed to analyze the three main types of metasurfaces: metafilms, metascreens, and metagratings. From these GSTCs we derive for each of these metasurfaces the plane-wave reflection (R) and transmission (T) coefficients. They are expressed in terms of the surface parameters that characterize the metasurface. These coefficients are then used to develop a retrieval approach for determining from measured or simulated data the uniquely defined effective surface parameters (i.e., the electric and magnetic surface susceptibilities and surface porosities) that characterize the each of the metasurfaces. Finally, in the last section, we present various other applications of the GSTCs.

1.2 Metasurfaces versus Frequency-Selective Surfaces

Before we introduce and discuss the different types of GSTCs for the various metasurfaces, we need to make the distinction between metasurfaces and frequency-selective surfaces. Depending on the wavelength and the periodicity of the inclusions that make up an engineered periodic structure, it may or may not be possible to model it as an effective medium (as for the case of a metamaterial) or using effective surface parameters (as for the case of a metasurface). In fact, the electromagnetic field interaction with these types of engineered structures can be divided into three separate regions of operation (see Fig. 1.5), with distinctive behaviors in

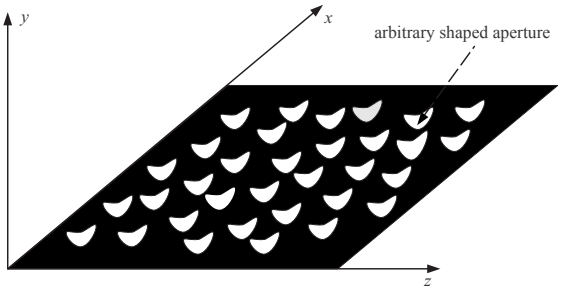

(a) array of arbitrarily shaped apertures in a conducting screen

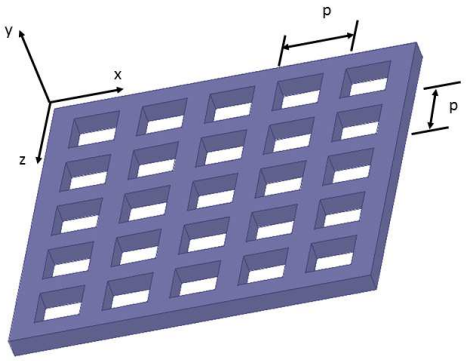

(b) metafilm: array of square apertures

Figure 1.2 Illustration of a metascreen, which consists of an array of arbitrarily apertures in a conducting screen located in the xz-plane: (a) array of arbitrarily shaped apertures and (b) array of square apertures.

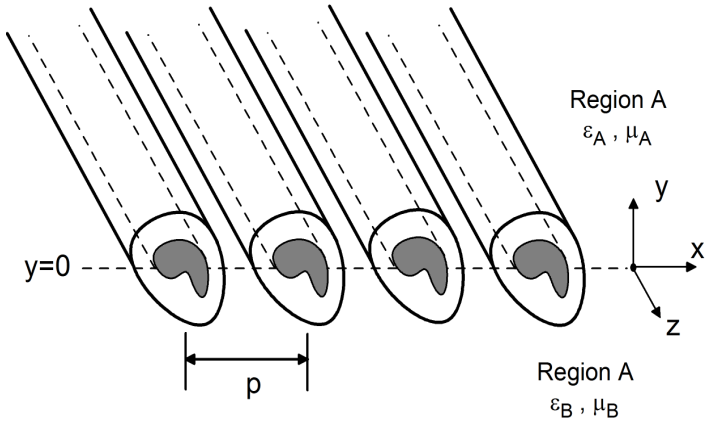

Figure 1.3 Illustration of a metagrating, which consists of an array of coated arbitrarily shaped and coated wires.

each region. It is important to be aware of this and to understand the behavior in each region when either performing measurements or analyzing metastructures at different length scales and/or frequencies, as will be described below. In addressing this, we will comment on (1) the difference between a metamaterial and a conventional photonic band gap (PBG) or electromagnetic band gap (EBG) structure, and in turn (2) the difference between a metasurface and a conventional frequency-selective surface (FSS).

Consider first three-dimensional metamaterials; these ideas will be extended below to metasurfaces. The behavior of such a composite material is qualitatively different in each of the three distinct regions shown in Fig. 1.5. Region 1 corresponds to the quasi-static region, which implies low frequencies; more specifically,

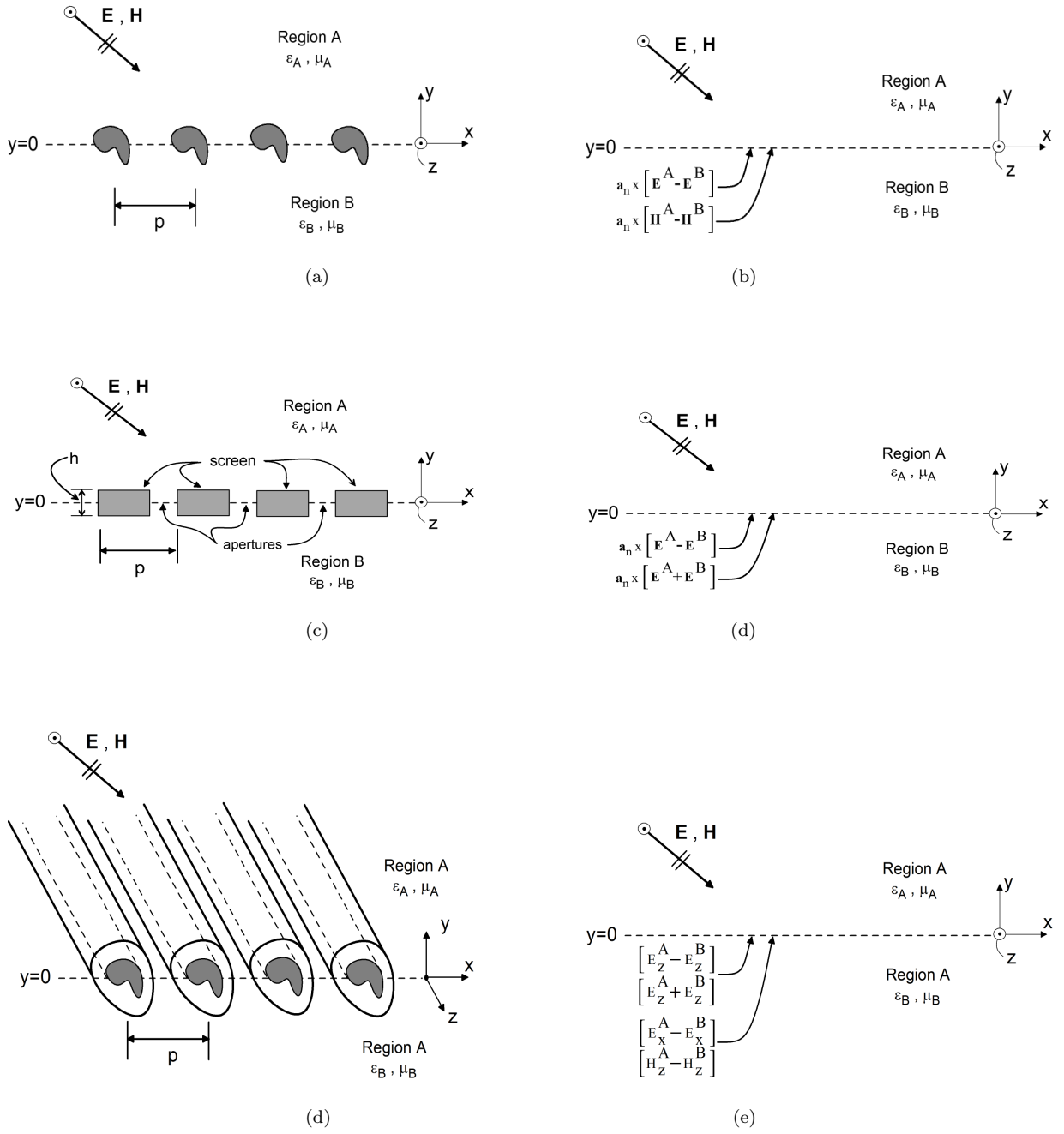

Figure 1.4 Reference planes for GSTC models: (a) a metafilm with arbitrarily shaped scatterers, (b) reference plane for a metafilm at which the GSTCs are applied (c) a metascreen with arbitrarily shaped apertures, (d) reference plane for a metascreen at which the GSTCs are applied, (e) a metagrating with arbitrary shaped coated wire grating, and (f) reference plane for a metagrating at which the GSTCs are applied.

frequencies at which the wavelength is much larger than the period of the structure (that is, the periodicity of the scatterers that compose the composite medium) and at which the scatterers are not resonant. These scatterers could have induced or permanent dipole moments, as is the case for atoms or molecules for classical materials, or these scatterers could be generic in shape and placed in a host matrix to obtain a man-made composite material designed to achieve some specified behavior. In this region, classical mixing formulas are used to obtain equivalent effective-material properties (permittivity ϵ, permeability μ, etc.).

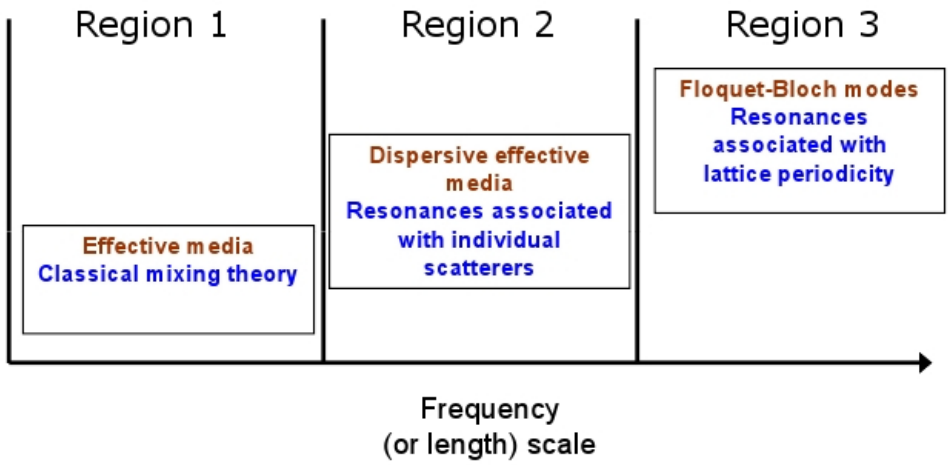

Figure 1.5 Three characteristic regions of composite material or metastructure behavior.

The determination of effective-medium properties and the modeling of electromagnetic response to inclusions embedded in a host material is a problem with a long history going back to Maxwell and Rayleigh, as well as Poisson, Clausius and Mossotti before that. Much work has been done since then to compute the effective properties of homogeneous composite materials, a survey of which can be found in [85]-[88].

Before we discuss the behavior in Region 2, let us examine Region 3. Here, the wavelength becomes comparable to or smaller than the period of the structure, and the fields no longer see the composite as an effective medium. At these frequencies, a more complicated field behavior exists and more elaborate techniques to analyze the EM field interaction with the composite periodic structures must be used (i.e., full-wave approaches). The classical analytical approach for this is the Floquet-Bloch mode expansion [88]-[95] of spatially modulated plane waves propagating in various directions. As the wavelength becomes smaller than the period, higher-order Floquet-Bloch modes must be considered. These higher-order modes then interfere with the fundamental wave propagating through the composite, so that stopbands and passbands will develop in the structure (in this case, the structures are often referred to as EBG or PBG structures [88], [89], [94], and [95]). The constructive and destructive interference of the various modes as the wave propagates through the composite are what give rise to the unique characteristics of EBG and PBG structures. It is important to note that such effects cannot be represented or captured by a conventional effective medium theory. These stopband and passband effects in EBG and PBG structures are caused by resonances associated with the periodicity of the structure.

Resonances associated with the scatterers themselves can cause interesting and unexpected effects in the effective material properties of a composite. Region 2 in Fig. 1.5 corresponds to a region where the period of the structure is still small compared to a wavelength, but the individual scatterers are designed in such a manner (either via their shape or their constitutive properties) such that the scatterers themselves can resonate. When this occurs, a new class of engineered materials (metamaterials) is realized, making possible a broad range of unique behavior not commonly found in nature (DNG or near-zero index materials, for example). Region 2, where the scatters resonate (but not the lattice, as is the case in region 3), is where metamaterials lie. The medium is dispersive here, but we may still characterize its electromagnetic behavior with the effective parameters ϵ and μ.

Similar to metamaterials, depending on the wavelength-to-period spacing, three regions of behavior will occur for electromagnetic interactions with a metasurface. For a two-dimensional lattice of scatterers or apertures, Region 1 in Fig. 1.5 corresponds to classical thin-film materials, while Region 3 in Fig. 1.5 corresponds to resonances associated with the periodicity of the scatterers or apertures. The conventional FSS and PBG surfaces [89, 94, 95] fall into this third region. On the other hand, when we talk about a metasurface, we are referring to an array of scatterers or apertures that lies in Region 2 (or even Region 1). Resonances of the surface may be associated with the resonances of the scatterers or apertures, but not

with the periodicity of the array. Ordinary FSSs are sometimes operated in this regime, but the distinction between this type of operation and that of Region 3 is not always made clear.

We emphasize that the characteristic behavior of Region 2 in Figure 1.5 may not always occur for a given metamaterial or metasurface. The scatterers or apertures need to be properly designed, such that the scatterers' (or apertures') resonances occur at a frequency well below that where the next higher-order Floquet-Bloch mode can propagate. For example, if the constituent materials or the sizes or shapes of the scatterers used in the material were not properly chosen [23], the scatterers' resonances could be pushed toward the Floquet-Bloch-mode region, and in this case an effective-medium model would not adequately describe the behavior of the composite material.

In summary, in Regions 1 and 2 of Figure 1.5 the interaction of an electromagnetic field with a metasurface is described by effective surface parameters of some kind, as will be discussed below. In Region 1 (analogous to the classical mixing theory region for the case of a metamaterial), the effective surface parameters are not frequency-dependent (except insofar as the constituent bulk properties have a frequency dependence). In Region 2 (the scatterers' or apertures' resonant region), the metasurface is still modeled by effective surface properties, which now may possess an inherent frequency dependence that make interesting resonant behaviors possible. In the last region (Region 3 in Figure 1.5), the electromagnetic field's interaction with the periodic array is very involved. We may no longer think of the surface as behaving like an interface with effective surface parameters. When the wavelength is comparable to the period, higher-order Floquet-Bloch modes must be considered, and one typically does not refer to these materials as metamaterials or metasurfaces in this region, but refers to them as EBG, PBG or FSS structures.

1.3 Characterization of Metasurfaces: Surface versus Bulk Properties

Like a metamaterial, the behavior of a metafilm is determined by the electric and magnetic polarizabilities of its constituent scatterers (or for a metascreen, of its constituent apertures). The traditional and most convenient method by which to model metamaterials is with effective-medium theory. Attempts to use a similar bulk-parameter analysis for metasurfaces have been less successful (see [27], [33], and [34] for a detailed discussion on this point). Indeed, some previous metafilm studies have modeled the film as a single-layer metamaterial in which effective bulk material properties of the metasurface are obtained by forcing the introduction of an arbitrary non-zero thickness parameter into the analysis. As we will demonstrate, several problems arise from the physically artificial character of this parameter; the bulk material property characterization of a metasurface is incorrect at a fundamental level. It is known that localized effects arise near the boundary of a metamaterial that can significantly modify effects such as plane-wave reflection and transmission [29, 30, 31, 42, 43, 96]; these are analogous to the effect of cutoff modes near the junction between two different waveguides. Classical algorithms for bulk parameter extraction do not account for these boundary effects, and indeed a metamaterial sample that is only one or a few layers thick should be expected to behave as "all boundary" without exhibiting a uniquely identifiable bulk behavior at all.

To illustrate this point, consider the equivalent-bulk layer representation of a metasurface shown in Fig. 1.6. The problem we face is that the thickness of a metasurface cannot be uniquely defined, nor can the effective material properties. In [29]-[34], it is shown that the effective surface parameters of a metafilm or metascreen are unique properties of the structure, and thus are the most appropriate way to characterize it. We will see below that the surface parameters for a metafilm are what we will call effective surface susceptibilities (defined below as χ_{MS} and χ_{ES}—the magnetic and electric surface susceptibilities, respectively) [27, 30], and for a metascreen, the so-called surface porosities (defined below as π_{MS} and π_{ES}—the magnetic and electric surface porosities, respectively) [27], [31]. Techniques for retrieving the surface parameters for a given metasurface based on reflection and transmission measurements (or simulations) are presented in [27], [33], [34], and [38], and will be discussed below.

The problems that arise when we try to represent a metasurface as a material with a bulk effective permittivity and permeability as in Figure 1.6 are demonstrated in Fig. 1.7(a), where retrieved values of ϵ_r for an array of lossy spherical particles as shown in Figure 1.1(b) are plotted for different values of the assumed thickness d. These results were obtained by computing numerically simulated values of the reflection and transmission coefficients for this array of spheres and then using the modified Nicolson-Ross-Weir (NRW) method [97]-[103] for determining the effective ϵ_r of the slab (see [34] for details; there is also

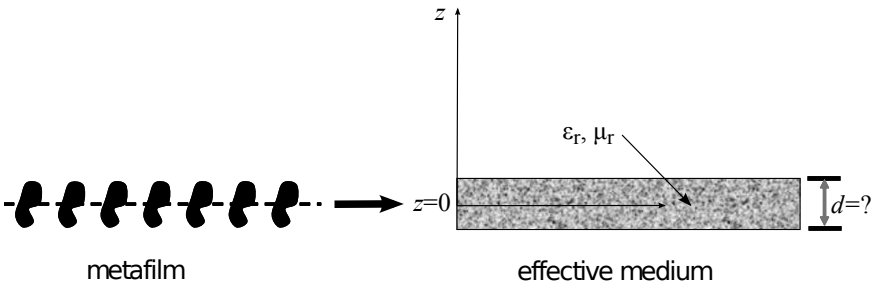

Figure 1.6 Representing a metafilm as a bulk effective medium with thickness d.

an effective μ_R which is not shown here). As we expect, these results show a functional dependence of ϵ_r on d. Fig. 1.7(b) shows results for $d(\epsilon_r - 1)$ for different values of d. We have also plotted the retrieved values of the surface susceptibility χ_{ES}^{yy} for this array that appears in (1.84) below (also obtained from using retrieval algorithms and the simulated numerical values of reflection and transmission coefficients [34], see also Section 1.6 below). The retrieved values for χ_{ES}^{yy} are the same as the analytical values given in [33]. The results shown in Fig. 1.7(b) illustrate that for sufficiently low frequencies, the product $d(\epsilon_r - 1)$ is independent of d and identical to χ_{ES}^{yy}. Although the connection between surface susceptibilities and the effective bulk properties of a slab was not discussed explicitly there, Smith *et al.* [21] do allude to the fact that the product of the slab thickness and the effective material properties of the slab should be constant. Further results for the surface susceptibilities of this same metafilm are shown in Figure 1.8(a)-(b), while results for an array of thin metallic scatterers (Figure 1.8(d)) are shown in Figure 1.8(c).

As we will see in section 1.4.2, a metascreen requires both surface susceptibilities and surface porosities for its complete characterization. Figure 1.9 shows plots of these quantities for a metascreen composed of an array of square apertures—again, these are unique and do not require the postulation of an arbitrary equivalent slab thickness.

When all is said and done, we would argue that a model for a metafilm that uses uniquely specified quantities (i.e., χ_{MS} or χ_{ES} as defined below [29], [30]) is more natural than an approach that involves two arbitrary quantities (d and ϵ_r). Likewise, for a metascreen we should use both surface susceptibilities (χ_{ES} and χ_{MS}) and surface porosities (π_{ES} and π_{MS}) as defined below [27], [31]. Even though it has been shown that the electric and magnetic surface parameters are the most appropriate manner to characterize metasurfaces, some researchers have continued to characterize them in terms of bulk effective material properties. If one insists on characterizing a metasurface as a thin material slab with bulk effective material properties and a thickness d, the only meaningful (and unique) parameters will be products such as $d(\epsilon_r - 1)$ and $d(\mu_r - 1)$, if the slab is centered at the plane containing the metafilm. A retrieval approach that gives unique quantities like χ_{MS}, χ_{ES}, π_{MS}, and π_{ES} is more natural than one that merely gives products of otherwise undetermined quantities [27, 33, 34, 38].

The effective surface parameters (surface susceptibilities and surface porosities) of the metasurface appear in effective boundary conditions called generalized sheet-transition conditions (GSTCs) [27], [29], [30], [31], and these parameters are all that are required to model the macroscopic interaction of any given metasurface with an electromagnetic field. The GSTCs allow this surface distribution of scatterers (or of apertures) to be replaced with boundary conditions that are applied at an infinitely thin equivalent surface (hence the name metasurface, metafilm or metascreen), as indicated in Fig. 1.4. The size, shape, and spacing of the scatterers (or apertures) are incorporated into the GSTCs through the effective surface susceptibilities and surface porosities.

1.4 Generalized Sheet Transition Conditions (GSTCs)

The GSTCs for a metasurface take on distinct functional forms depending on whether it is a metafilm, a metascreen, or a metagrating. In this section, we present the GSTCs required to analyze these three kinds of metastructure.

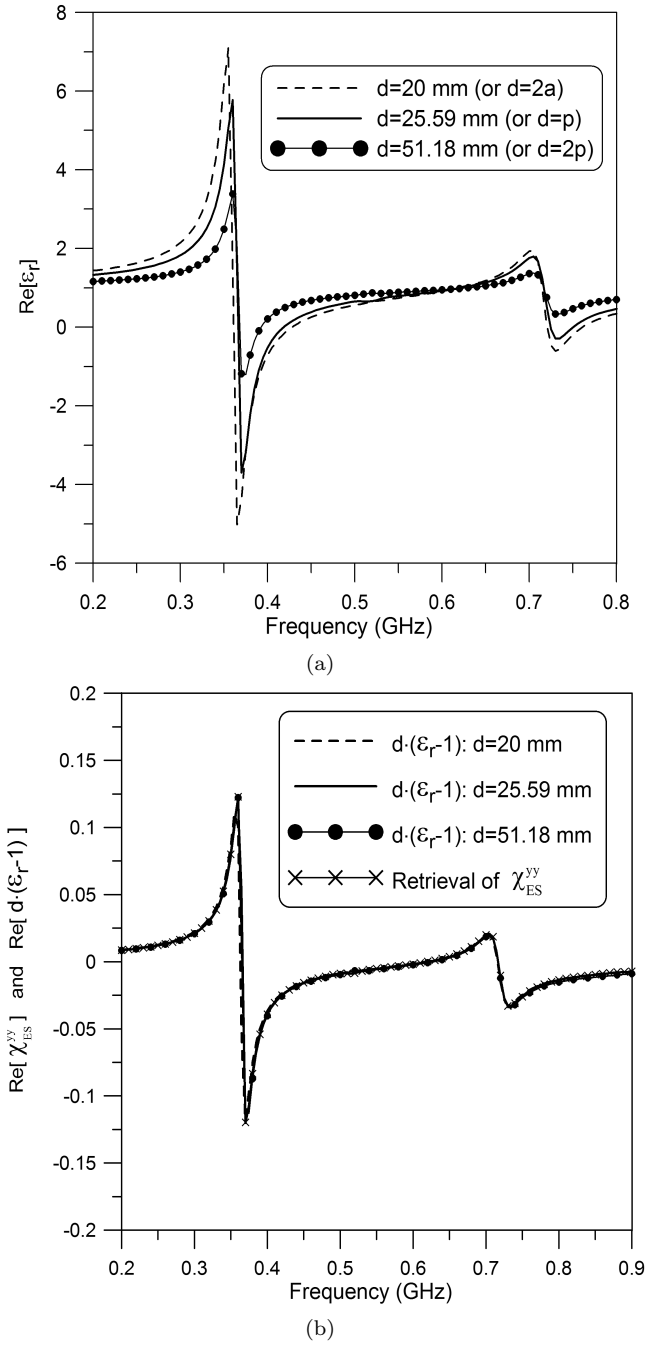

Figure 1.7 Results for an array of lossy spheres with radius $a = 10$ mm, period $p = 25.59$ mm, $\epsilon_{r2} = 2$, $\mu_{r2} = 900$, and loss tangent $\tan\delta = 0.04$: (a) Retrieved ϵ_r and (b) $d(\epsilon_r - 1)$ and χ_{ES}^{yy}.

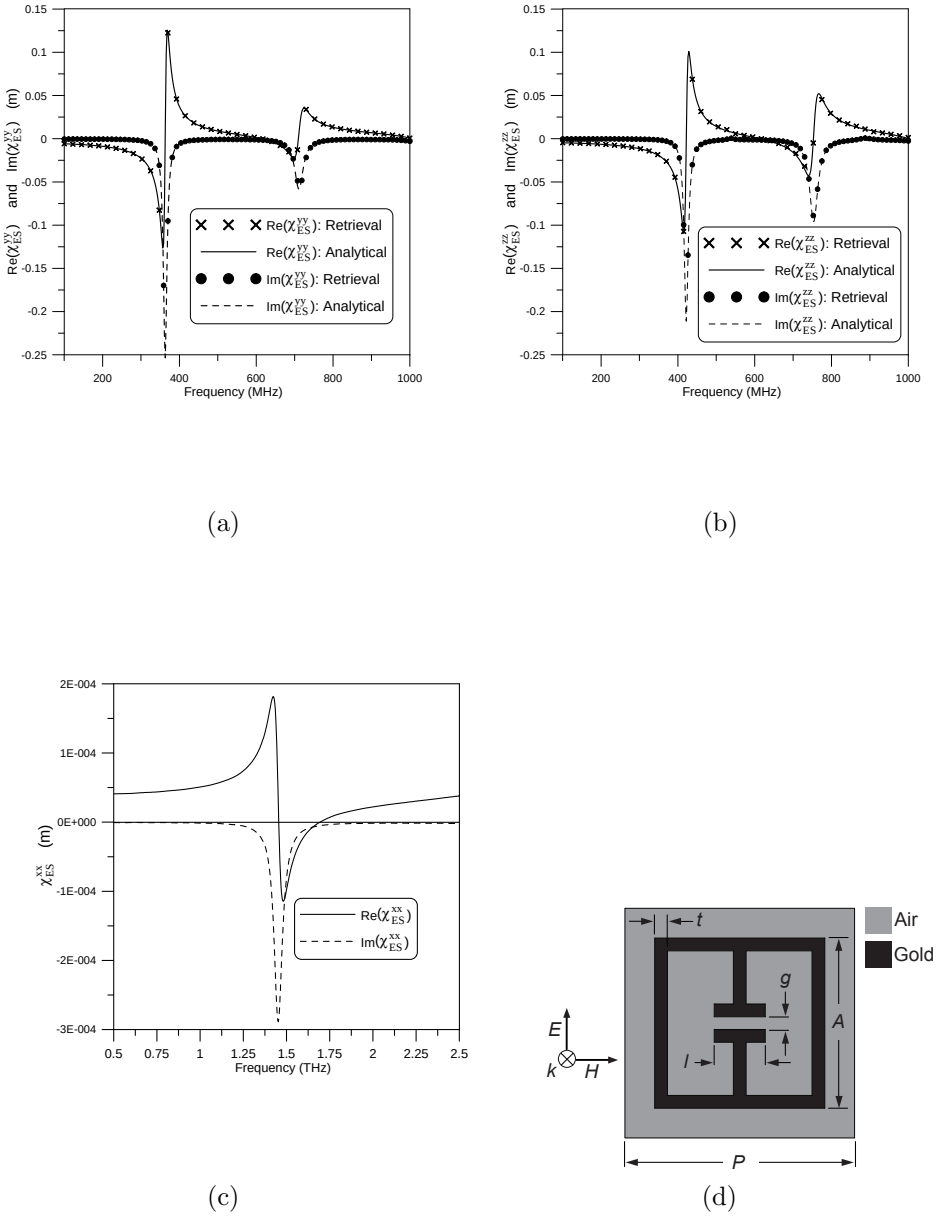

Figure 1.8 Surface electric susceptibilities for two metafilms: (a) χ_{ES}^{yy} and (b) χ_{ES}^{zz} for a metafilm of spherical particles ($a = 10$ mm, $p = 25.59$ mm, $\epsilon_r = 2$, $\mu_r = 900$, and $\tan\delta = 0.04$); (c) surface electric susceptibility χ_{ES}^{zz} for the metafilm array of thin metallic scatterers shown in (d) with $t = 3$ μm, $A = 40$ μm, $p = 54$ μm, and $l = 12$ μm.

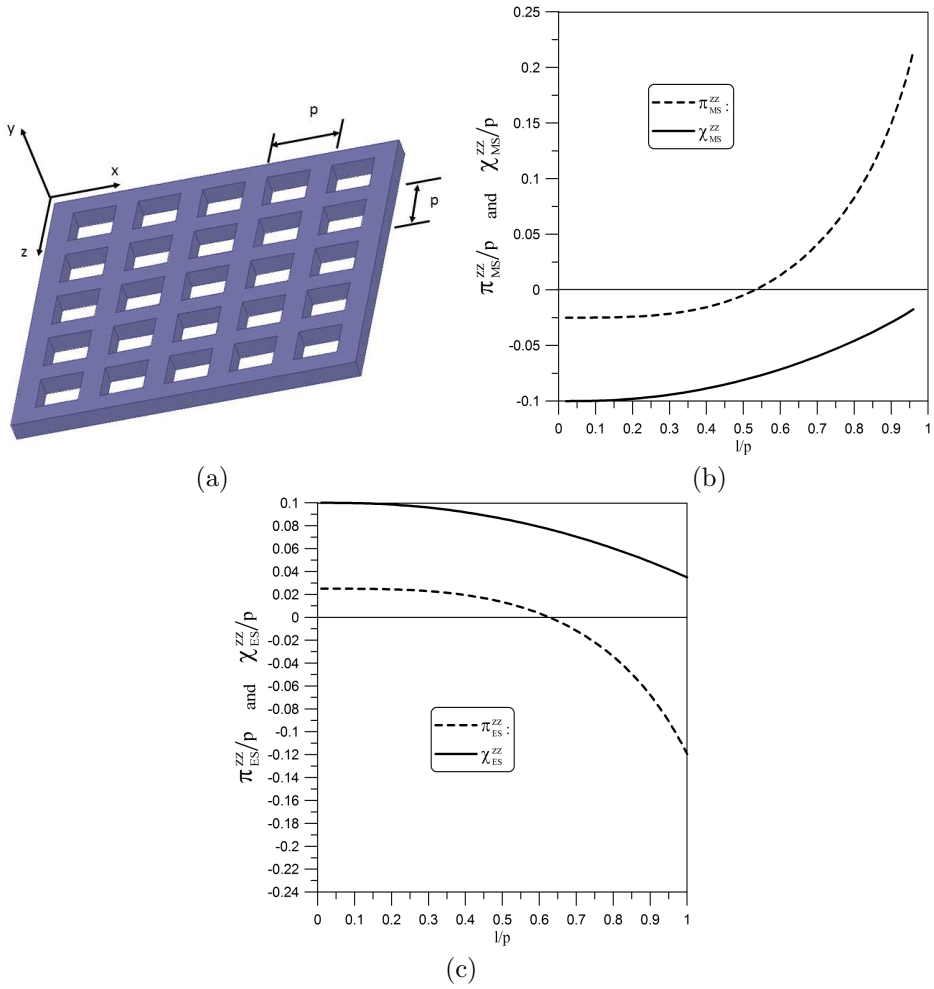

Figure 1.9 Surface susceptibilities and surface porosities for a metascreen composed of an array of apertures : (a) array of square apertures of length l, (b) χ^{zz}_{MS} and π^{zz}_{MS} for square aperture array ($h = 10$ mm and $p = 100$ mm), and (c) χ^{yy}_{ES} and π^{yy}_{ES} for circular aperture array ($h = 5$ mm and $p = 100$ mm).

1.4.1 GSTCs for a Metafilm

As stated above, a metafilm is a metasurface that has a "cermet" topology, which refers to an array of isolated (non-touching) scatterers (see Fig. 1.1). For a metafilm, the GSTCs specify the jumps in the tangential components of the electric (E) and magnetic (H) fields across the metafilm [see Figs. 1.4(a) and 1.4(c)] and take on the following form [27]-[30]:

$$\mathbf{a}_y \times \left[\mathbf{E}^{\mathrm{A}} - \mathbf{E}^{\mathrm{B}}\right]_{y=0} = -\, j\omega\mu_0 \left(\overleftrightarrow{\boldsymbol{\chi}}_{MS} \cdot \tilde{\mathbf{H}}_{\mathrm{av}}\right)_t - \mathbf{a}_y \times \nabla_t \left(\mathbf{a}_y \cdot \overleftrightarrow{\boldsymbol{\chi}}_{ES} \cdot \tilde{\mathbf{E}}_{\mathrm{av}}\right) \tag{1.1}$$

and

$$\mathbf{a}_y \times \left[\mathbf{H}^{\mathrm{A}} - \mathbf{H}^{\mathrm{B}}\right]_{y=0} = j\omega\epsilon_0 \left(\overleftrightarrow{\boldsymbol{\chi}}_{ES} \cdot \tilde{\mathbf{E}}_{\mathrm{av}}\right)_t - \mathbf{a}_y \times \nabla_t \left(\mathbf{a}_y \cdot \overleftrightarrow{\boldsymbol{\chi}}_{MS} \cdot \tilde{\mathbf{H}}_{\mathrm{av}}\right) \ , \tag{1.2}$$

where the subscript "t" represents the x and y components and the average fields are defined by

$$\mathbf{E}_{\mathrm{av}} = \frac{1}{2}\left(\mathbf{E}^{\mathrm{A}} + \mathbf{E}^{\mathrm{B}}\right) \quad \text{and} \quad \mathbf{H}_{\mathrm{av}} = \frac{1}{2}\left(\mathbf{H}^{\mathrm{A}} + \mathbf{H}^{\mathrm{B}}\right) \ . \tag{1.3}$$

The superscripts A and B correspond to the regions below and above the reference plane of the metafilm. The parameters in the GSTCs in eqs. (1.1) and (1.2) are surface susceptibility dyadics and are defined as

$$\begin{aligned} \overleftrightarrow{\boldsymbol{\chi}}_{ES} \;=\; & \chi_{ES}^{xx}\mathbf{a}_x\mathbf{a}_x + \chi_{ES}^{xy}\mathbf{a}_x\mathbf{a}_y + \chi_{ES}^{xz}\mathbf{a}_x\mathbf{a}_z \\ & + \chi_{ES}^{yx}\mathbf{a}_y\mathbf{a}_x + \chi_{ES}^{yy}\mathbf{a}_y\mathbf{a}_y + \chi_{ES}^{yz}\mathbf{a}_y\mathbf{a}_z \\ & + \chi_{ES}^{zx}\mathbf{a}_x\mathbf{a}_x + \chi_{ES}^{zy}\mathbf{a}_z\mathbf{a}_y + \chi_{ES}^{zz}\mathbf{a}_z\mathbf{a}_z \ , \end{aligned} \tag{1.4}$$

$$\begin{aligned} \overleftrightarrow{\boldsymbol{\chi}}_{MS} \;=\; & \chi_{MS}^{xx}\mathbf{a}_x\mathbf{a}_x + \chi_{MS}^{xy}\mathbf{a}_x\mathbf{a}_y + \chi_{MS}^{xz}\mathbf{a}_x\mathbf{a}_z \\ & + \chi_{MS}^{yx}\mathbf{a}_y\mathbf{a}_x + \chi_{MS}^{yy}\mathbf{a}_y\mathbf{a}_y + \chi_{MS}^{yz}\mathbf{a}_y\mathbf{a}_z \\ & + \chi_{MS}^{zx}\mathbf{a}_x\mathbf{a}_x + \chi_{MS}^{zy}\mathbf{a}_z\mathbf{a}_y + \chi_{MS}^{zz}\mathbf{a}_z\mathbf{a}_z \ . \end{aligned} \tag{1.5}$$

The surface susceptibilities have units of length. Note that the coordinate system used here is the same as that used in [30], but different from the one used in [29], [33], and [34].

1.4.2 GSTCs for a Metascreen

Metascreens are metasurfaces with a "fishnet" structure (see Fig. 1.2), which are characterized by periodically spaced apertures in an otherwise relatively impenetrable surface. This fundamentally different topology requires a different functional form of GSTCs than what applies to a metafilm: a set of BCs for the jumps in both tangential E and H fields at its reference surface. As it turns out, GSTCs can still be used for a metascreen, but the topology demands a different form for them, for the following reason. For a problem involving two regions separated by a boundary surface, one needs at least two effective boundary conditions (EBCs) to constrain the tangential E- and/or H-fields at that boundary. A metascreen differs from a metafilm in that there is the possibility of having tangential surface currents (flowing on the surface of the screen along the z and x directions). Typically these currents would only be known once the tangential components of the H-field are known.

This concept can be illustrated by the case of an electromagnetic field at the surface of a perfect electric conductor (PEC). For a PEC, only the BC for the tangential E-field at the PEC (i. e., $\mathbf{E}_t = 0$ on the PEC) is used in solving boundary problems for the field. The tangential H-field at the PEC is related to the surface current flowing on the PEC and this current is only known once the H-field has been determined, so this second boundary condition is not used to solve for the fields. It is useful, therefore, to classify EBCs either as *essential* for the solution of an electromagnetic boundary problem, or applicable only *a posteriori* when quantities such as surface current or charge density are to be computed from the fields. For a metascreen, any EBC for the tangential H field is an *a posteriori* BC and can only be used once the fields have been solved for. Thus, the required *essential* BCs for metascreen should constrain only tangential E, and should be expressed as conditions on the jump in the tangential E-field and on the sum (twice the average) of the tangential E-fields, i.e., on

$$\begin{aligned} \left[E_x^A - E_x^B\right]_{y=0} \quad ; \quad \left[E_z^A - E_z^B\right]_{y=0} \\ \left[E_x^A + E_x^B\right]_{y=0} \quad ; \quad \left[E_z^A + E_z^B\right]_{y=0} \ , \end{aligned} \tag{1.6}$$

where the superscripts A and B correspond to the regions above and below the reference plane of the metascreen, respectively. We add that these types of GSTCs (on both the jump in, and the average of, the E-field at the interface) also appear in the analysis of a wire grating (or metagrating) [32], as we will see in the next subsection.

The required GSTCs for a metascreen are given by [27], [31]:

$$\begin{aligned}\mathbf{a}_y \times \left[\mathbf{E}^{\mathrm{A}}(\mathbf{r}_o) - \mathbf{E}^{\mathrm{B}}(\mathbf{r}_0)\right] &= -\mathbf{a}_y \times \left[\chi_{ES}^{Ayy}\,\nabla_t E_y^A(\mathbf{r}_o) + \chi_{ES}^{Byy}\,\nabla_t E_y^B(\mathbf{r}_o)\right] \\ &\quad -\mathbf{a}_x\, j\omega\mu_0\, \left[\chi_{MS}^{Axx} H_x^A(\mathbf{r}_o) + \chi_{MS}^{Bxx} H_x^B(\mathbf{r}_o)\right. \\ &\quad\quad \left. +\chi_{MS}^{Axz} H_z^A(\mathbf{r}_o) + \chi_{MS}^{Bxz} H_z^B(\mathbf{r}_o)\right] \\ &\quad -\mathbf{a}_z\, j\omega\mu_0\, \left[\chi_{MS}^{Azx} H_x^A(\mathbf{r}_o) + \chi_{MS}^{Bzx} H_x^B(\mathbf{r}_o)\right. \\ &\quad\quad \left. +\chi_{MS}^{Azz} H_z^A(\mathbf{r}_o) + \chi_{MS}^{Bzz} H_z^B(\mathbf{r}_o)\right]\end{aligned} \tag{1.7}$$

and

$$\begin{aligned}\mathbf{a}_y \times \left[\mathbf{E}^{\mathrm{A}}(\mathbf{r}_o) + \mathbf{E}^{\mathrm{B}}(\mathbf{r}_0)\right] &= -\mathbf{a}_y \times \left[\pi_{ES}^{Ayy}\,\nabla_t E_y^A(\mathbf{r}_o) - \pi_{ES}^{Byy}\,\nabla_t E_y^B(\mathbf{r}_o)\right] \\ &\quad -\mathbf{a}_x\, j\omega\mu_0\, \left[\pi_{MS}^{Axx} H_x^A(\mathbf{r}_o) - \pi_{MS}^{Bxx} H_x^B(\mathbf{r}_o)\right. \\ &\quad\quad \left. +\pi_{MS}^{Axz} H_z^A(\mathbf{r}_o) - \pi_{MS}^{Bxz} H_z^B(\mathbf{r}_o)\right] \\ &\quad -\mathbf{a}_z\, j\omega\mu_0\, \left[\pi_{MS}^{Azx} H_x^A(\mathbf{r}_o) - \pi_{MS}^{Bzx} H_x^B(\mathbf{r}_o)\right. \\ &\quad\quad \left. +\pi_{MS}^{Azz} H_z^A(\mathbf{r}_o) - \pi_{MS}^{Bzz} H_z^B(\mathbf{r}_o)\right]\end{aligned} \tag{1.8}$$

As before, χ_{ES} and χ_{MS} are effective electric and magnetic surface susceptibilities, respectively, while π_{ES} and π_{MS} are interpreted as effective electric and magnetic surface porosities of the metascreen. Like the surface susceptibilities, the surface porosities have units of length.

1.4.3 GSTCs for a Metagrating

A metagrating [32] is a metasurface composed of a grating of arbitrary-shaped parallel material-coated wires as shown in Fig. 1.3. A metagrating behaves like a metafilm to electric fields perpendicular to the wire axes and like a metascreen for electric fields parallel those axes. Thus, the form of GSTCs required for a metagrating is a combination of those of the metafilm and metascreen. The GSTCs for the metagrating are given by [32]

$$\begin{aligned}\mathbf{a}_y \times \left[\mathbf{E}^{A}(\mathbf{r}_o) - \mathbf{E}^{B}(\mathbf{r}_o)\right] &= -j\omega\mu_0\, \chi_{MS}^{zz} H_{z,av}(\mathbf{r}_o)\, \mathbf{a}_z - j\omega\, \chi_{MS}^{xy} B_{y,av}(\mathbf{r}_o)\, \mathbf{a}_x \\ &\quad +j\omega\, \left[\chi_{MS}^{Axx}\, B_x^A(\mathbf{r}_o) + \chi_{MS}^{Bxx}\, B_x^B(\mathbf{r}_o)\right]\, \mathbf{a}_x \\ &\quad -\mathbf{a}_y \times \left[\chi_{ES}^{yx}\, \nabla E_{x,av}(\mathbf{r}_o)\right] \\ &\quad -\mathbf{a}_y \times \left[\chi_{ES}^{Ayy} \nabla E_y^A(\mathbf{r}_o) + \chi_{ES}^{Byy} \nabla E_y^B(\mathbf{r}_o)\right]\ ,\end{aligned} \tag{1.9}$$

$$\begin{aligned}H_z^A(\mathbf{r}_o) - H_z^B(\mathbf{r}_o) &= j\omega\epsilon_0\, \chi_{ES}^{xx}\, E_{x,av}(\mathbf{r}_o) \\ &\quad +j\omega\epsilon_0\, \left[\chi_{ES}^{Axy}\, E_y^A(\mathbf{r}_o) + \chi_{ES}^{Bxy}\, E_y^B(\mathbf{r}_o)\right] \\ &\quad -\tfrac{1}{\mu_0}\, \chi_{MS}^{yy}\, \tfrac{\partial B_{y,av}(\mathbf{r}_o)}{\partial z} \\ &\quad -\tfrac{1}{\mu_0}\, \left[\chi_{MS}^{Ayx}\, \tfrac{\partial B_x^A(\mathbf{r}_o))}{\partial z} + \chi_{MS}^{Byx}\, \tfrac{\partial B_x^B(\mathbf{r}_o)}{\partial z}\right]\ ,\end{aligned} \tag{1.10}$$

and

$$\begin{aligned}E_z^A(\mathbf{r}_o) + E_z^B(\mathbf{r}_o) &= -j\omega\pi_{MS}^{xy} B_{y,av}(\mathbf{r}_o) \\ &\quad -j\omega\, \left[\pi_{MS}^{Axx}\, B_x^A(\mathbf{r}_o) - \pi_{MS}^{Bxx}\, B_x^B(\mathbf{r}_o)\right] \\ &\quad -\pi_{ES}^{xy}\, \tfrac{\partial E_{x,av}(\mathbf{r}_o)}{\partial z} \\ &\quad -\pi_{ES}^{Ayy}\, \tfrac{\partial E_y^A(\mathbf{r}_o)}{\partial z} - \pi_{ES}^{Byy}\, \tfrac{\partial E_y^B(\mathbf{r}_o)}{\partial z}\ ,\end{aligned} \tag{1.11}$$

where certain average fields at the interface have been defined as:

$$\begin{aligned} E_{x,av}(\mathbf{r}_o) &= \frac{E_x^A(\mathbf{r}_o) + E_x^B(\mathbf{r}_o)}{2} \\ B_{y,av}(\mathbf{r}_o) &= \frac{B_y^A(\mathbf{r}_o) + B_y^B(\mathbf{r}_o)}{2} \\ H_{z,av}(\mathbf{r}_o) &= \frac{H_z^A(\mathbf{r}_o) + H_z^B(\mathbf{r}_o)}{2} \ . \end{aligned} \tag{1.12}$$

The coefficients χ_{ES} and χ_{MS} are effective electric and magnetic surface susceptibilities of the metagrating, while $\pi_{MS,ES}$ are effective electric and magnetic surface *porosities* of the metagrating; both have units of length.

1.5 Reflection and Transmission Coefficients

The plane-wave reflection and transmission coefficients for three types of metasurfaces are derived in this section. We present results for both a transverse electric (TE) and transverse magnetic (TM) polarized plane wave incident onto the metasurface.

1.5.1 Metafilms

As seen from the GSTCs (1.1) and (1.2), the electric and magnetic surface susceptibilities may have cross-polarization (or off-diagonal) terms $\chi_{ES,MS}^{xz,zx}$, $\chi_{ES,MS}^{zy,yz}$, and $\chi_{ES,MS}^{xy,yx}$. These terms can result in coupling between TE and TM fields. Initially, we will assume for simplicity that the scatterers are sufficiently symmetric that these off-diagonal terms are zero. These assumptions correspond to many metafilms that are encountered in practice; the more general case will be treated later. The symmetry of the scatterers results in:

$$\chi_{ES,MS}^{xz,zx} = \chi_{ES,MS}^{zy,yz} = \chi_{ES,MS}^{xy,yx} \equiv 0 \ . \tag{1.13}$$

Under this condition, the surface susceptibility dyadics reduce to:

$$\begin{aligned} \overleftrightarrow{\chi}_{ES} &= \chi_{ES}^{xx}\mathbf{a}_x\mathbf{a}_x + \chi_{ES}^{yy}\mathbf{a}_y\mathbf{a}_y + \chi_{ES}^{zz}\mathbf{a}_z\mathbf{a}_z \\ \overleftrightarrow{\chi}_{MS} &= \chi_{MS}^{xx}\mathbf{a}_x\mathbf{a}_x + \chi_{MS}^{yy}\mathbf{a}_y\mathbf{a}_y + \chi_{MS}^{zz}\mathbf{a}_z\mathbf{a}_z \end{aligned} \tag{1.14}$$

1.5.1.1 TE Polarization for a Metafilm Let a metafilm be located in the plane $y = 0$ in free space. Assume that a TE polarized plane wave is incident onto the metafilm as shown in Fig. 1.10, such that the total E-field in region A ($y > 0$) is given by $\mathbf{E} = \mathbf{E}^i + \mathbf{E}^r$, where the incident and reflected fields are

$$\begin{aligned} \mathbf{E}^i &= \mathbf{a}_z E_0 e^{-j\mathbf{k}_i\cdot\mathbf{r}} \\ \mathbf{E}^r &= \mathbf{a}_z R_{TE} E_0 e^{-j\mathbf{k}_r\cdot\mathbf{r}} \end{aligned} \ . \tag{1.15}$$

The transmitted field in region B ($y < 0$) is given by

$$\mathbf{E}^t = \mathbf{a}_z T_{TE} E_0 e^{-j\mathbf{k}_t\cdot\mathbf{r}} \ , \tag{1.16}$$

where

$$\begin{aligned} \mathbf{k}_t = \mathbf{k}_i &= \{\mathbf{a}_x \sin\theta - \mathbf{a}_y \cos\theta\}\, k_0 \\ \mathbf{k}_r &= \{\mathbf{a}_x \sin\theta + \mathbf{a}_y \cos\theta\}\, k_0 \end{aligned} \ , \tag{1.17}$$

and $k_0 = \omega\sqrt{\mu_0\epsilon_0}$ is the wavenumber of free space. In (1.15) and (1.16), R_{TE} and T_{TE} are the reflection and transmission coefficient, respectively. From Maxwell's equations, the incident, reflected and transmitted

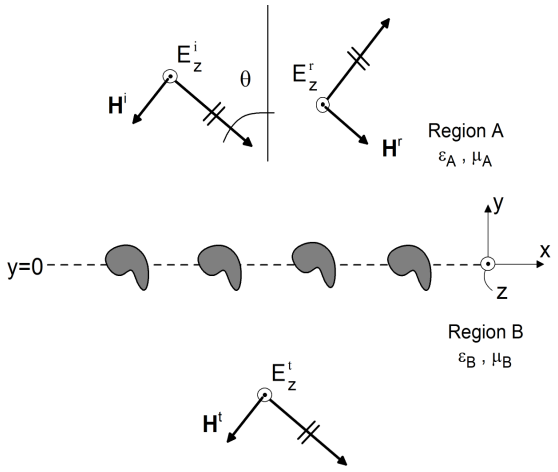

Figure 1.10 TE polarized plane-wave incident onto a metastructure.

H-fields are given by:

$$\begin{aligned}\mathbf{H}^i &= \left(\tfrac{k_0 E_0}{\omega\mu}\right)\{-\mathbf{a}_x\cos\theta-\mathbf{a}_y\sin\theta\}\,e^{-j\mathbf{k}_i\cdot\mathbf{r}}\\ \mathbf{H}^r &= \left(\tfrac{k_0 E_0 R_{TE}}{\omega\mu}\right)\{\mathbf{a}_x\cos\theta-\mathbf{a}_y\sin\theta\}\,e^{-j\mathbf{k}_r\cdot\mathbf{r}}\\ \mathbf{H}^t &= -\left(\tfrac{k_0 E_0 T_{TE}}{\omega\mu}\right)\{\mathbf{a}_x\cos\theta+\mathbf{a}_y\sin\theta\}\,e^{-j\mathbf{k}_t\cdot\mathbf{r}}\end{aligned}\quad . \tag{1.18}$$

Substituting the electric and magnetic field components given in (1.15), (1.16) and (1.18), into the GSTCs (1.1) and (1.2) results in

$$R_{TE}(\theta)=\frac{-j\frac{k_0}{2\cos\theta}\left(\chi^{zz}_{ES}+\chi^{yy}_{MS}\sin^2\theta-\chi^{xx}_{MS}\cos^2\theta\right)}{1-\left(\frac{k_0}{2}\right)^2\chi^{xx}_{MS}\left(\chi^{zz}_{ES}+\chi^{yy}_{MS}\sin^2\theta\right)+j\frac{k_0}{2\cos\theta}\left(\chi^{zz}_{ES}+\chi^{xx}_{MS}\cos^2\theta+\chi^{yy}_{MS}\sin^2\theta\right)} \tag{1.19}$$

and

$$T_{TE}(\theta)=\frac{1+\left(\frac{k_0}{2}\right)^2\chi^{xx}_{MS}\left(\chi^{zz}_{ES}+\chi^{yy}_{MS}\sin^2\theta\right)}{1-\left(\frac{k_0}{2}\right)^2\chi^{xx}_{MS}\left(\chi^{zz}_{ES}+\chi^{yy}_{MS}\sin^2\theta\right)+j\frac{k_0}{2\cos\theta}\left(\chi^{zz}_{ES}+\chi^{xx}_{MS}\cos^2\theta+\chi^{yy}_{MS}\sin^2\theta\right)} \tag{1.20}$$

1.5.1.2 TM Polarization for a Metafilm Assume that a TM polarized H-field plane wave is incident onto the metafilm shown in Fig. 1.11, such that the H-field components of the incident, reflected, and transmitted plane waves are given by

$$\begin{aligned}\mathbf{H}^i &= \mathbf{a}_z\tfrac{E_0}{\zeta_0}e^{-j\mathbf{k}_i\cdot\mathbf{r}}\\ \mathbf{H}^r &= -\mathbf{a}_z R_{TM}\tfrac{E_0}{\zeta_0}e^{-j\mathbf{k}_r\cdot\mathbf{r}}\\ \mathbf{H}^t &= \mathbf{a}_z T_{TM}\tfrac{E_0}{\zeta_0}e^{-j\mathbf{k}_t\cdot\mathbf{r}}\end{aligned}\quad . \tag{1.21}$$

where $\zeta_0=\sqrt{\mu_0/\epsilon_0}$ is the wave impedance of free space. From Maxwell's equations, the incident, reflected and transmitted E-fields are given by:

$$\begin{aligned}\mathbf{E}^i &= E_0\left(\mathbf{a}_x\cos\theta+\mathbf{a}_y\sin\theta\right)e^{-j\mathbf{k}_i\cdot\mathbf{r}}\\ \mathbf{E}^r &= E_0\left(\mathbf{a}_x\cos\theta-\mathbf{a}_y\sin\theta\right)R_{TM}e^{-j\mathbf{k}_r\cdot\mathbf{r}}\\ \mathbf{E}^t &= E_0\left(\mathbf{a}_x\cos\theta+\mathbf{a}_y\sin\theta\right)T_{TM}\;e^{-j\mathbf{k}_t\cdot\mathbf{r}}\end{aligned}\quad . \tag{1.22}$$

Substituting these expressions into the GSTCs given in (1.1) and (1.2) we obtain:

$$R_{TM}(\theta)=\frac{-j\frac{k_0}{2\cos\theta}\left(\chi^{xx}_{ES}\cos^2\theta-\chi^{zz}_{MS}-\chi^{yy}_{ES}\sin^2\theta\right)}{1-\left(\frac{k_0}{2}\right)^2\chi^{xx}_{ES}\left(\chi^{zz}_{MS}+\chi^{yy}_{ES}\sin^2\theta\right)+j\frac{k_0}{2\cos\theta}\left(\chi^{zz}_{MS}+\chi^{xx}_{ES}\cos^2\theta+\chi^{yy}_{ES}\sin^2\theta\right)}\quad , \tag{1.23}$$

and

$$T_{TM}(\theta)=\frac{1+\left(\frac{k_0}{2}\right)^2\chi^{xx}_{ES}\left(\chi^{zz}_{MS}+\chi^{yy}_{ES}\sin^2\theta\right)}{1-\left(\frac{k_0}{2}\right)^2\chi^{xx}_{ES}\left(\chi^{zz}_{MS}+\chi^{yy}_{ES}\sin^2\theta\right)+j\frac{k_0}{2\cos\theta}\left(\chi^{zz}_{MS}+\chi^{xx}_{ES}\cos^2\theta+\chi^{yy}_{ES}\sin^2\theta\right)}\quad . \tag{1.24}$$

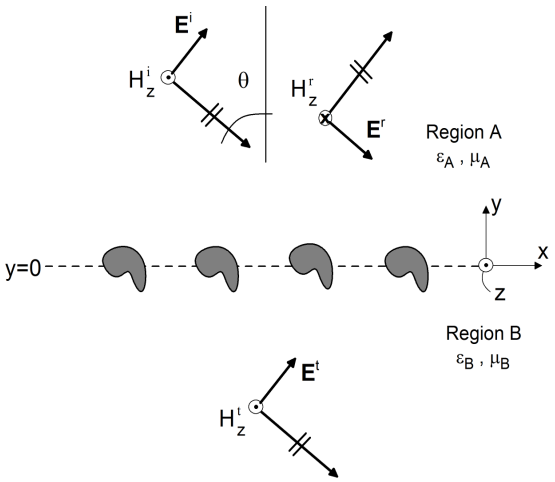

Figure 1.11 TM polarized plane-wave incident onto a metastructure.

1.5.1.3 Cross-Polarized Terms When the full surface susceptibility dyadics are included, the reflection and transmission coefficients are more complicated. In fact, the cross-polarization surface susceptibilities result in coupling (or mode conversion) between TE and TM modes when a plane-wave is incident onto a metafilm. For an asymmetric metafilm, an incident TE plane wave can result in both TE and TM waves as defined in Fig. 1.12. To account for the possibility of polarization conversion, the reflected and transmitted fields [for the TE incident wave as indicated in eq. (1.15)] are expressed as

$$\begin{aligned}\mathbf{E}^r &= \mathbf{a}_z E_0\ R_{TE} e^{-j\mathbf{k}_r\cdot\mathbf{r}} \\ &\quad +E_0\ R_{TE}^{TM}\ (\mathbf{a}_x\cos\theta - \mathbf{a}_y\sin\theta)\ e^{-j\mathbf{k}_r\cdot\mathbf{r}}\end{aligned}\ , \tag{1.25}$$

and

$$\begin{aligned}\mathbf{E}^t &= \mathbf{a}_z E_0\ T_{TE}\ e^{-j\mathbf{k}_t\cdot\mathbf{r}} \\ &\quad +E_0\ T_{TE}^{TM}\ (\mathbf{a}_x\cos\theta + \mathbf{a}_y\sin\theta)\ e^{-j\mathbf{k}_t\cdot\mathbf{r}}\end{aligned}\ , \tag{1.26}$$

where

$$\mathbf{k}_t = \mathbf{k}_i \quad \text{and} \quad \mathbf{k}_r = \{\mathbf{a}_x\sin\theta + \mathbf{a}_y\cos\theta\}\, k_0\ , \tag{1.27}$$

and R_{TE} and T_{TE} are the (co-polarized) reflection and transmission coefficients of a TE wave, and R_{TE}^{TM} and T_{TE}^{TM} are the (cross-polarized) reflection and transmission coefficients of a TM wave for an incident TE wave.

Upon substituting these expressions for the fields into the GSTCs, the reflection and transmission coefficients for a TE incident plane-wave are found to be [104] and [105]

$$R_{TE}(\theta) = -\frac{\mathcal{A}\mathcal{B} - k_0^2\chi_{MS}^{yx}\chi_{MS}^{xy}}{2(\mathcal{A}\mathcal{C} + k_0^2\chi_{MS}^{yx}\chi_{MS}^{xy})} + \frac{\mathcal{E}\mathcal{N} - k_0^2\chi_{ES}^{yx}\chi_{ES}^{xy}}{2(\mathcal{D}\mathcal{E} + k_0^2\chi_{ES}^{yx}\chi_{ES}^{xy})} \tag{1.28}$$

$$T_{TE}(\theta) = \frac{\mathcal{A}\mathcal{B} - k_0^2\chi_{MS}^{yx}\chi_{MS}^{xy}}{2(\mathcal{A}\mathcal{C} + k_0^2\chi_{MS}^{yx}\chi_{MS}^{xy})} + \frac{\mathcal{E}\mathcal{N} - k_0^2\chi_{ES}^{yx}\chi_{ES}^{xy}}{2(\mathcal{D}\mathcal{E} + k_0^2\chi_{ES}^{yx}\chi_{ES}^{xy})} \tag{1.29}$$

$$R_{TE}^{TM}(\theta) = -\frac{jk_0\chi_{MS}^{yx}(\mathcal{B} - \mathcal{C})}{2(\mathcal{A}\mathcal{C} + k_0^2\chi_{MS}^{yx}\chi_{MS}^{xy})} + \frac{jk_0\chi_{ES}^{xy}(\mathcal{N} - \mathcal{D})}{2(\mathcal{D}\mathcal{E} + k_0^2\chi_{ES}^{yx}\chi_{ES}^{xy})} \tag{1.30}$$

$$T_{TE}^{TM}(\theta) = \frac{jk_0\chi_{MS}^{yx}(\mathcal{B} - \mathcal{C})}{2(\mathcal{A}\mathcal{C} + k_0^2\chi_{MS}^{yx}\chi_{MS}^{xy})} + \frac{jk_0\chi_{ES}^{xy}(\mathcal{N} - \mathcal{D})}{2(\mathcal{D}\mathcal{E} + k_0^2\chi_{ES}^{yx}\chi_{ES}^{xy})} \tag{1.31}$$

where

$$\mathcal{A} = 2 + \tfrac{jk_0}{\cos\theta}\chi_{MS}^{yy} + \tfrac{jk_0}{\cos\theta}\chi_{ES}^{zz}\sin^2\theta \quad ; \quad \mathcal{B} = 2 - jk_0\chi_{MS}^{xx}\cos\theta\ , \tag{1.32}$$

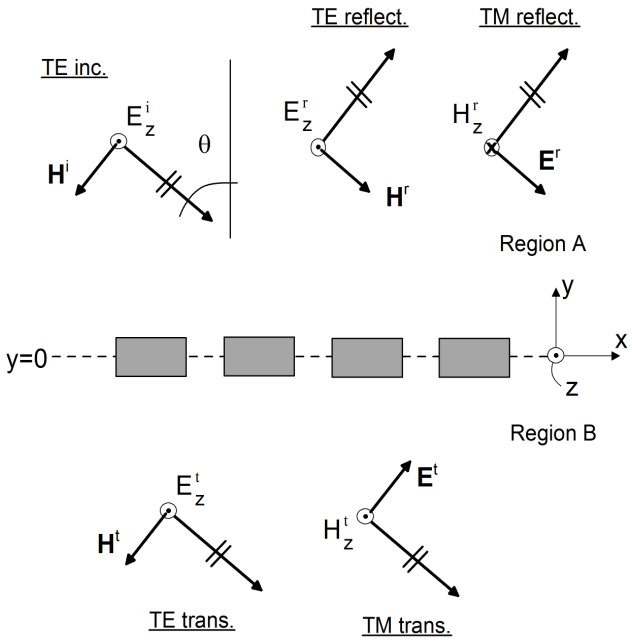

Figure 1.12 TE Plane wave incident onto a asymmetric metastructure.

$$\mathcal{N} = 2 - \tfrac{jk_0}{\cos\theta}\chi_{ES}^{yy} - \tfrac{jk_0}{\cos\theta}\chi_{MS}^{zz}\sin^2\theta \quad ; \quad \mathcal{E} = 2 + jk_0\chi_{ES}^{xx}\cos\theta \ , \tag{1.33}$$

and

$$\mathcal{D} = 2 + \tfrac{jk_0}{\cos\theta}\chi_{ES}^{yy} + \tfrac{jk_0}{\cos\theta}\chi_{MS}^{zz}\sin^2\theta \quad ; \quad \mathcal{C} = 2 + jk_0\chi_{MS}^{xx}\cos\theta \ . \tag{1.34}$$

From these expressions, we see that due to the anisotropic terms in the GSTCs, polarization conversion will occur, in that an incident TE wave will generate TM waves in addition to the expected TE waves. If the cross-coupling terms are zero, then R_{TE}^{TM} and T_{TE}^{TM} are also zero; and we are left with a pure TE reflection and transmitted field.

For an asymmetric metafilm, a TM plane wave can also result in both TE and TM waves. Assume that a TM polarized plane wave is incident onto the metafilm as shown in Fig. 1.13, such that the incident electric field is given by:

$$\mathbf{E}^i \ = \ E_0\left(\mathbf{a}_x\cos\theta + \mathbf{a}_y\sin\theta\right)e^{-j\mathbf{k}_i\cdot\mathbf{r}} \ . \tag{1.35}$$

Similar to the derivation above, to account for the possibility of the metafilm converting the incident TM wave into both TE and TM waves (see Fig. 1.13), the reflected and transmitted fields are expressed as

$$\begin{aligned}\mathbf{E}^r \ = \ & \mathbf{a}_z E_0 \ R_{TM}^{TE} \ e^{-j\mathbf{k}_r\cdot\mathbf{r}} \\ & + E_0 \ R_{TM}\left(\mathbf{a}_x\cos\theta - \mathbf{a}_y\sin\theta\right) \ e^{-j\mathbf{k}_r\cdot\mathbf{r}}\end{aligned} \ , \tag{1.36}$$

and

$$\begin{aligned}\mathbf{E}^t \ = \ & \mathbf{a}_z E_0 \ T_{TM}^{TE} e^{-j\mathbf{k}_t\cdot\mathbf{r}} \\ & + E_0 \ T_{TM} \ \left(\mathbf{a}_x\cos\theta + \mathbf{a}_y\sin\theta\right) \ e^{-j\mathbf{k}_t\cdot\mathbf{r}}\end{aligned} \ , \tag{1.37}$$

where R_{TM} and T_{TM} are the (co-polarized) reflection and transmission coefficients of the TM wave, and R_{TM}^{TE} and T_{TM}^{TE} are the (cross-polarized) reflection and transmission coefficients of a TE wave for a incident TM wave.

Upon substituting the expressions above into the GSTCs, the reflection and transmission coefficients are found to be [104] and [105]

$$R_{TE}(\theta) = -\frac{\mathcal{C}\,\mathcal{M} - k_0^2\chi_{MS}^{yx}\chi_{MS}^{xy}}{2(\mathcal{A}\mathcal{C} + k_0^2\chi_{MS}^{yx}\chi_{MS}^{xy})} + \frac{\mathcal{D}\,\mathcal{F} - k_0^2\chi_{ES}^{yx}\chi_{ES}^{xy}}{2(\mathcal{D}\,\mathcal{E} + k_0^2\chi_{ES}^{yx}\chi_{ES}^{xy})} \tag{1.38}$$

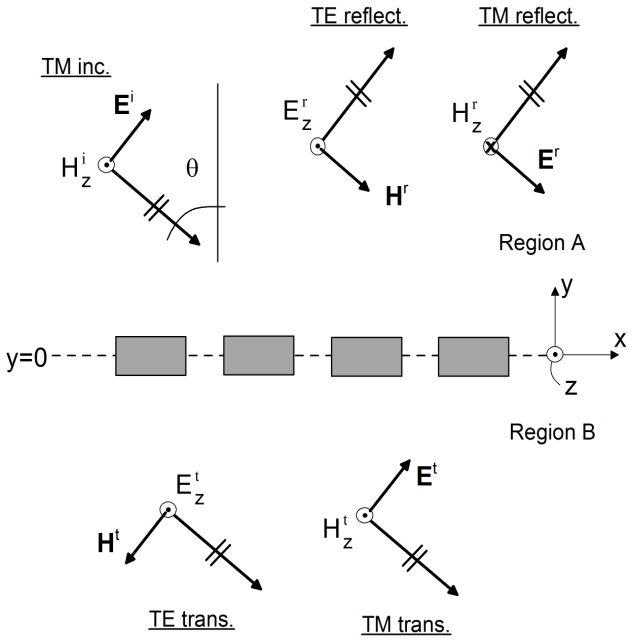

Figure 1.13 TM Plane wave incident onto a asymmetric metastructure.

$$T_{TE}(\theta) = \frac{\mathcal{C}\,\mathcal{M} - k_0^2\chi_{MS}^{yx}\chi_{MS}^{xy}}{2(\mathcal{A}\mathcal{C} + k_0^2\chi_{MS}^{yx}\chi_{MS}^{xy})} + \frac{\mathcal{D}\,\mathcal{F} - k_0^2\chi_{ES}^{yx}\chi_{ES}^{xy}}{2(\mathcal{D}\,\mathcal{E} + k_0^2\chi_{ES}^{yx}\chi_{ES}^{xy})} \tag{1.39}$$

$$R_{TE}^{TM}(\theta) = -\frac{jk_0\chi_{MS}^{yx}(\mathcal{M} + \mathcal{A})}{2(\mathcal{A}\mathcal{C} + k_0^2\chi_{MS}^{yx}\chi_{MS}^{xy})} + \frac{jk_0\chi_{ES}^{xy}(\mathcal{E} - \mathcal{D})}{2(\mathcal{D}\,\mathcal{E} + k_0^2\chi_{ES}^{yx}\chi_{ES}^{xy})} \tag{1.40}$$

$$T_{TE}^{TM}(\theta) = \frac{jk_0\chi_{MS}^{yx}(\mathcal{B} + \mathcal{A})}{2(\mathcal{A}\mathcal{C} + k_0^2\chi_{MS}^{yx}\chi_{MS}^{xy})} - \frac{jk_0\chi_{ES}^{xy}(\mathcal{E} + \mathcal{F})}{2(\mathcal{D}\,\mathcal{E} + k_0^2\chi_{ES}^{yx}\chi_{ES}^{xy})} \tag{1.41}$$

where

$$\mathcal{M} = 2 - \tfrac{jk_0}{\cos\theta}\chi_{ES}^{MS} - \tfrac{jk_0}{\cos\theta}\chi_{ES}^{zz}\sin^2\theta \quad ; \quad \mathcal{F} = 2 - jk_0\chi_{ES}^{xx}\cos\theta \ , \tag{1.42}$$

and $\mathcal{A}$, $\mathcal{B}$, $\mathcal{C}$, $\mathcal{D}$, $\mathcal{N}$, $\mathcal{E}$ are given in eqs. (1.32)-(1.34). From these expressions, we see that due to the anisotropic terms in the GSTC mode conversion will occur in that an incident TM mode will generate a TE mode. If the cross-coupling terms ($\chi_{MS}^{xz,zx}$ and $\pi_{MS}^{xz,zx}$) are zero, then $R_{TM}^{TE} = 0$ and $T_{TM}^{TE} = 0$; and R_{TM} and T_{TM} reduce to the pure TM reflected and transmitted field.

1.5.2 Metascreens

As seen from the GSTCs in (1.7) and (1.8), the magnetic surface parameters for a metascreen may have cross-polarization (or off-diagonal) terms π_{MS}^{xz}, π_{MS}^{zx}, χ_{MS}^{xz}, and χ_{MS}^{zx}. As for a metafilm, these terms can result in coupling between TE and TM fields. Initially, we will assume for simplicity that the apertures are sufficiently symmetric that these off-diagonal terms are zero. We will also assume that regions A and B are both free space, and that the screen possesses mirror symmetry about the reference plane $y = 0$. These assumptions correspond to many metascreens that are encountered in practice; the more general case will be treated below. Symmetry of the apertures results in:

$$\pi_{MS}^{xz} = \pi_{MS}^{zx} = \chi_{MS}^{xz} = \chi_{MS}^{zx} \equiv 0 \ , \tag{1.43}$$

and the symmetry with respect to either side of the metascreen results in

$$\begin{aligned} \pi_{ES}^{Ayy} = \pi_{ES}^{Byy} \equiv 2\pi_{ES}^{yy} \quad &; \quad \chi_{ES}^{Ayy} = \chi_{ES}^{Byy} \equiv \tfrac{1}{2}\chi_{ES}^{yy} \\ \pi_{MS}^{Axx} = \pi_{MS}^{Bxx} \equiv \quad 2\pi_{MS}^{xx} \quad &; \quad \chi_{MS}^{Axx} = \chi_{MS}^{Bxx} \equiv \tfrac{1}{2}\chi_{MS}^{xx} \\ \pi_{MS}^{Azz} = \pi_{MS}^{Bzz} \equiv \quad 2\pi_{MS}^{zz} \quad &; \quad \chi_{MS}^{Azz} = \chi_{MS}^{Bzz} \equiv \tfrac{1}{2}\chi_{MS}^{zz} \end{aligned} \quad . \tag{1.44}$$

Under these conditions, the GSTCs become:

$$\begin{aligned} \mathbf{a}_y \times \left[\mathbf{E}^{\mathrm{A}}(\mathbf{r}_o) - \mathbf{E}^{\mathrm{B}}(\mathbf{r}_o)\right] \quad = \quad & -j\omega\mu_0 \left[\mathbf{a}_x \chi_{MS}^{xx} H_{x,\mathrm{av}}(\mathbf{r}_o) + \mathbf{a}_z \chi_{MS}^{zz} H_{z,\mathrm{av}}(\mathbf{r}_o)\right] \\ & -\chi_{ES}^{yy} \mathbf{a}_y \times \nabla_t E_{y,\mathrm{av}}(\mathbf{r}_o) \end{aligned} \quad , \tag{1.45}$$

and

$$\begin{aligned} \mathbf{a}_y \times \mathbf{E}_{\mathrm{av}}(\mathbf{r}_o) \quad = \quad & -j\omega\mu_0 \left\{\mathbf{a}_x \pi_{MS}^{xx} \left[H_x^A(\mathbf{r}_o) - H_x^B(\mathbf{r}_o)\right] + \mathbf{a}_z \pi_{MS}^{zz} \left[H_z^A(\mathbf{r}_o) - H_z^B(\mathbf{r}_o)\right]\right\} \\ & -\pi_{ES}^{yy} \mathbf{a}_y \times \nabla_t \left[E_y^A(\mathbf{r}_o) - E_y^B(\mathbf{r}_o)\right] \end{aligned} \quad . \tag{1.46}$$

where

$$H_{x,\mathrm{av}}(\mathbf{r}_o) = \frac{1}{2}\left[H_x^A(\mathbf{r}_o) + H_x^B(\mathbf{r}_o)\right] \quad \text{and} \quad \mathbf{E}_{\mathrm{av}}(\mathbf{r}_o) = \frac{1}{2}\left[\mathbf{E}^A(\mathbf{r}_o) + \mathbf{E}^B(\mathbf{r}_o)\right] \tag{1.47}$$

represent the average of the fields on the two sides of the reference plane at $y = 0$.

1.5.2.1 TE Polarization for a Metascreen Let a metascreen be located in the plane $y = 0$ in free space. If we assume a TE polarized plane wave is incident onto the metastructure shown in Fig. 1.10, then the reflected and transmitted E and H fields are given in eqs. (1.15), (1.16) and (1.18). Substituting the fields into the GSTCs given in eqs. (1.45) and (1.46), we obtain the reflection and transmission coefficients for a TE incident field [38]:

$$R_{TE}(\theta) = \frac{1 + k_0^2\, \chi_{MS}^{xx}\, \pi_{MS}^{xx}\, \cos^2\theta}{k_0^2 \chi_{MS}^{xx}\, \pi_{MS}^{xx}\, \cos^2\theta - j\frac{k_0}{2}\left(\chi_{MS}^{xx} + 4\pi_{MS}^{xx}\right)\cos\theta - 1} \tag{1.48}$$

and

$$T_{TE}(\theta) = \frac{\frac{i\, k_0 \cos\theta}{2}\left[\chi_{MS}^{xx} - 4\pi_{MS}^{xx}\right]}{k_0^2 \chi_{MS}^{xx}\, \pi_{MS}^{xx}\, \cos^2\theta - j\frac{k_0}{2}\left(\chi_{MS}^{xx} + 4\pi_{MS}^{xx}\right)\cos\theta - 1} \tag{1.49}$$

Note that for this polarization only two surface parameters (χ_{MS}^{xx} and π_{MS}^{xx}) are needed to determine $R_{TE}(\theta)$ and $T_{TE}(\theta)$. This is in contrast to a metafilm, where three different surface parameters are needed to determine these coefficients [27], [33]-[35].

1.5.2.2 TM Polarization for a Metascreen Assume that a TM polarized H-field plane wave is incident onto the metastructure shown in Fig. 1.11, such that the E and H-field components of the incident, reflected, and transmitted plane waves are given by eqs. (1.21) and 1.22). Substituting the field into the GSTCs (1.45) and (1.46), the reflection and transmission coefficients for a TM incident field are found to be [38]:

$$R_{TM}(\theta) = \frac{-1 - \frac{k_0^2}{\cos^2\theta}\,\mathcal{A}\,\mathcal{B}}{1 - \frac{k_0^2}{\cos^2\theta}\mathcal{A}\mathcal{B} + \frac{j\, k_0}{2\cos\theta}\left(\mathcal{A} + 4\,\mathcal{B}\right)} \quad , \tag{1.50}$$

and

$$T_{TM}(\theta) = -\frac{\frac{jk_0}{\cos\theta}\left[\mathcal{A} - 4\mathcal{B}\right]}{1 - \frac{k_0^2}{\cos^2\theta}\mathcal{A}\mathcal{B} + \frac{j\, k_0}{2\cos\theta}\left(\mathcal{A} + 4\,\mathcal{B}\right)} \quad , \tag{1.51}$$

where

$$\begin{aligned} \mathcal{A} &= \chi_{MS}^{zz} + \chi_{ES}^{yy}\, \sin^2\theta \\ \mathcal{B} &= \pi_{MS}^{zz} + \pi_{ES}^{yy}\, \sin^2\theta \end{aligned} \quad . \tag{1.52}$$

Note that for this polarization four surface parameters (χ_{MS}^{zz}, π_{MS}^{zz}, χ_{ES}^{yy}, and π_{ES}^{yy}) are needed to determine $R_{TM}(\theta)$ and $T_{TM}(\theta)$. This is in contrast to a metafilm, where only three different surface parameters are needed to determine these quantities [27], [33]-[35].

1.5.2.3 Cross-Polarized Terms As for the metafilm, cross-polarization terms in the GSTCs result in coupling between TE and TM fields (i.e., TE polarized fields will generate TM fields, and vice-versa). Here we will assume the apertures are symmetric with respect to the plane $y = 0$ and that the material properties in region A and region B are the same. These two assumptions correspond to most metascreens encountered in practice and result in

$$\begin{aligned}
\pi_{MS}^{Axz} = \pi_{MS}^{Bxz} = \pi_{MS}^{xz} \quad &\text{and} \quad \pi_{MS}^{Azx} = \pi_{MS}^{Bzx} = \pi_{MS}^{zx} \\
\chi_{MS}^{Axz} = \chi_{MS}^{Bxz} = \chi_{MS}^{xz} \quad &\text{and} \quad \chi_{MS}^{Azx} = \chi_{MS}^{Bzx} = \chi_{MS}^{zx} \\
\pi_{ES}^{Ayy} = \pi_{ES}^{Byy} = \pi_{ES}^{yy} \quad &\text{and} \quad \chi_{ES}^{Ayy} = \chi_{ES}^{Byy} = \chi_{ES}^{yy} \\
\pi_{MS}^{Axx} = \pi_{MS}^{Bxx} = \pi_{MS}^{xx} \quad &\text{and} \quad \chi_{MS}^{Axx} = \chi_{MS}^{Bxx} = \chi_{MS}^{xx} \\
\pi_{MS}^{Azz} = \pi_{MS}^{Bzz} = \pi_{MS}^{zz} \quad &\text{and} \quad \chi_{MS}^{Azz} = \chi_{MS}^{Bzz} = \chi_{MS}^{zz}
\end{aligned} \quad . \tag{1.53}$$

Under these conditions, the GSTCs reduce to a simpler form:

$$\begin{aligned}
\mathbf{a}_y \times \left[\mathbf{E}^{\mathrm{A}}(\mathbf{r}_o) - \mathbf{E}^{\mathrm{B}}(\mathbf{r}_0)\right] \;=\; & -\mathbf{a}_x\, j\omega\mu_0 \left\{\chi_{MS}^{xx}\left[H_x^A(\mathbf{r}_o) + H_x^B(\mathbf{r}_o)\right] + \chi_{MS}^{xz}\left[H_z^A(\mathbf{r}_o) + H_z^B(\mathbf{r}_o)\right]\right\} \\
& -\mathbf{a}_z\, j\omega\mu_0 \left\{\chi_{MS}^{zz}\left[H_z^A(\mathbf{r}_o) + H_z^B(\mathbf{r}_o)\right] + \chi_{MS}^{zx}\left[H_x^A(\mathbf{r}_o) + H_x^B(\mathbf{r}_o)\right]\right\} \\
& -\mathbf{a}_y \times\; \chi_{ES}^{yy}\left[\nabla_t E_y^A(\mathbf{r}_o) + \nabla_t E_y^B(\mathbf{r}_o)\right]
\end{aligned} \quad , \tag{1.54}$$

and

$$\begin{aligned}
\mathbf{a}_y \times \left[\mathbf{E}^{\mathrm{A}}(\mathbf{r}_o) + \mathbf{E}^{\mathrm{B}}(\mathbf{r}_0)\right] \;=\; & -\mathbf{a}_x\, j\omega\mu_0 \left\{\pi_{MS}^{xx}\left[H_x^A(\mathbf{r}_o) - H_x^B(\mathbf{r}_o)\right] + \pi_{MS}^{xz}\left[H_z^A(\mathbf{r}_o) - H_z^B(\mathbf{r}_o)\right]\right\} \\
& -\mathbf{a}_z\, j\omega\mu_0 \left\{\pi_{MS}^{zz}\left[H_z^A(\mathbf{r}_o) - H_z^B(\mathbf{r}_o)\right] + \pi_{MS}^{zx}\left[H_x^A(\mathbf{r}_o) - H_x^B(\mathbf{r}_o)\right]\right\} \\
& -\mathbf{a}_y \times\; \pi_{ES}^{yy}\left[\nabla_t E_y^A(\mathbf{r}_o) - \nabla_t E_y^B(\mathbf{r}_o)\right]
\end{aligned} \quad . \tag{1.55}$$

Using the incident, reflected, and transmitted fields as defined in eqs. (1.25) and (1.26) in the GSTCs (1.54) and (1.55), the reflection and transmission coefficients (as defined in Fig. 1.12) for a TE incident plane wave are obtained [39]:

$$R_{TE}(\theta) = 1 - \frac{A}{X\left(A + \frac{V}{4X}\right)} - \frac{B}{Y\left(B + \frac{4W}{Y}\right)} \quad , \tag{1.56}$$

$$\begin{aligned}
T_{TE}(\theta) \;=\; & -\frac{\frac{1}{4}\frac{V}{X}}{X\left(\mathcal{A} + \frac{V}{4X}\right)} + \frac{4\frac{W}{Y}}{Y\left(\mathcal{B} + \frac{4W}{Y}\right)} \\
& + \frac{j2k_0\pi_{MS}^{xx}\cos\theta}{Y} - \frac{j\frac{k_0}{2}\chi_{MS}^{xx}\cos\theta}{X}
\end{aligned} \quad , \tag{1.57}$$

$$R_{TE}^{TM}(\theta) = -\frac{j\frac{k_0}{2}\chi_{MS}^{zx}\cos\theta}{X\left(\mathcal{A} + \frac{V}{4X}\right)} - \frac{j2k_0\pi_{MS}^{zx}\cos\theta}{Y\left(\mathcal{B} + \frac{4W}{Y}\right)} \quad , \tag{1.58}$$

and

$$T_{TE}^{TM}(\theta) = \frac{j\frac{k_0}{2}\chi_{MS}^{zx}\cos\theta}{X\left(\mathcal{A} + \frac{V}{4X}\right)} - \frac{j2k_0\pi_{MS}^{zx}\cos\theta}{Y\left(\mathcal{B} + \frac{4W}{Y}\right)} \quad , \tag{1.59}$$

where

$$\mathcal{A} = \cos\theta + j\frac{k_o}{2}\chi_{MS}^{zz} + j\frac{k_o}{2}\chi_{ES}^{yy}\sin^2\theta \quad , \tag{1.60}$$

and

$$\mathcal{B} = \cos\theta + j2\,k_0\pi_{MS}^{zz} + j2\,k_0\pi_{ES}^{yy}\sin^2\theta \quad , \tag{1.61}$$

$$X = 1 + j\frac{k_0}{2}\chi_{MS}^{xx}\cos\theta \quad , \quad Y = 1 + j2k_0\pi_{MS}^{xx}\cos\theta \quad , \tag{1.62}$$

$$V = k_0^2\chi_{MS}^{xz}\chi_{MS}^{zx}\cos\theta \quad , \quad W = k_0^2\pi_{MS}^{xz}\pi_{MS}^{zx}\cos\theta \quad . \tag{1.63}$$

From these expressions, we see that due to the anisotropic terms in the GSTCs ($\chi_{MS}^{xz,zx}$ and $\pi_{MS}^{xz,zx}$), polarization conversion will occur, so that an incident TE wave will generate a TM wave. If the anisotropic terms

are zero (i.e., $\chi_{MS}^{xz,zx}=0$, $\pi_{MS}^{xz,zx}=0$), then $R_{TE}^{TM}=0$ and $T_{TE}^{TM}=0$; and R_{TE} and T_{TE} reduce to those given above [38]. In this case, we are left with pure TE reflected and transmitted fields as defined above.

Using the incident, reflected, and transmitted fields as defined in eqs. (1.35)-(1.37) in the same GSTCs as for the incident TE case, the reflection and transmission coefficients (as defined in Fig. 1.13) for a TM incident plane wave are found to be [39]:

$$R_{TM}(\theta)=1-\frac{\cos\theta}{\mathcal{A}+\frac{V}{4X}}-\frac{\cos\theta}{\mathcal{B}+\frac{4W}{Y}}\ , \tag{1.64}$$

$$T_{TM}(\theta)=\frac{\cos\theta}{\mathcal{A}+\frac{V}{4X}}-\frac{\cos\theta}{\mathcal{B}+\frac{4W}{Y}}\,, \tag{1.65}$$

$$R_{TM}^{TE}(\theta)=-\frac{j\frac{k_o}{2}\chi_{MS}^{xz}\cos\theta}{X\left[\mathcal{A}+\frac{V}{4X}\right]}-\frac{jk_o\pi_{MS}^{xz}\cos\theta}{Y\left[\mathcal{B}+\frac{4W}{Y}\right]}\ , \tag{1.66}$$

and

$$T_{TM}^{TE}(\theta)=\frac{j\frac{k_o}{2}\chi_{MS}^{xz}\cos\theta}{X\left[\mathcal{A}+\frac{V}{4X}\right]}-\frac{jk_o\pi_{MS}^{xz}\cos\theta}{Y\left[\mathcal{B}+\frac{4W}{Y}\right]}\ . \tag{1.67}$$

We see that due to the anisotropic terms in the GSTCs, polarization conversion will occur, and an incident TM wave will generate a TE wave. If the anisotropic terms are zero (i.e., $\chi_{MS}^{xz,zx}=0$, $\pi_{MS}^{xz,zx}=0$), then $R_{TM}^{TE}=0$ and $T_{TM}^{TE}=0$; and R_{TM} and T_{TM} reduce to those given above [38], and we are left with pure TM reflected and transmitted fields as defined above.

1.5.3 Metagratings

The GSTCs for the metagrating can be separated into two different sets of expressions that apply to either a TE or a TM incident plane wave. For the TE polarized case, the GSTCs reduce to [32]:

$$\left[E_z^A(\mathbf{r}_o)-E_z^B(\mathbf{r}_o)\right] \;=\; -j\,\omega\mu_0\,\left[\mu_0\mu_A\chi_{MS}^{Axx}\,H_x^A(\mathbf{r}_o)+\mu_0\mu_B\chi_{MS}^{Bxx}\,H_x^B(\mathbf{r}_o)\right] \tag{1.68}$$

$$\left[E_z^{A1}(\mathbf{r}_o)+E_z^{B1}(\mathbf{r}_o)\right] \;=\; -j\omega\,\left[\mu_A\pi_{MS}^{Axx}\,H_x^A(\mathbf{r}_o)-\mu_B\pi_{MS}^{Bxx}\,H_x^B(\mathbf{r}_o)\right]\ , \tag{1.69}$$

while for the TM polarized case, they reduce to [32]:

$$\begin{aligned}\left[E_x^A(\mathbf{r}_o)-E_x^B(\mathbf{r}_o)\right] \;=\;& +j\,\omega\,\chi_{MS}^{zz}\,H_{z,av}(\mathbf{r}_o)\\ &+\chi_{ES}^{yx}\tfrac{\partial}{\partial x}E_{x,av}(\mathbf{r}_o)\\ &+\tfrac{\partial}{\partial x}\left[\chi_{ES}^{Ayy}E_y^A(\mathbf{r}_o)+\chi_{ES}^{Byy}E_y^B(\mathbf{r}_o)\right]\end{aligned} \tag{1.70}$$

$$\begin{aligned}\left[H_{zA}^1(\mathbf{r}_o)-H_{zB}^1(\mathbf{r}_o)\right] \;=\;& j\omega\epsilon_0\,\chi_{ES}^{xx}\,E_{x,av}(\mathbf{r}_o)\\ &+j\omega\epsilon_0\,\left[\chi_{ES}^{Axy}\,E_y^A(\mathbf{r}_o)+\chi_{ES}^{Bxy}\,E_y^B(\mathbf{r}_o)\right]\ .\end{aligned} \tag{1.71}$$

The forms of these reduced conditions are such that no polarization conversion will occur so long as the incident wave is either TE or TM to the z-direction.

1.5.3.1 TE Polarization for a Metagrating Let a metagrating be located in the plane $y=0$ in free space. If we assume a TE polarized plane wave is incident onto the metagrating shown in Fig. 1.10, then reflected and transmission E and H field are given in eqs. (1.15), (1.16) and (1.18). Substituting the fields into the GSTCs (1.68) and (1.69) gives the reflection and transmission coefficients for a TE incident field:

$$R_{TE}=\frac{2-jk_0\left(\chi_{MS}^{Axx}-\chi_{MS}^{Bxx}+\pi_{MS}^{Axx}-\pi_{MS}^{Bxx}\right)\cos\theta+k_0^2\left(\chi_{MS}^{Bxx}\pi_{MS}^{Axx}+\chi_{MS}^{Axx}\pi_{MS}^{Bxx}\right)\cos^2\theta}{-2-jk_0\left(\chi_{MS}^{Axx}+\chi_{MS}^{Bxx}+\pi_{MS}^{Axx}+\pi_{MS}^{Bxx}\right)\cos\theta+k_0^2\left(\chi_{MS}^{Bxx}\pi_{MS}^{Axx}+\chi_{MS}^{Axx}\pi_{MS}^{Bxx}\right)\cos^2\theta} \tag{1.72}$$

and

$$T_{TE} = \frac{j2k_0\left(\chi_{MS}^{Axx} - \pi_{MS}^{Axx}\right)\cos\theta}{-2 - jk_0\left(\chi_{MS}^{Axx} + \chi_{MS}^{Bxx} + \pi_{MS}^{Axx} + \pi_{MS}^{Bxx}\right)\cos\theta + k_0^2\left(\chi_{MS}^{Bxx}\pi_{MS}^{Axx} + \chi_{MS}^{Axx}\pi_{MS}^{Bxx}\right)\cos^2\theta} \tag{1.73}$$

For a symmetric wire grating

$$\begin{aligned}\chi_{MS}^{Axx} &= \chi_{MS}^{Bxx} = \chi_{MS}^{xx}\\ \pi_{MS}^{Axx} &= \pi_{MS}^{Bxx} = \pi_{MS}^{xx}\end{aligned} \tag{1.74}$$

and in that case the reflection and transmission coefficients reduce to

$$R_{TE} = \frac{1 + k_0^2\chi_{MS}^{xx}\pi_{MS}^{xx}\cos^2\theta}{-1 - jk_0\left(\chi_{MS}^{xx} + \chi_{MS}^{xx}\right)\cos\theta + k_0^2\chi_{MS}^{xx}\pi_{MS}^{xx}\cos^2\theta} \tag{1.75}$$

$$T_{TE} = \frac{jk_0\left(\chi_{MS}^{xx} - \pi_{MS}^{xx}\right)\cos\theta}{-1 - jk_0\left(\chi_{MS}^{xx} + \chi_{MS}^{xx}\right)\cos\theta + k_0^2\chi_{MS}^{xx}\pi_{MS}^{xx}\cos^2\theta} \tag{1.76}$$

These have same the functional form as those given by Wainstein for an uncoated wire grating [106, eq. (2.30)].

1.5.3.2 TM Polarization for a Metagrating To simplify the formulas in the TM case, we will assume that no coupling terms are present:

$$\chi_{ES}^{Axy} = \chi_{ES}^{Bxy} = \chi_{ES}^{yx} \equiv 0 \ . \tag{1.77}$$

The more general case can be derived (following a similar procedure) if desired. Assume that a TM polarized plane wave is incident onto the metascreen shown in Fig. 1.11, such that the E and H-field components of the incident, reflected, and transmitted plane waves are given by eqs. (1.22) and (1.21). Substituting the field into the GSTCs (1.70) and (1.71), the reflection coefficient for a TM incident field is found to be:

$$R_{TM} = -\frac{N_R}{\left(-2j + k_0\ \chi_{ES}^{xx}\cos\theta\right)\left(-2j\cos\theta + k_0\left[\chi_{MS}^{Bzz} - \left(\chi_{ES}^{Ayy} + \chi_{ES}^{Byy}\right)\sin^2\theta\right]\right)} \tag{1.78}$$

where

$$N_R = k_0\left[-2j\chi_{ES}^{xx}\cos^2\theta + k_0\,\chi_{SE}^{xx}\left(\chi_{ES}^{Ayy} - \chi_{ES}^{Byy}\right)\cos\theta\,\sin^2\theta + 2j\left(\chi_{MS}^{Bzz} - \left(\chi_{ES}^{Ayy} + \chi_{ES}^{Byy}\right)\sin^2\theta\right)\right] \ . \tag{1.79}$$

The transmission coefficient for a TM incident field is given by:

$$T_{TM} = \frac{\cos\theta\left(4 + k_0^2\chi_{MS}^{Bzz}\chi_{ES}^{xx} - 2k_0^2\chi_{ES}^{xx}\chi_{ES}^{Ayy}\sin^2\theta\right)}{\left(-2j + k_0\ \chi_{ES}^{xx}\cos\theta\right)\left(-2j\cos\theta + k_0\left[\chi_{MS}^{Bzz} - \left(\chi_{ES}^{Ayy} + \chi_{ES}^{Byy}\right)\sin^2\theta\right]\right)} \ . \tag{1.80}$$

For the case of a symmetric metagrating,

$$\begin{aligned}\chi_{SE}^{Ayy} &= \chi_{SE}^{Byy} = \chi_{SE}^{yy}\\ \chi_{SE}^{Axy} &= \chi_{SE}^{Bxy} = \chi_{SE}^{yx} \equiv 0\end{aligned} \tag{1.81}$$

and the reflection and transmission coefficients reduce to

$$R_{TM} = \frac{-2jk_0\left(\chi_{MS}^{zz} - 2\chi_{ES}^{yy}\sin^2\theta - \chi_{ES}^{xx}\cos^2\theta\right)}{\left(-2j + k_0\chi_{ES}^{xx}\cos\theta\right)\left(-2j\cos\theta + k0\left(\chi_{MS}^{zz} - 2\chi_{ES}^{yy}\sin^2\theta^2\right)\right)} \tag{1.82}$$

and

$$T_{TM} = \frac{\cos\theta\left(4 + k_0^2\chi_{MS}^{zz}\chi_{ES}^{xx} - 2k_0^2\chi_{SE}^{xx}\chi_{ES}^{yy}\sin^2\theta\right)}{\left(-2j + k_0\chi_{ES}^{xx}\cos\theta\right)\left(-2j\cos\theta + k0\left(\chi_{MS}^{zz} - 2\chi_{SE}^{yy}\sin^2\theta^2\right)\right)} \tag{1.83}$$

These have the same functional form as Wainstein's for an uncoated wire grating [106, eq. (2.31)].

1.6 Determining the Surface Parameters

The surface parameters that appear explicitly in the various boundary conditions for different types of metasurfaces are uniquely defined, and are their best quantitative characterization when their microscopic scale is small compared to a wavelength. At times, these surface parameters can be difficult to determine. For specific geometries, there are various approximate expressions to be found throughout the literature that are based on dipole interactions. However, these approximate expressions are limited in their range of application. The electric and magnetic susceptibilities for an array of spherical particles are given in [33] and [35]. The surface susceptibilities for an array of square patches are given in [37] and [107], and the surface susceptibility of an array circular wires is given in [32]. The electric and magnetic surface porosities for arrays of circular apertures or square apertures are given in [108] and [109]. The magnetic surface porosity for an array of wires is given in [32].

The surface susceptibilities and porosities can also be determined by solving the static field problems defined in [30]-[32], giving a framework for calculating the surface parameters for metafilms, metascreens, and metagratings. As shown in these references, the solution of these static field problems can be computationally challenging for arbitrarily shaped structures.

Alternatively to using approximate expressions or solving the static field problems, we can derive expressions that allow for the surface parameters to be retrieved from measured or simulated values of R and T. This method is analogous to the modified Nicolson-Ross-Weir (NRW) approach used for retrieving the effective permeability and permittivity of a metamaterial [97]-[103], which has been extended to the retrieval of the surface parameters for metafilms and metascreens [33], [34], and [38]. In this section, the GSTCs for the various metasurfaces presented above will be used here to develop retrieval techniques for the surface parameters of metafilms, metascreens, and metagratings.

1.6.1 Retrieval Expressions for Metafilms

Once the reflection and transmission coefficients are obtained (either from measurements or from numerical calculations), the surface susceptibilities can be determined. For the case of scatterers that have diagonal surface susceptibility dyadics, two different sets of R and T data are required (one at normal incidence and one at oblique incidence) for each polarization. For the TE polarized wave, the three unknown surface susceptibilities are determined from eqs. (1.56) and (1.57) to give:

$$\chi_{MS}^{xx} = \frac{2j}{k_0}\frac{R_{TE}(0) - T_{TE}(0) + 1}{R_{TE}(0) - T_{TE}(0) - 1}, \quad \chi_{ES}^{zz} = \frac{2j}{k_0}\frac{R_{TE}(0) + T_{TE}(0) - 1}{R_{TE}(0) + T_{TE}(0) + 1}, \tag{1.84}$$

and

$$\chi_{MS}^{yy} = -\frac{\chi_{ES}^{yy}}{\sin^2(\theta)} + \frac{2j\cos(\theta)}{k_0\sin^2(\theta)}\frac{R_{TE}(\theta) + T_{TE}(\theta) - 1}{R_{TE}(\theta) + T_{TE}(\theta) + 1} \ . \tag{1.85}$$

In these expressions, $R_{TE}(0)$ and $T_{TE}(0)$ are the reflection and transmission coefficients at normal incidence ($\theta = 0^\circ$), while $R_{TE}(\theta)$ and $T_{TE}(\theta)$ are the reflection and transmission coefficients at some oblique incidence angle, sufficiently different from $\theta = 0$. If experimental data is used, two angles other than $\theta = 0$ may be required because measuring the reflection coefficients at $\theta = 0$ can be difficult; this leads to a different set of equations than those presented above.

For the TM polarized wave, the three unknown surface susceptibilities are determined from eqs. (1.64) and (1.65) to give [33], [34]:

$$\chi_{ES}^{xx} = \frac{2j}{k_0}\frac{R_{TM}(0) + T_{TM}(0) - 1}{R_{TM}(0) + T_{TM}(0) + 1}, \quad \chi_{MS}^{zz} = \frac{2j}{k_0}\frac{R_{TM}(0) - T_{TM}(0) + 1}{R_{TM}(0) - T_{TM}(0) - 1}, \tag{1.86}$$

and

$$\chi_{ES}^{yy} = -\frac{\chi_{MS}^{yy}}{\sin^2(\theta)} + \frac{2j\cos(\theta)}{k_0\sin^2(\theta)}\frac{T_{TM}(\theta) - 1 - R_{TM}(\theta)}{T_{TM}(\theta) + 1 - R_{TM}(\theta)} \tag{1.87}$$

Similar to the TE case, $R_{TM}(0)$ and $T_{TM}(0)$ are the reflection and transmission coefficients at normal incidence, while $R_{TM}(\theta)$ and $T_{TM}(\theta)$ are the reflection and transmission coefficients at some oblique incidence angle, sufficiently different from $\theta = 0$.

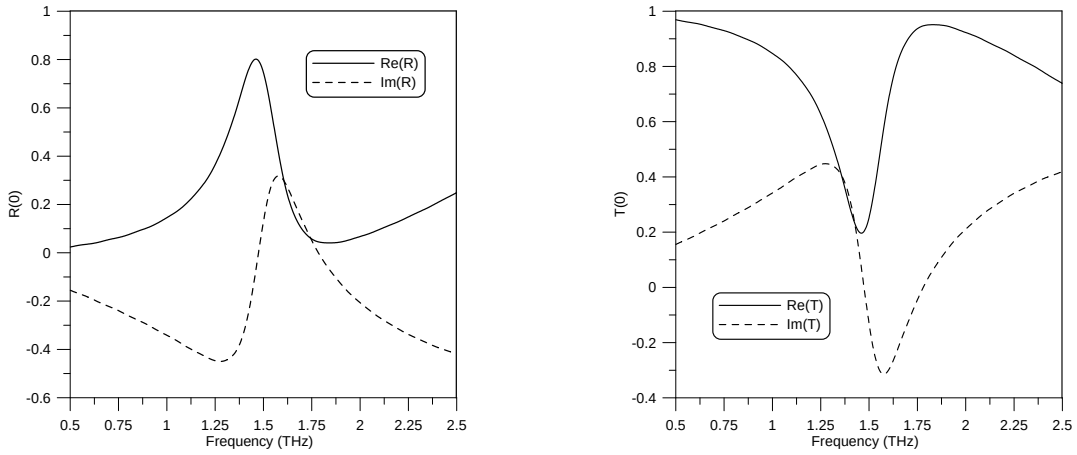

(a) $R_{TM}(0)$ (b) $T_{TM}(0)$

Figure 1.14 Numerically computed $R_{TM}(0)$ and $T_{TM}(0)$ (referred to $y = 0$) for the array of metallic scatterers shown in Fig. 1.8(d).

In the retrieval approaches for both polarizations, it is important to realize that the reference plane for $R_{TE,TM}(0)$, $T_{TE,TM}(0)$, $R_{TM}(\theta)$ and $T_{TM}(\theta)$ is required to be located at $y = 0$. This is a consequence of how the GSTCs were derived in [29] and [30]. The GSTCs (and the surface parameters) would need to be modified for different choices of reference plane location [106], [110], and [111]. In order to illustrate the validity of these expressions for retrieving the surface susceptibilities of a metafilm, we will next consider some examples.

We first use the retrieval method to determine the surface susceptibilities of a metafilm composed of the metallic scatterers shown in Fig. 1.8(d). The TM mode reflection ($R_{TM}(0)$) and transmission coefficients ($T_{TM}(0)$) at an incidence angle of zero degrees for this structure were obtained from a commercial finite-element EM field solver. These numerical results are shown in Fig. 1.14, for the E-field polarized along the x-axis and the reference plane of $R_{TM}(0)$ and $T_{TM}(0)$ located at $y = 0$. These values are used in eq. (1.86) to obtain χ_{ES}^{xx}, a plot of which was shown in Fig. 1.8c.

In the next example, we consider a metafilm composed of a square array of spherical particles, as shown in Fig. 1.1(b). For this metafilm, $a = 10$ mm, $p = 25.59$ mm, $\epsilon_r = 2$, $\mu_r = 900$, $\tan\delta = 0.04$. The TE reflection and transmission coefficients at incidence angles of 0° and 30° for this structure were obtained from a commercial finite-element EM field solver, and are shown in Fig. 1.15. These values were then used in eqs. (1.84) and (1.85) to obtain χ_{ES}^{xx} and χ_{ES}^{yy}, which are shown in Figs. 1.8a and 1.8b. In [35] and [33] it is shown that if the scatterers are spaced sufficiently far from each other, the components of the electric and magnetic surface susceptibility dyadics can be determined by means of "sparse-array" approximation formulas. These approximate analytical values are also plotted in Figs. 1.8a and 1.8b. From this comparison, we see that the surface susceptibilities obtained from the retrieval approach are virtually identical to those obtained from the approximate analytical expressions.

1.6.2 Retrieval Expressions for Metascreens

For a metascreen, we see from (1.48) and (1.49) that only two surface parameters (χ_{MS}^{xx} and π_{MS}^{xx}) determine $R_{TE}(\theta)$ and $T_{TE}(\theta)$. Using these two expressions, the two unknown surface parameters are determined from

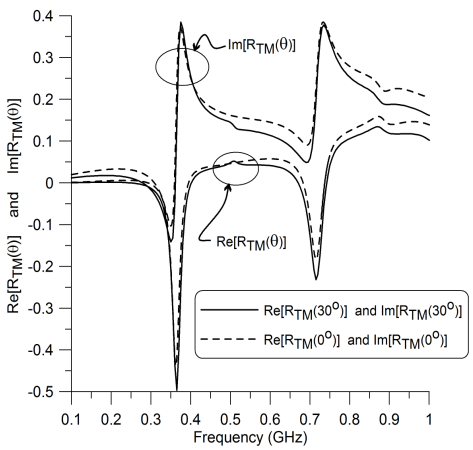

(a) $R_{TM}(0)$ and $R_{TM}(30°)$

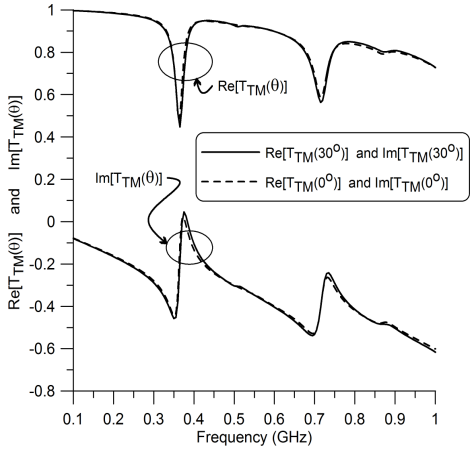

(b) $T_{TM}(0)$ and $T_{TM}(30°)$

Figure 1.15 Numerically computed $R_{TM}(0)$ and $T_{TM}(0)$ (referred to $y = 0$) for the array of spherical particles shown in Fig. 1.1(b).

[38]:

$$\pi_{MS}^{xx} = \frac{j}{2k_0}\frac{R_{TE}(0) + T_{TE}(0) + 1}{R_{TE}(0) + T_{TE}(0) - 1} \quad , \tag{1.88}$$

and

$$\chi_{MS}^{xx} = \frac{2j}{k_0}\frac{R_{TE}(0) - T_{TE}(0) + 1}{R_{TE}(0) - T_{TE}(0) - 1} \tag{1.89}$$

where $R_{TE}(0)$ and $T_{TE}(0)$ are the reflection and transmission coefficients at normal incidence ($\theta = 0°$). Any angle for $R_{TE}(\theta)$ and $T_{TE}(\theta)$ in (1.88) and (1.89) could have been used, but $\theta = 0°$ is a convenient choice. If $R_{TE}(0)$ and $T_{TE}(0)$ are known, either from experimental measurements or from a numerical simulation of the metascreen, then (1.88) and (1.89) can be used to retrieve the values of χ_{MSS}^{xx} and π_{MS}^{xx}.

From (**??**) and (**??**) we see that $R(\theta)$ and $T(\theta)$ depend on four of the surface parameters. Thus, unlike the TE polarization case, two sets of $R_{TM}(\theta)$ and $T_{TM}(\theta)$ data are required to determine all four unknowns for the TM polarized wave [38]:

$$\pi_{MS}^{zz} = \frac{j}{2k_0}\frac{R_{TM}(0) + T_{TM}(0) + 1}{R_{TM}(0) + T_{TM}(0) - 1} \tag{1.90}$$

$$\chi_{MS}^{zz} = \frac{2j}{k_0}\frac{R_{TM}(0) - T_{TM}(0) + 1}{R_{TM}(0) - T_{TM}(0) - 1} \tag{1.91}$$

$$\pi_{ES}^{yy} = -\frac{\pi_{MS}^{zz}}{\sin^2\theta} + \frac{j\cos\theta}{2k_0\sin^2\theta}\frac{R_{TM}(\theta) + T_{TM}(\theta) + 1}{R_{TM}(\theta) + T_{TM}(\theta) - 1} \quad , \tag{1.92}$$

and

$$\chi_{ES}^{yy} = -\frac{\chi_{MS}^{zz}}{\sin^2\theta} + \frac{2j\cos\theta}{k_0\sin^2\theta}\frac{R_{TM}(\theta) - T_{TM}(\theta) + 1}{R_{TM}(\theta) - T_{TM}(\theta) - 1} \tag{1.93}$$

where $R_{TM}(0)$ and $T_{TM}(0)$ are the reflection and transmission coefficients at normal incidence ($\theta = 0°$), while $R_{TM}(\theta)$ and $T_{TM}(\theta)$ are the reflection and transmission coefficients at some oblique incidence angle, sufficiently different from $\theta = 0°$. With $R_{TM}(0)$, $T_{TM}(0)$, $R_{TM}(\theta)$ and $T_{TM}(\theta)$ available from either simulation or experiment, (1.90)-(1.93) can be used to retrieve the four unknown surface parameters (χ_{MS}^{zz}, π_{MS}^{zz}, χ_{ES}^{yy}, and π_{ES}^{yy}).

Here we consider two examples for retrieving the surface parameters of a metascreen. We first consider an array of circular apertures in a perfectly conductor of thickness h as shown in Fig. 1.16(a). For this metascreen, $p = 100$ mm, the thickness $h = 10$ mm, and a is the radius of the apertures (which will be

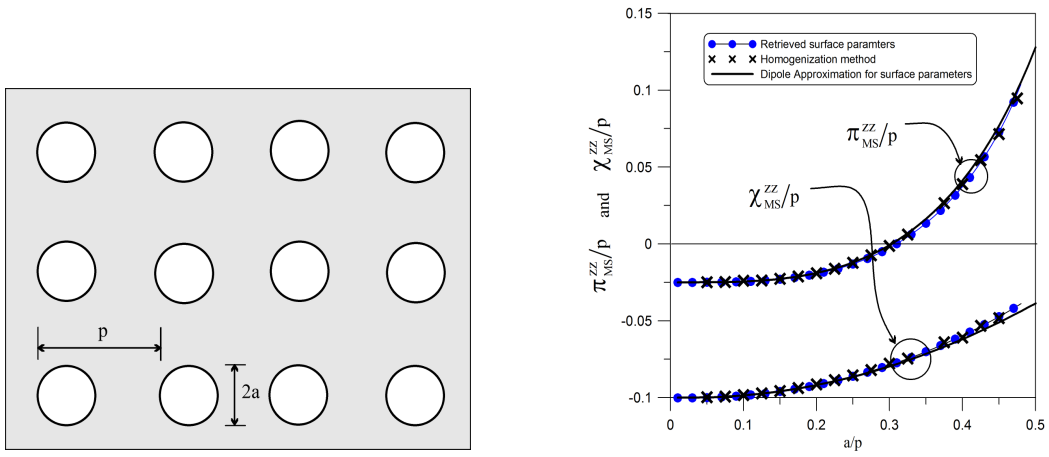

(a) (b)

Figure 1.16 Metascreen: (a) circular apertures and (b) magnetic surface susceptibility and surface porosity for an array of circular apertures: $p = 100$ mm and $h = 10$ mm.

varied). The reflection and transmission coefficients for the metascreen were determined numerically from the finite-element software HFSS (mentioning this product does not imply an endorsement, but serves to clarify the numerical program used) for both $\theta = 0°$ and $\theta = 30°$ at a frequency of 500 MHz and a/p ranging from 0 to 0.5. The numerical values for $R_{TM}(0)$, $T_{TM}(0)$, $R_{TM}(\theta)$ and $T_{TM}(\theta)$ at the reference plane $y = 0$, and were used in (1.90) and (1.91) to determine the two magnetic surface parameters (χ^{zz}_{MS} and π^{zz}_{MS}). Fig. 1.16(b) show the retrieved magnetic surface parameters for a range of a. Using dipole-interaction approximations, closed-form results for these surface porosities and susceptibilities have been obtained in [108] for an array of circular apertures. These approximations are also shown in Fig. 1.16(b). The surface susceptibilities and porosities can also be determined by solving the static field problem as defined in [31]. These homogenization-based surface parameters are also shown in Fig. 1.16b. From the comparison, we see that the retrieved surface magnetic susceptibility and surface magnetic porosity correlate very well with the other two approaches for the whole range of $a/p = 0$ to $a/p = 0.49$.

Next, we consider an array of square apertures in a perfectly conducting plate as shown in Fig. 1.17(a). For this array, $p = 100$ mm, the thickness is $h = 10$ mm, and l is the length of the side of the square (which will be varied). The numerical values for $R_{TM}(0)$, $T_{TM}(0)$, $R_{TM}(\theta)$ and $T_{TM}(\theta)$ at the reference plane $y = 0$, and were used in (1.90)-(1.93) to determine the two magnetic surface parameters (χ^{zz}_{MS} and π^{zz}_{MS}). Fig. 1.17(b) shows the retrieved magnetic surface parameters for a range of l. In this figure, we also show the dipole-approximation from [108] and results from the homogenization model [31]. From the comparison, we see that the retrieved surface magnetic susceptibility and surface magnetic porosity correlate very well with the other two approaches for the whole range of l/p, except that the dipole approximation for π^{zz}_{MS} becomes somewhat inaccurate for $l/p > 0.5$. Retrieved results for other apertures are found in [38].

1.6.3 Retrieval Expressions for Metagratings

As was the case for a TE incident wave onto a metascreen, we see from (1.75) and (1.76) that only two surface parameters (χ^{xx}_{SM} and π^{xx}_{MS}) determine $R_{TE}(\theta)$ and $T_{TE}(\theta)$ for a metagrating. Using these two expressions, the two unknown surface parameters are determined from:

$$\pi^{xx}_{MS} = \frac{j}{k_0}\frac{R_{TE}(0) + T_{TE}(0) + 1}{R_{TE}(0) + T_{TE}(0) - 1} \quad , \tag{1.94}$$

and

$$\chi^{xx}_{MS} = \frac{j}{k_0}\frac{R_{TE}(0) - T_{TE}(0) + 1}{R_{TE}(0) - T_{TE}(0) - 1} \quad . \tag{1.95}$$

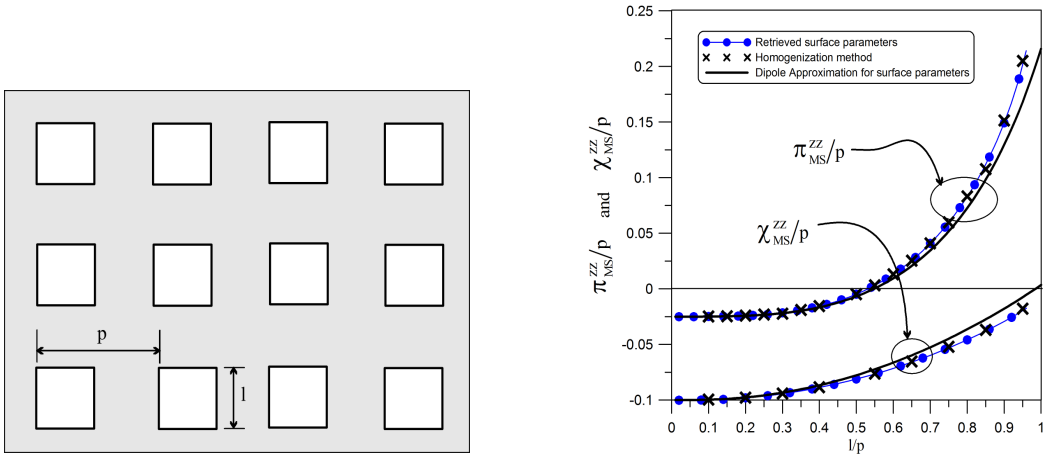

(a) (b)

Figure 1.17 Metascreen: (a) square apertures and (b) magnetic surface susceptibility and surface porosity for an array of circular apertures: $p = 100$ mm and $h = 10$ mm.

From (1.82) and (1.83) we see that $R_{TM}(\theta)$ and $T_{TM}(\theta)$ for the symmetric case depend on three surface parameters. Thus, unlike the TE polarization case, two sets of $R_{TM}(\theta)$ and $T_{TM}(\theta)$ data are required to determine all three unknowns for the TM polarized wave:

$$\chi^{zz}_{MS} = \frac{2j}{k_0}\frac{R_{TM}(0) - T_{TM}(0) + 1}{R_{TM}(0) - T_{TM}(0) - 1} \tag{1.96}$$

$$\chi^{xx}_{ES} = \frac{2j}{k_0}\frac{R_{TM}(0) + T_{TM}(0) - 1}{R_{TM}(0) + T_{TM}(0) + 1}\ , \tag{1.97}$$

and

$$\chi^{yy}_{ES} = \frac{\chi^{zz}_{MS}}{2\sin^2\theta} + \frac{j\cos\theta}{k_0\sin^2\theta}\frac{R_{TM}(\theta) + \frac{jk_0}{2}\chi^{xx}_{ES}\left[1 + R_{TM}(\theta)\right]\cos\theta}{1 - R_{TM}(\theta) - \frac{jk_0}{2}\chi^{xx}_{ES}R_{TM}(\theta)\cos\theta}\ . \tag{1.98}$$

As an example, we consider the uncoated circular wire grating shown in Fig. 1.18(a). This metagrating has only three non-zero surface parameters (χ^{xx}_{MS}, χ^{xx}_{ES}, and π^{xx}_{MS}) [32]. The retrieved surface parameters are shown in Fig. 1.18(b) for a range of wire radius a, together with Wainstein's analytical results [106] and results from homogenization [32] for comparison.

1.7 Some Applications of GSTCs

However they are obtained, we have seen how the surface susceptibilities and porosities together with the GSTCs allow the plane-wave reflection and transmission coefficients to be computed. In this section we will discuss the use of GSTCs to the modeling of metasurfaces in a number of other applications.

1.7.1 Guided-waves on a Single Metasurface

As is the case for an ordinary dielectric slab, a metasurface may also support surface waves under suitable conditions. However, unlike a conventional dielectric slab, forward and backward surface waves as well as complex modes may be excited simultaneously on the metasurface; this is a direct consequence of engineering the properties of the constituent scatterers or apertures. In fact, the scatterers that compose a metafilm can be judiciously chosen such that surface waves and/or complex modes will be present only at certain desired frequencies. Conditions for guided waves can be supported on a metafilm are given in detail in [36]. Here

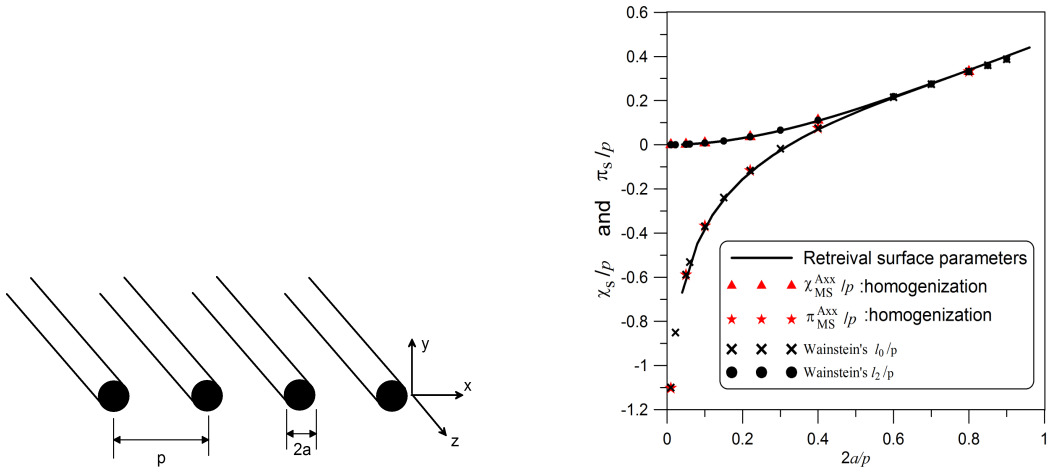

(a) wire grating (b) surface parameters

Figure 1.18 Metagrating: (a) uncoated wire grating and (b) magnetic and electric surface susceptibility and surface porosity for an array of wires of radius a. Also shown in this figure are results from [106]

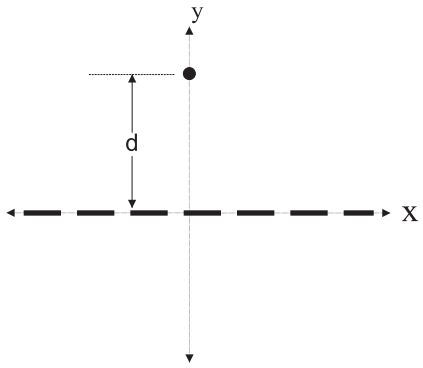

Figure 1.19 Line source above a metafilm. The line source is either an electric or magnetic current source located at $z = d$ and the metafilm is represented by the dashed line at $z = 0$.

we will merely summarize the use of GSTCs in this analysis, which could be extended to other metasurfaces such as metascreens or metagratings if desired.

Consider an electric line source oriented in the z-direction, at a distance d above and parallel to a metafilm of infinite extent in the xy-plane (see Fig. 1.19, and note the change in coordinate system compared to that used in [36]). The scatterers of the metafilm are assumed to be of rather arbitrary shape, but with enough symmetry that (1.13)-(1.14) hold. If the regions above and below the metafilm consist of the same dielectric material, the problem space can be divided into three sections. Region I ($y > d$) extends to infinity in the $+y$-direction, while region III ($y < 0$) extends to infinity in the $-y$-direction. Region II ($0 < y < d$) is the area between the plane of the line source and the metafilm.

Using a spectral-domain approach and applying the GSTCs at $y = 0$ and the appropriate jump conditions at the source location (i.e., $y = d$), the scattered field for $y > 0$ is given by [36]

$$E_s = -\frac{\omega\mu_0}{4\pi}\int_{-\infty}^{\infty}\frac{e^{-j\rho\,(y+d)}e^{-j\nu\,x}}{\rho}RS_{TE}(\nu)\;d\nu \tag{1.99}$$

where

$$RS_{TE}(\nu) = \frac{-j\left[\frac{k_0^2}{2\rho}\chi_{ES}^{zz}+\frac{\nu^2}{2\rho}\chi_{MS}^{yy}-\frac{\rho}{2}\chi_{MS}^{xx}\right]}{1-\chi_{MS}^{xx}\left(\frac{k_0^2}{4}\chi_{ES}^{zz}+\frac{\nu^2}{4}\chi_{MS}^{yy}\right)+j\left[\frac{k_0^2}{2\rho}\chi_{ES}^{zz}+\frac{\nu^2}{2\rho}\chi_{MS}^{yy}+\frac{\rho}{2}\chi_{MS}^{xx}\right]} \tag{1.100}$$

Table 1.1 Conditions for surface waves and guided modes for an electric-line source (as well as expressions for the propagation constant). These results are valid for pure real surface susceptibilities. Note that the total number of guided waves increases by one if $\mathrm{Re}(\chi_{MS}^{xx}) < 0$.

Constraints on χ_{ES} and χ_{MS}		Number of guided waves	*Even*-class poles	Type of guided wave
$\chi_{MS}^{yy} > 0$	$\chi_{ES}^{zz} \geq \frac{1}{k^2 \chi_{MS}^{yy}} - \chi_{MS}^{yy}$	2	$\rho_{E_{1,2}} = \frac{-j \pm \sqrt{k^2 \left(\chi_{ES}^{zz} + \chi_{MS}^{yy}\right) \chi_{MS}^{yy} - 1}}{\chi_{MS}^{yy}}$	complex mode
	$-\chi_{MS}^{yy} < \chi_{ES}^{zz} \leq \frac{1}{k^2 \chi_{MS}^{yy}} - \chi_{MS}^{yy}$	2	$\rho_{E_{1,2}} = -j \left[\frac{1 \pm \sqrt{1 - k^2 \left(\chi_{ES}^{zz} + \chi_{MS}^{yy}\right) \chi_{MS}^{yy}}}{\chi_{MS}^{yy}} \right]$	surface wave
	$\chi_{ES}^{zz} \leq -\chi_{MS}^{yy}$	1	$\rho_{E_1} = -j \left[\frac{1 + \sqrt{1 - k^2 \left(\chi_{ES}^{zz} + \chi_{MS}^{yy}\right) \chi_{MS}^{yy}}}{\chi_{MS}^{yy}} \right]$	surface wave
	$\chi_{ES}^{zz} = 0$	2	$\rho_{E_{1,2}} = -j \left[\frac{1 \pm \sqrt{1 - k^2 \left(\chi_{MS}^{yy}\right)^2}}{\chi_{MS}^{yy}} \right]$	surface wave
$\chi_{MS}^{yy} < 0$	$\chi_{ES}^{zz} > -\chi_{MS}^{yy}$	1	$\rho_{E_1} = -j \left[\frac{1 - \sqrt{1 - k^2 \left(\chi_{ES}^{zz} + \chi_{MS}^{yy}\right) \chi_{MS}^{yy}}}{\chi_{MS}^{yy}} \right]$	surface wave
$\chi_{MS}^{yy} = 0$	$\chi_{ES}^{zz} > 0$	1	$\rho_{E_1} = \frac{-jk^2}{2} \chi_{ES}^{zz}$	surface wave

and ρ and ν are associated with an incidence angle θ by

$$\rho = k_0 \cos\theta \quad , \quad \nu = k_0 \sin\theta \tag{1.101}$$

The poles of the reflection coefficient RS_{TE} are functions of the surface susceptibilities of the metafilm. Once these poles are determined, the propagation constant of a surface wave along the metafilm (i.e., along the x-axis) for this guided-wave pole is given by:

$$\nu = \sqrt{k^2 - \rho_s^2} \tag{1.102}$$

where ρ_s is given in Table 1.1 under various conditions for an electric line source; values for a magnetic line source are given in Table 1.2 [36]. When the surface susceptibilities of the metasurface meet certain of these conditions, surface waves or complex modes can be excited.

As an example, consider a metafilm composed of spherical particles that have a radius of $a = 10$ mm and are placed in an array with a period of $p = 25.67$ mm (see Fig. 1.1(b)). The material properties of these particles were chosen to be $\epsilon_r = 100$, $\mu_r = 1$, and $\tan\delta = 1 \times 10^{-4}$—representative of some commercially available ceramics at microwave frequencies. Values for $\chi_{MS}^{yy,xx}$, $\chi_{ES}^{yy,xx}$, χ_{ES}^{zz} χ_{MS}^{zz} as functions of frequency for this array are given in [36]. The symmetry of the spherical particles means that $\chi_{ES}^{zz} = \chi_{ES}^{xx}$ and $\chi_{MS}^{zz} = \chi_{MS}^{xx}$. Fig. 1.20 shows the magnitudes of the electric fields for an electric line-source excitation for this array at two different frequencies (1.5 GHz and 2.0 GHz), as computed by a commercial finite-element program, with the line source placed 45.59 mm above the metafilm. This figure shows the presence of one surface wave and a pair of complex modes at the lower frequency [Fig 1.20(a)], while Fig 1.20(b)] illustrates what happens at the higher frequency when two surface waves are present.

Fig. 1.21 shows the magnitude of the E-field for a magnetic line source place above the same array. Fig. 1.21(a) illustrates the presence of one surface wave, while Fig. 1.21(b) illustrates the existence of a complex mode. By varying the properties of the scatterers, the surface susceptibilities will change, and hence, from the results in Tables 1.1 and 1.2, it is possible to have a surface wave and/or complex mode exist at any desired frequency, i.e., to realize a frequency-agile guided-wave structure.

Table 1.2 Conditions for surface waves and guided modes for an magnetic-line source (as well as expressions for the propagation constant). These results are valid for pure real surface susceptibilities. Note that the total number of guided waves increases by one if $\mathrm{Re}(\chi_{ES}^{xx}) < 0$.

Constraints on χ_{ES} and χ_{MS}		Number of guided waves	*Even*-class poles	Type of guided wave
$\chi_{ES}^{yy} > 0$	$\chi_{MS}^{zz} \geq \frac{1}{k^2 \chi_{ES}^{yy}} - \chi_{ES}^{yy}$	2	$\rho_{E_{1,2}} = \frac{-j \pm \sqrt{k^2 \left(\chi_{MS}^{zz} + \chi_{ES}^{yy}\right) \chi_{ES}^{yy} - 1}}{\chi_{ES}^{yy}}$	complex mode
	$-\chi_{ES}^{yy} < \chi_{MS}^{zz} \leq \frac{1}{k^2 \chi_{ES}^{yy}} - \chi_{ES}^{yy}$	2	$\rho_{E_{1,2}} = -j \left[\frac{1 \pm \sqrt{1 - k^2 \left(\chi_{MS}^{zz} + \chi_{ES}^{yy}\right) \chi_{ES}^{yy}}}{\chi_{ES}^{yy}} \right]$	surface wave
	$\chi_{MS}^{zz} \leq -\chi_{ES}^{yy}$	1	$\rho_{E_1} = -j \left[\frac{1 + \sqrt{1 - k^2 \left(\chi_{MS}^{zz} + \chi_{ES}^{yy}\right) \chi_{ES}^{yy}}}{\chi_{ES}^{yy}} \right]$	surface wave
	$\chi_{MS}^{zz} = 0$	2	$\rho_{E_{1,2}} = -j \left[\frac{1 \pm \sqrt{1 - k^2 \left(\chi_{ES}^{yy}\right)^2}}{\chi_{ES}^{yy}} \right]$	surface wave
$\chi_{ES}^{yy} < 0$	$\chi_{MS}^{zz} > -\chi_{ES}^{yy}$	1	$\rho_{E_1} = -j \left[\frac{1 - \sqrt{1 - k^2 \left(\chi_{MS}^{zz} + \chi_{ES}^{yy}\right) \chi_{ES}^{yy}}}{\chi_{ES}^{yy}} \right]$	surface wave
$\chi_{ES}^{yy} = 0$	$\chi_{MS}^{zz} > 0$	1	$\rho_{E_1} = \frac{-jk^2}{2} \chi_{MS}^{zz}$	surface wave

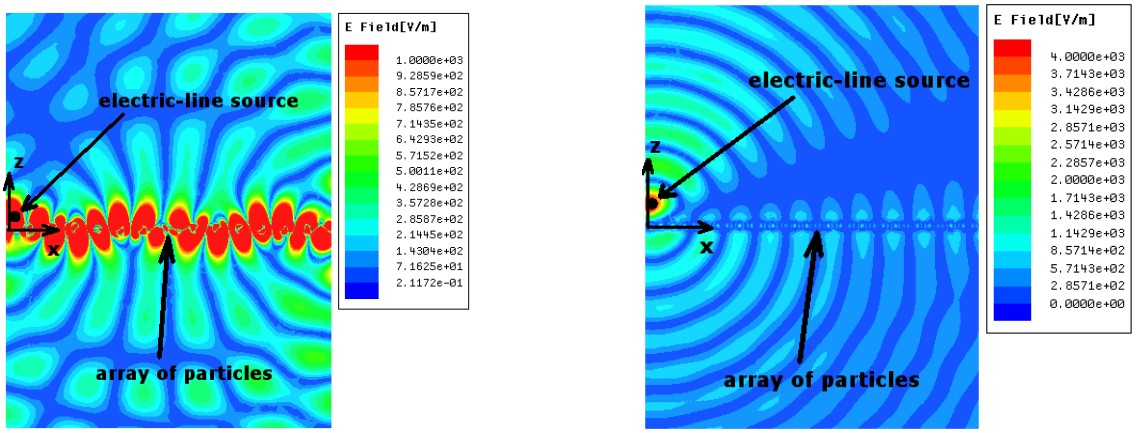

(a) f=1.50 GHz (b) f=2.0 GHz

Figure 1.20 Magnitude of the E-field from a electric-line source placed 45.49 mm above an array of spherical particles: (a) f=1.50 GHz (one surface wave and a complex mode pair) and (b) f=2.0 GHz (two surface waves). For an array of spherical particles consisting of $a = 10$ mm, $p = 25.67$ mm , $\epsilon_r = 100$, $\mu_r = 1$, and $\tan\delta = 1 \times 10^{-4}$

Leaky waves are also possible for this metafilm. The angle at which energy propagates away from the surface for a leaky wave is given by [141].

$$\theta_{LEAKY} = \arcsin\left(\frac{Re[\nu]}{k_0}\right) \tag{1.103}$$

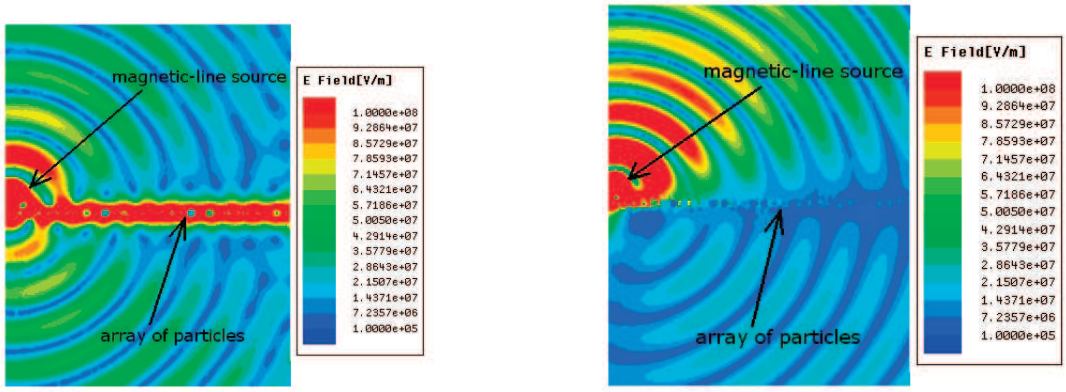

(a) f=1.42 GHz (b) f=1.5 GHz

Figure 1.21 Magnitude of the E-field (on a linear scale) from a magnetic line source placed 45.49 mm above an array of spherical particles: (a) f=1.42 GHz: one surface wave, and (b) f=1.5 GHz: complex mode.

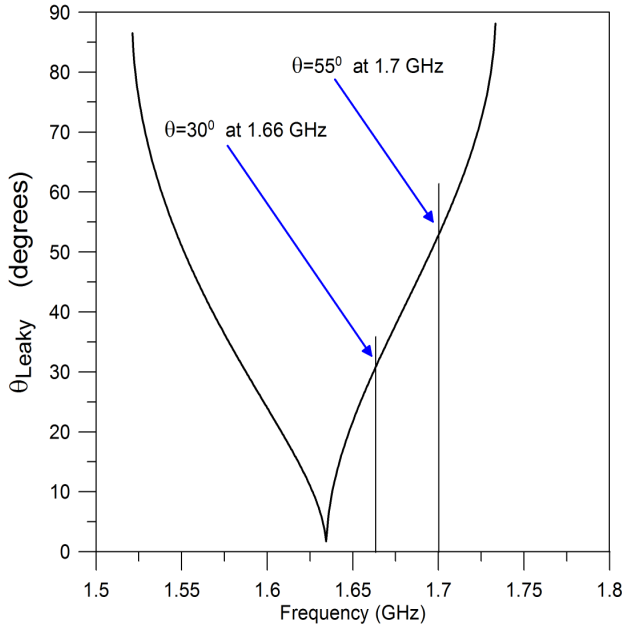

Figure 1.22 Leaky-wave angle versus frequency for an array of spherical particles with $a = 10$ mm, $p = 25.67$ mm , $\epsilon_r = 100$, $\mu_r = 1$, and $\tan\delta = 1 \times 10^{-4}$.

under the restriction that

$$Re[\nu] < k_0 \ . \tag{1.104}$$

Fig. 1.22 shows θ_{LEAKY} as a function of frequency for the same array of spherical particles as that used above. These results were obtained by using (1.103) and the surface parameters for the array given in [36]. To validate these results, Fig. 1.23 shows the magnitudes of the E-field for frequencies of 1.70 GHz, 1.66 GHz and 1.64 GHz. These results were obtained with a commercial finite-element program for the same array as used in Fig. 1.22. These results illustrate that little energy is flowing along the x-axis, while energy is propagating at some angle away from the metasurface as a leaky wave. The angles at which the energy propagates away from the surface correspond to those given in Fig. 1.22.

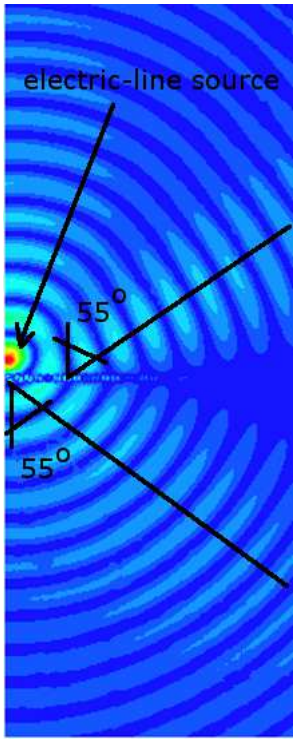

(a) f=1.70 GHz: $\theta_l = 55°$,

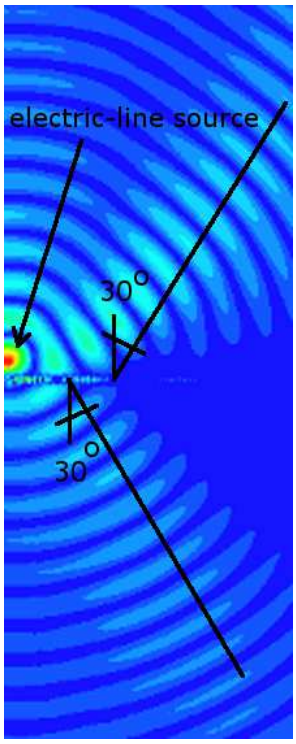

(b) f=1.66 GHz: $\theta_l = 30°$,

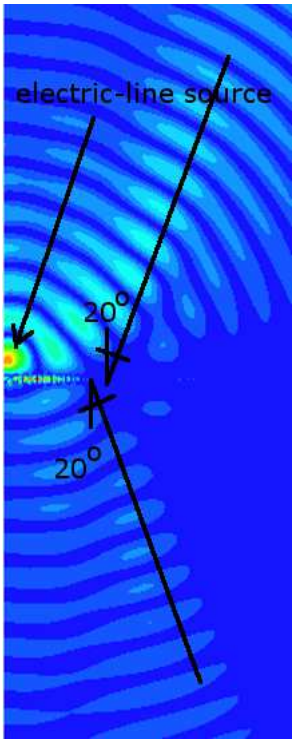

(b) f=1.64 GHz: $\theta_l = 20°$

Figure 1.23 Magnitude of E-field and Poynting's vector for an electric line source along the y-axis placed 45.49 mm above an array of spherical particles: (a) f=1.70 GHz , (b) f=1.66 GHz , and (c) f=1.64 GHz.

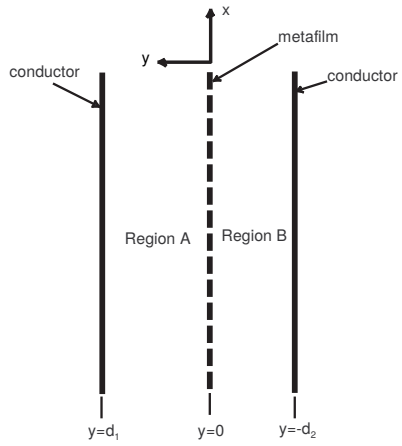

Figure 1.24 Resonator: a metafilm placed between two parallel metal plates.

1.7.2 Resonator Size Reduction

Engheta [142, 143] has demonstrated that the classical lower bound on the size of a resonant structure can be reduced if a cavity is partially filled with a negative-index material. Extending this idea, it was shown in [37, 144] that the same thing could be accomplished with a metasurface. The advantage of a metasurface is that because it requires less physical space than a 3D metamaterial, a cavity or resonator with a metasurface can in principle be made smaller than those that use 3D metamaterials.

Consider the resonator shown in Fig. 1.24. This resonator consists of perfectly conducting metallic walls at $y = d_1$ and $y = -d_2$ with a metafilm placed at $y = 0$. The resonator is divided into two regions (labeled A and B). It will be assumed for simplicity that both regions are filled with the same homogeneous medium. An x-polarized electric field, independent of x and z, is assumed. The electric field in region A is then given by

$$\bar{E}_A = \bar{a}_x \left[E_1\ e^{-j\beta y} + E_2\ e^{j\beta y}\right] \tag{1.105}$$

and in region B by

$$\bar{E}_B = \bar{a}_x \left[E_3\ e^{-j\beta y} + E_4\ e^{j\beta y}\right] \tag{1.106}$$

where $\beta = \omega\sqrt{\mu\epsilon} = 2\pi/\lambda$ is the wavenumber in the resonator medium, $\bar{a}_x$ is a unit vector, and E_1, E_2, E_3, and E_4 are constants to be determined from the boundary conditions. Applying the boundary condition that the total electric field on the two perfect conductors at $y = d_1$ and $y = -d_2$ must be zero, we obtain relationships between E_1 and E_2 from the $y = d_1$ plane boundary condition and between E_4 and E_3 from the $y = -d_2$ plane boundary condition. The GTSCs for the metafilm are then applied at $y = 0$ in order to obtain the phase-matching condition for the resonator [37]. The phase-matching conditions required at resonance for the separation distance $d_1 = d_2 = d$ between two metal plates with a metasurface placed in the center is given by [37]:

$$\begin{aligned} d &= \tfrac{\lambda}{2}\left[1 + n\pi - \tfrac{2}{\pi}\tan^{-1}\left(\tfrac{\pi}{\lambda}\ \chi_{ES}\right)\right] \\ d &= \tfrac{\lambda}{2}\left[2n\pi - \tfrac{2}{\pi}\tan^{-1}\left(\tfrac{\pi}{\lambda}\ \chi_{MS}\right)\right] \end{aligned} \quad \text{for} \quad n = 0, 1, 2, 3, ... \tag{1.107}$$

where $n = 0$ is not allowed if $\chi_{MS} \geq 0$ [37]. From these expressions it is seen that by judiciously choosing the metasurface, it is possible to have a resonator that overcomes the $\lambda/2$ size limit. Various cases for different conditions on the surface parameters are given in [37].

As an example, consider a metafilm composed of thin square perfectly conducting patches placed between two metal plates. The square match metafilm is shown in Fig. 1.25(a). Fig. 1.25(b) shows the resonant frequency (f_r) versus l/p (where p is the period and l is the length of the side of one of the squares) for three different plate separations. For reference, the classical result $d = \lambda/2$ occurs when $l/p = 0$. To verify these theoretical results, this resonator was analyzed with the commercial finite-element (FEM) software code HFSS from Ansoft Corporation (mentioning this product does not imply an endorsement, but serves

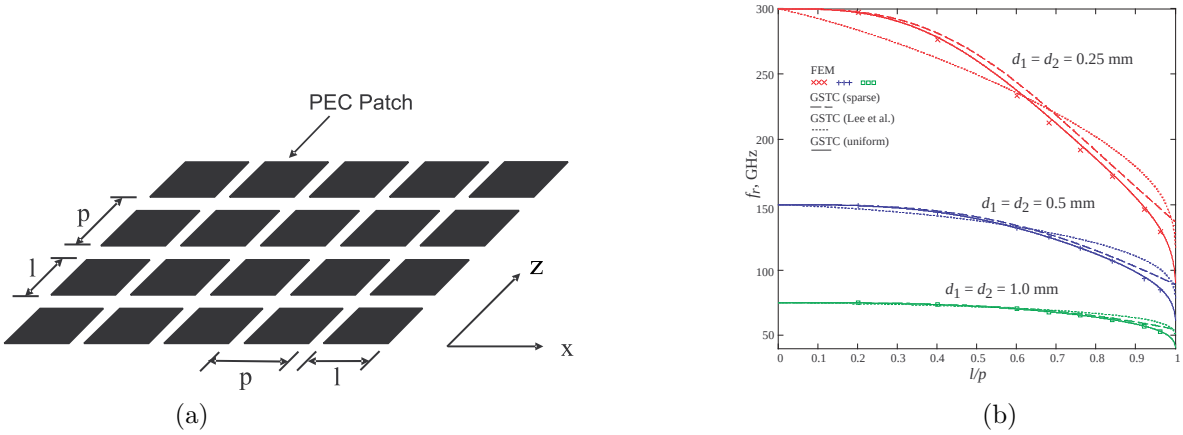

Figure 1.25 Resonant frequency of air-filled parallel-plate resonator loaded with square-patch capacitive metafilm: (a) array of square conducting patches and (b) resonant frequency.

Table 1.3 Resonant frequency reduction as a function of l/p for a parallel-plate resonator with a metafilm consisting of square metal patches with $p = 500$ μm.

Reduction in f_r			
l/p	$d_1 + d_2 = 0.5$ mm	$d_1 + d_2 = 1.0$ mm	$d_1 + d_2 = 2.0$ mm
0	0 %	0 %	0 %
0.4	7.3 %	3.8 %	1.9 %
0.6	20.9 %	11.9 %	6.4 %
0.8	38.4 %	25.2 %	14.9 %
0.96	56.1 %	42.6 %	29.0 %

to clarify the numerical program used). It is seen that the capacitive metasurface can significantly reduce the resonant frequency for a given resonator size d, or equivalently reduce the size of the resonator needed to obtain a desired resonant frequency. The reduction in resonant frequency of the resonator for the simple square-patch metafilm resonator is shown in Table 1.3 for $p = 500$ μm. In this table, the percent reduction (which is also a measure of size reduction possible for a given resonant frequency) is listed for different values of l/p. The results in this table show that a square-patch metafilm placed at the center of a resonator can reduce the size by as much as 56 %. If metasurfaces are designed with scatterers having more elaborate polarizability characteristics (e.g., judiciously chosen resonant behavior) it should in principle be possible to achieve even greater reduction in size. In fact, by controlling the properties of the metasurface, a frequency-agile resonator could be realized.

Losses in the materials making up the metafilm will have a limiting effect on the performance of these resonators. Losses show up in the GSTC formulation as complex values of the effective surface susceptibilities. To investigate losses, we consider a nonmagnetic dielectric cylinder with radius a, height l (oriented along the y-axis) and permittivity ϵ_r relative to the surrounding medium, see Fig 1.26. If $l \ll a$, this is a thin dielectric disk. Analytical formulas for the surface parameters for an array of dielectric cylinder, which can be applied to the lossy case simply by making the cylinder's permittivity complex, are given in [37]. The resonant frequencies obtained by solution of the GSTC-based equation were compared with FEM results.

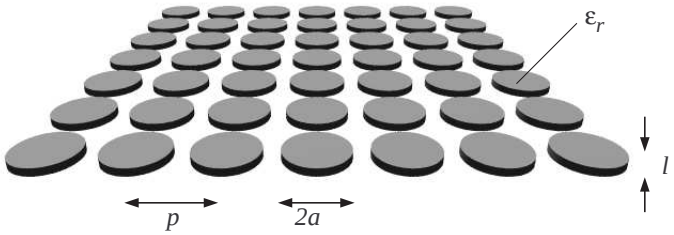

Figure 1.26 A surface array of cylindrical dielectric pucks with relative permittivity ϵ_r, radius a and height l.

The results are summarized in Tables 1.4 and 1.5. Agreement between the GSTC model and the FEM results is good.

For reference, recall that this resonator will have a resonant frequency of $f_r = 10$ GHz with no metafilm present. Is lowest resonant frequency will be $f_r = 2.887$ GHz when completely filled with the dielectric medium used for the pucks, with a quality factor $Q = 25$ given the loss tangent of 0.04. We observe that there is a trade-off between the reduction in resonant frequency (or resonator size) that we can achieve, and the value of Q. This is quite natural from a physical point of view, since as the polarizability of the metafilm scatterers increases, the proportion of field energy located in the lossy region increases.

Table 1.4 Resonant frequency and Q as functions of $l/2a$ for a parallel-plate resonator with a metafilm consisting of cylindrical dielectric pucks with $\epsilon_r = 12$, $\tan\delta = 0.04$, $d_1 = d_2 = 7.5$ mm, $p = 10$ mm and $a = 4.6$ mm.

	GSTC		FEM	
$l/2a$	f_r, GHz	Q	f_r, GHz	Q
0.05	8.756	147	8.626	116
0.1	8.116	120	7.919	93
0.2	7.297	106	7.058	81
0.3	6.718	100	6.533	78

Table 1.5 Resonant frequency and Q as functions of $l/2a$ for a parallel-plate resonator with a metafilm consisting of cylindrical dielectric pucks with $\epsilon_r = 12$, $\tan\delta = 0.04$, $d_1 = d_2 = 7.5$ mm, $p = 10$ mm and $a = 4.0$ mm.

	GSTC		FEM	
$l/2a$	f_r, GHz	Q	f_r, GHz	Q
0.05	9.160	221	9.077	179
0.1	8.707	178	8.593	144
0.2	8.100	155	7.986	129
0.3	7.652	144	7.580	124

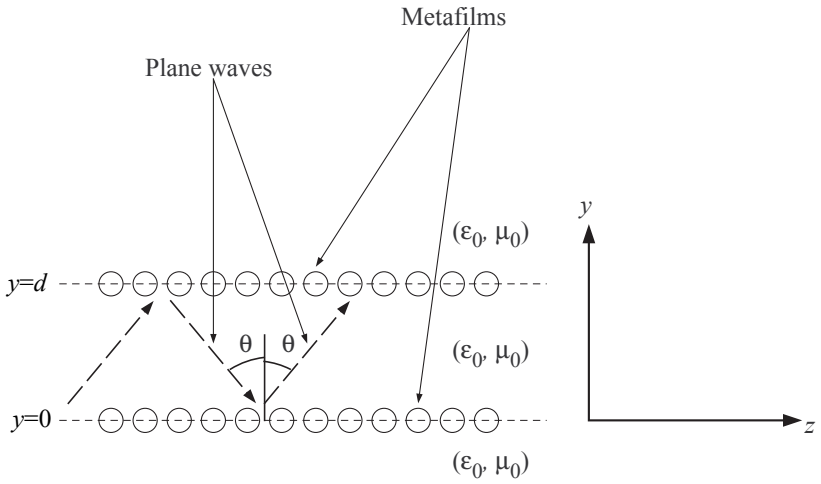

Figure 1.27 An illustration of a waveguide composed of two metafilms separated by a distance d.

1.7.3 Waveguides

Because metasurfaces can be designed to give total reflection of an incident plane wave, it should be possible to trap and guide electromagnetic energy in a region between two metasurfaces [40]. This class of metasurface waveguides is illustrated in Fig. 1.27 (note the change in coordinate system compared to that used in [40]). This waveguide consists of a region of space $0 < y < d$ bounded by two identical parallel metafilms. All regions are assumed to be air, so we may take their material properties to be those of free space.

Assume that we have a a TE mode polarized in the x-direction, propagating in the z-direction, and with a time dependence $e^{j\omega t}$. The field between the metafilms is given by the superposition of two plane waves incident at the angle θ to the $\pm y$-directions, as shown in Fig. 1.2:

$$E_x = \left(E_1 e^{-jk_y y} + E_2 e^{+jk_y y}\right) e^{-j\beta z} \qquad 0 < y < d \ , \tag{1.108}$$

where $\beta = k_0 \sin\theta$ is the unknown propagation constant, which must be determined, $k_y = \sqrt{k_0^2 - \beta^2} = k_0 \cos\theta$, and $k_0 = \omega\sqrt{\mu_0 \epsilon_0}$ is the wave number of free space. Outside this region, the field is written as outgoing (or attenuating) waves:

$$E_x = E_3 e^{-jk_y y} e^{-j\beta z} \qquad y > d \ , \tag{1.109}$$

$$E_x = E_4 e^{+jk_y y} e^{-j\beta z} \qquad y < 0 \ , \tag{1.110}$$

Equations (1.56) and (1.57) show that, in order for total reflection to occur, the normalized propagation constant must obey

$$n_e = \frac{\beta}{k_0} = \sqrt{\frac{\chi_{MS}^{yy}\chi_{ES}^{xx} + \frac{4}{k_0^2}}{-\chi_{MS}^{yy}\chi_{MS}^{xx}}} \tag{1.111}$$

[see also eq. (1.114) below]. This quantity will generally be complex for leaky modes. Once the scatterers that compose the metafilm are chosen to meet the above criterion, and β is determined, the transverse wavenumber in the x direction is given by

$$k_x = \sqrt{k_0^2 - \beta^2} = k_0\sqrt{1 - n_e^2} \tag{1.112}$$

and the separation distance d between the two metasurfaces is given by:

$$d = \frac{\left(n + \frac{1}{2}\right)\pi + 2\tan^{-1}\left(\frac{k_x \chi_{MS}^{yy}}{2}\right)}{k_x} \quad \text{for} \quad n = 1, 2, 3, ... \tag{1.113}$$

It is desirable to find conditions for which the imaginary part of n_e is as small as possible, and we need to ensure that $\mathrm{Im}(n_e) < 0$ and $0 < \mathrm{Re}(n_e) < 1$ (the latter because otherwise the mode will basically be a surface wave localized near the two metasurfaces and will likely suffer increased attenuation as a result). Similar sets of expressions for the TM modes along with an example are given in [40].

This waveguide can be compact, with low material and radiation losses. If the metafilms were constructed of a polymer type of material, it would be possible to have a flexible waveguiding structure. It is also possible to control the surface properties of the scatterers (and in turn the surface parameters), which would result in controllable or smart, frequency-agile waveguiding structures.

1.7.4 Controllable Reflections and Transmissions

Given a generic metasurface, one could use any of a number of commercial computational codes to analyze the interaction of an electromagnetic field with that metasurface. However, as we saw in Section 1.5, the GSTCs allow us to obtain closed-form expressions for the plane-wave reflection and transmission coefficients, the advantage of which is that one can get some physical insight into the relationship of the surface parameters to the reflection and transmission behavior. Expressions given in Section 1.5 illustrate that if the surface parameters (surface susceptibilities and/or porosities) can be changed, it will be possible to control the reflection and transmission behavior of the surface.

1.7.4.1 Metafilm From equations (1.56)-(1.65) one can write down the relationship between the electrical and magnetic surface susceptibilities needed to have either total reflection or total transmission for a metafilm. For total reflection, the following conditions must be satisfied:

$$\begin{aligned} k_0^2\,\chi_{MS}^{xx}\left(\chi_{ES}^{zz}+\chi_{MS}^{yy}\sin^2\theta\right) &= -4 \quad \text{for} \quad \text{TE}\ , \\ k_0^2\,\chi_{ES}^{xx}\left(\chi_{MS}^{zz}+\chi_{ES}^{yy}\sin^2\theta\right) &= -4 \quad \text{for} \quad \text{TM}\ , \end{aligned} \tag{1.114}$$

while for total transmission, the required conditions are

$$\begin{aligned} \chi_{ES}^{zz}+\chi_{MS}^{yy}\sin^2\theta-\chi_{MS}^{xx}\cos^2\theta &= 0 \quad \text{for} \quad \text{TE}\ , \\ -\chi_{MS}^{zz}-\chi_{ES}^{yy}\sin^2\theta+\chi_{ES}^{xx}\cos^2\theta &= 0 \quad \text{for} \quad \text{TM}\ , \end{aligned} \tag{1.115}$$

1.7.4.2 Metascreen Using eqs. (1.48)-(**??**), for a metascreen the following conditions must by satisfied for total reflection

$$\begin{aligned} \chi_{MS}^{xx} &= 4\pi_{MS}^{xx} \quad \text{for} \quad \text{TE}\ , \\ \chi_{MS}^{zz}+\chi_{ES}^{yy}\,\sin^2\theta &= 4\left[\pi_{MS}^{zz}-\pi_{ES}^{yy}\,\sin^2\theta\right] \quad \text{for} \quad \text{TM}\ , \end{aligned} \tag{1.116}$$

while for total transmission, the required conditions are

$$\begin{aligned} k_0^2\ \chi_{MS}^{xx}\pi_{MS}^{xx}\cos^2\theta &= -1 \quad \text{for} \quad \text{TE}\ , \\ \left(\chi_{MS}^{zz}+\chi_{ES}^{yy}\,\sin^2\theta\right)\left(\pi_{MS}^{zz}-\pi_{ES}^{yy}\,\sin^2\theta\right) &= -\tfrac{\cos^2\theta}{k_0^2} \quad \text{for} \quad \text{TM}\ , \end{aligned} \tag{1.117}$$

1.7.4.3 Metagrating Using eqs. (1.75)-(1.83), for a metagrating the following conditions must by satisfied for total reflection

$$\begin{aligned} \chi_{MS}^{xx} &= \pi_{MS}^{xx} \quad \text{for} \quad \text{TE}\ , \\ k_o^2\chi_{MS}^{zz}\chi_{ES}^{xx}-2k_0^2\chi_{ES}^{xx}\chi_{ES}^{yy}\sin^2\theta &= -4 \quad \text{for} \quad \text{TM}\ , \end{aligned} \tag{1.118}$$

while for total transmission, the required conditions are

$$\begin{aligned} k_0^2\ \chi_{MS}^{xx}\pi_{MS}^{xx}\cos^2\theta &= -1 \quad \text{for} \quad \text{TE}\ , \\ \chi_{SM}^{zz}-2\chi_{SE}^{yy}\sin^2\theta-\chi_{SE}^{xx}\cos^2\theta &= 0 \quad \text{TM}\ , \end{aligned} \tag{1.119}$$

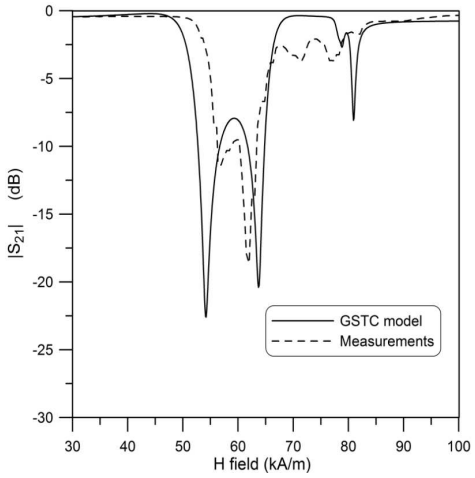

Figure 1.28 Controlling the transmission properties of a surface with an external dc magnetic field., see [41].

In principle, control of the reflection and transmission behavior can be done in a number of ways, e.g., (1) by changing the electrical or magnetic surface parameters or (2) by changing the properties (either the material properties or the geometry) of the substrate on which the metasurfaces lie. For example, a metafilm made up of spherical magnetic particles can be controlled. Such a controllable surface has been realized by using a metafilm of spherical YIG particles and controlling the surface parameters (the magnetic surface susceptibilities) with a DC magnetic bias field [41]. Fig. 1.28 shows the transmission behavior of such a metafilm as a function of the external DC magnetic field.

Other approaches have been used to control the surface behavior of a metasurface, and a significant amount of research is ongoing in the area of dynamically controllable metasurfaces, as we discuss in Sections VII and IX of [27]. For example, the highly resonant nature of metasurfaces provides a means for tuning the frequency response of these structures. Many metasurfaces are constructed from metallic inclusions that have plasma resonances governed largely by the choice of their geometry. Aside from the specific geometry, the resonances of these metallic inclusions may also be controlled by affecting the capacitive and or inductive properties that dictate the plasma resonances. The electric coupled resonator is a structure that provides a means for directly perturbing the capacitive response by altering the electrical properties of the material occupying the electrical gap. One way to accomplish this is to cause different fluids to flow in a channel over the gap; for details see [44]. Such a structure is shown in Fig. 1.29 and other fluid-tunable structures are considered in [44].

1.7.4.4 Angularly Independent Behavior and Anisotropic Metastructures The use of metasurfaces with anisotropic parameters can achieve a number of useful results not possible with isotropic metasurfaces. In particular, if the surface parameters are varied along the surface, interesting properties might be achieved. For example, it is possible to design a metasurface so as to focus an EM plane wave to a desired region in space, much like a focusing antenna array. If the surface parameters of the metasurface were designed in a manner such that they could be changed at will, one could as a result have a metasurface capable of changing the direction and frequency where the energy is focused, i.e., a frequency- and space-agile surface. One can also design a metasurface that converts one type of polarization to another. These concepts are currently under investigation.

Another example deals with how to obtain (at least in some parameter range) angularly independent behavior of the reflection and transmission [45]. Consider a metafilm. For a given incidence angle, eqs. (1.114) gives the relationships between the electric and magnetic surface susceptibilities required to obtain total reflection. This suggests a mechanism by which one could achieve approximate angular independence of such total reflection. For instance, in the TE case when $\chi_{ES}^{zz} \gg \chi_{MS}^{yy}$, the angular dependence becomes less significant, because the first term in the parentheses of the first equation in (1.114) dominates over the second angularly dependent term. Similarly, in the TM case, when $\chi_{MS}^{zz} \gg \chi_{ES}^{yy}$, the angular dependence likewise

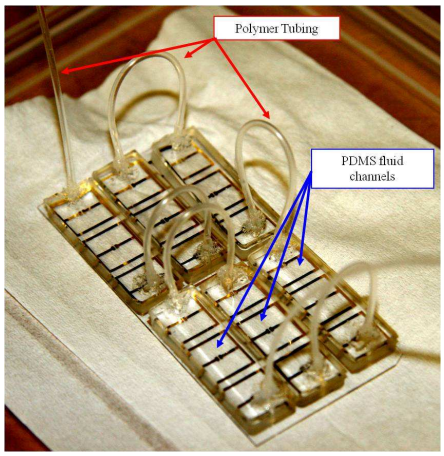

Figure 1.29 A fluid-tunable metafilm composed of a 36 array of metallic resonators fabricated from gold on glass with PDMS (polydomethykiloxane) fluid-channel sections, see [44].

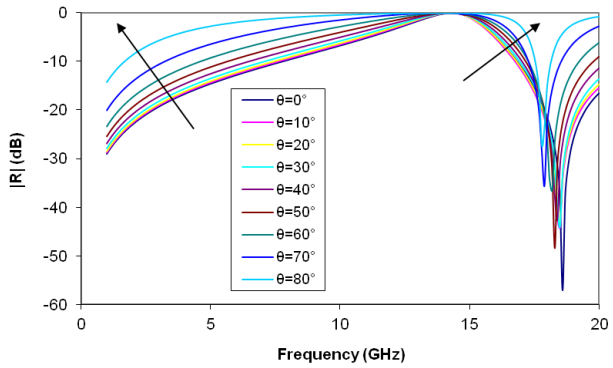

Figure 1.30 The reflection coefficient for a TE-polarized incident plane wave for an electrical resonator metasurface structure., see [45].

becomes weak. These conditions could occur, for example, at certain resonance frequencies of the scatterers that constitute the metafilm. When the indicated terms are dominant, the total reflection conditions become:

$$\begin{aligned} \chi_{MS}^{xx}\chi_{ES}^{yy} &= -\tfrac{4}{k_0^2} \quad \text{for} \quad \text{TE} \\ \chi_{ES}^{xx}\chi_{MS}^{yy} &= -\tfrac{4}{k_0^2} \quad \text{for} \quad \text{TM} \end{aligned} \quad . \tag{1.120}$$

Similar expressions can be derived for other types of metastructures. Thus, if a metasurface is designed such that the transverse components of the surface susceptibilities are highly resonant, as compared to the normal components, then the metasurface may exhibit angle-independent behavior. Fig. 1.30 shows one example of this, where we have plotted the reflection coefficient of a metasurface composed of the metallic structure shown in Fig. 1(b) in [45]. In this figure we see that at about 14 GHz the surface exhibits a nearly angle-independent behavior up to incidence angles as large as 60°.

One can extend this concept to many other types of structures. For example, it can be shown that highly anisotropic slabs of materials can exhibit angle-independent behavior as well. This can be seen by examining the reflection properties of an inhomogeneous anisotropic slab, as discussed in [45, eqns. (31)-(38)].

Additionally, the mathematically constructed perfectly matched layer (PML) [83] that has been introduced into computational electromagnetics for reducing non-physical reflections at radiation boundaries also requires such angle independence. Such PMLs may be physically realizable by use of the concept of metasurfaces. The idea of designing a metasurface structure to use as PML in computational codes is under investigation.

This mechanism offers a unique way to match lossy materials for the purpose of developing compact electromagnetic absorbers and make possible unique designs of impedance-matching surfaces. Compact absorbers based on such ideas have recently begun to appear in the literature [46]-[51]. These structures typically are designed with a metasurface on the front side of a lossy substrate backed by a metal plate. These structures may be narrowband, but are quite compact in size. An additional benefit of using the metasurface is the fact that these structures show substantial angle independence (as discussed above). These structures have been demonstrated both numerically and experimentally [46], [48], [50].

Various groups have also investigated the use of metasurfaces to develop impedance-matching surfaces, a wide-angle impedance-matching surface having been fabricated [52]. This structure has highly anisotropic properties, which as we saw above can enable angularly independent behavior. There is a great deal of attention of using meatsurfaces for tailoring wave fronts and for polarization conversion [74]-[81]. Other applications of metasurfaces include biomedical, microwave-assisted chemistry, and terahertz devices to name a few (see [27] for a list of references). In fact, new applications for metasurfaces are emerging almost daily as researchers understand their potential in all fields of physics and engineering.

1.8 Impedance-Type Boundary Conditions

Some researchers prefer to express the GSTCs in the form of impedance-type boundary conditions [111], [145]-[148]. For plane wave fields, whose variation parallel to a metafilm is of the form:

$$e^{-j\mathbf{k}\cdot\mathbf{r}_t} \quad , \tag{1.121}$$

where

$$\mathbf{k} = k_x\mathbf{a}_x + k_y\mathbf{a}_y \quad \text{and} \quad \mathbf{r}_t = x\mathbf{a}_x + y\mathbf{a}_y, \tag{1.122}$$

we can use Maxwell's equations to write the GSTCs for the metafilm given in eqs. (1.1) and (1.2) as

$$\mathbf{a}_y \times \left[\mathbf{E}^{\mathrm{A}} - \mathbf{E}^{\mathrm{B}}\right]_{y=0} = -\overline{\overline{\boldsymbol{Z}}}_{MS} \cdot \mathbf{H}_{t,av} \ , \tag{1.123}$$

$$\mathbf{a}_y \times \left[\mathbf{H}^{\mathrm{A}} - \mathbf{H}^{\mathrm{B}}\right]_{y=0} = \overline{\overline{\boldsymbol{Y}}}_{ES} \cdot \mathbf{E}_{t,av} \ . \tag{1.124}$$

$$\tag{1.125}$$

Here, the spatially dispersive ($\mathbf{k}$-dependent) surface transfer admittance and transfer impedance dyadics are given by

$$\overline{\overline{\boldsymbol{Y}}}_{ES} = j\omega\overline{\overline{\boldsymbol{\chi}}}_{ES} + \frac{j\overline{\overline{\boldsymbol{\chi}}}_{MS}}{\omega\mu}(\mathbf{a}_z \times \mathbf{k})(\mathbf{a}_z \times \mathbf{k}) \ , \tag{1.126}$$

$$\overline{\overline{\boldsymbol{Z}}}_{MS} = j\omega\overline{\overline{\boldsymbol{\chi}}}_{MS} + \frac{j\overline{\overline{\boldsymbol{\chi}}}_{ES}}{\omega\epsilon}(\mathbf{a}_z \times \mathbf{k})(\mathbf{a}_z \times \mathbf{k}) \ . \tag{1.127}$$

Boundary conditions of this form can also be interpreted as lumped elements in equivalent transmission-line circuits [146]. The GSTCs for metascreens and the metagratings can also be cast in impedance boundary condition forms if desired.

1.9 Isolated Scatterers and One-Dimensional Arrays

Can metastructures also be realized with one-dimensional structures or single isolated scatterers? The two-dimensional metamaterial (i.e., metasurface) concept can be extended even further to the concept of using only a linear array rather than a surface array. Furthermore, one can use only a single sub-wavelength

resonant structure for some desired effect or behavior. In fact, we have already begun to see a few applications of this concept. One in particular is the use of a unit-cell in the design of electrically small antennas. In antenna applications, the unit cell acts like a parasitic element to the radiating element of the antenna and serves as a means to match the electrically small radiating element to both (1) the feeding transmission line and (2) free space. Such designs have been shown to enable efficient electrically-small antennas [112]-[119]. Nanoparticles have also been used for tuning "so-called" optical nanoantennas [120]. An additional example is the use of a one-dimensional unit cell as a tuning structure for planar transmission lines [121]. Another emerging area of application is the use of one-dimensional chains of nanoparticles as waveguides supporting surface waves, of which examples can be found in [122]-[128].

1.10 Summary

The recent development of various engineered materials (3-D metamaterials, 2-D metasurfaces, single arrays and single particles) is bringing us closer to realizing the exciting predictions made over one hundred years ago by the work of Lamb (1904), Schuster (1904), and Pocklington (1905) [129]-[131]. Although early investigators in the fledgling area of metamaterials attributed the first study of such media to Veselago [132] in 1967, the aforementioned authors anticipated some of his work by many decades, and L. I. Mandel'shtam (1945) [133, 134], Malyuzhinets (1951) [135] and Sivukhin (1957) [136] had all previously discussed the properties of wave propagation in backward-wave media. Some other historical (or "pre-historical") surveys have been given in [137]-[140].

In this chapter, we have discussed two-dimensional metamaterials, referred to as metasurfaces. We have defined three major types of metasurfaces: metafilms, metascreens, and metagratings, each having a distinct surface topology. We introduced the GSTCs required to accurately model these three different types of metasurface. From these GSTCs, we derived the reflection and transmission coefficients for each metasurface. These coefficients are expressed in terms of the surface parameters that characterize the metasurface. The coefficients are then used to develop a retrieval approach for determining the uniquely defined effective surface parameters that characterize the each of the metasurfaces from measured or simulated data. We concluded the chapter with a presentation of various other applications of the GSTCs.

The application of metasurfaces at frequencies from microwave to optical and beyond has attracted great interest in recent years [27], [28], [35]-[84]. Metasurfaces allow for controllable smart surfaces, miniaturized cavity resonators, novel waveguiding structures, compact and wide-angle absorbers, impedance matching surfaces, biomedical devices, tailoring wave fronts, polarization conversion, antennas, and high-speed switching devices, to name only a few. While there is still much work to be done in the understanding, analysis, design, and fabrication of these engineered materials, the potential of these materials has forever changed the landscape of RF, microwaves, optics and photonics for the future. It seems that nearly every day, new applications of these metasurfaces emerge as researchers begin to tap into their potential and understand how to design and utilize them.

REFERENCES

1. S. Zouhdi, A. Sihvola and M. Arsalane (eds.), Advances in Electromagnetics of Complex Media and Metamaterials, Boston , Kluwer Academic Pub., 2002.
2. N. Engheta and R.W. Ziolkowski, Electromagnetic Metamaterials: Physics and Engineering Explorations, Hoboken, NJ, John Wiley & Sons, 2006.
3. G.V. Eleftheriades and K.G. Balmain, Negative Refraction Metamaterials: Fundamental Principles and Applications, Hoboken, NJ, John Wiley & Sons, 2005.
4. V.G. Veselago, "The electrodynamics of substances with simultaneously negative values of ϵ and μ" [in Russian], Usp. Fiz. Nauk, 92, 1967, pp. 517-526 [Engl. transl. in Sov. Phys. Uspekhi, 10, 1968, pp. 509-514].
5. D.R. Smith, W.J. Padilla, D.C. Vier, S.C. Nemat-Nasser and S. Schultz, "Composite medium with simultaneously negative permeability and permittivity," *Phys. Rev. Lett.*, 84, 2000, pp. 4184-4186.
6. R. Marques, J. Martel, F. Mesa and F. Medina, "A new 2D isotropic left-handed metamaterial design: theory and experiment," *Micr. Opt. Technol. Lett.*, 35, no. 5, 2002, pp. 405-408.
7. C. L. Holloway, E. F. Kuester, J. Baker-Jarvis and P. Kabos, "A double negative (DNG) composite medium composed of magneto-dielectric spherical particles embedded in a matrix," *IEEE Trans. Ant. Prop.*, 51, no. 10, 2003, pp. 2596-2603.
8. A. Sihvola, "Metamaterials in electromagnetics," *Metamaterials*, 1, no. 1, 2007, pp. 2-11.
9. E. Shamonina and L. Solymar, "Metamaterials: How the subject started," *Metamaterials*, 1, no. 1, 2007, pp. 12-18.
10. M. Lapine and S. Tretyakov, "Contemporary notes on metamaterials," *IET Microw. Antennas Propag.*, 1, no. 1, 2007, pp. 3-11.
11. J.B. Pendry, A.J. Holden, W.J. Stewart, and I. Youngs, "Extremely low frequency plasmons in metallic mesostructure," *Phys. Rev. Lett.*, vol. 76, pp. 4773-4776, 1996.
12. P J.B. Pendry, A.J. Holden, D.J. Robbins, and W.J. Stewart, "Magnetism from conductors and enhanced nonlinear phenomena," *IEEE Trans. Micr. Theory Tech.*, Vol. 47, pp. 2075-2084, 1999.
13. C.A. Kyriazidou, H.F. Contopanagos, W.M. Merrill, and N.G. Alexópoulos, "Artificial versus natural crystals: effective wave impedance of printed photonic bandgap materials," *IEEE Trans. Ant. Prop.*, Vol. 48, pp. 95-105, 2000.
14. C.A. Kyriazidou, R.E. Daiz, and N.G. Alexópoulos, "Novel material with narrow-band transparency window in the bulk," *IEEE Trans. Ant. Prop.*, Vol. 48, pp. 107-116, 2000.

Please enter `\offprintinfo{(Title, Edition)}{(Author)}`
at the beginning of your document.

15. D.R. Smith, D.C. Vier, N. Kroll, and Schultz, "Direct calculation of permeability and permittivity for a left-handed metamaterial," *Appl. Phys. Lett.*, Vol. 77, pp. 2246-2248, 2000.
16. S.G. Johnson and J.D. Joannopoulos, "Three-dimensionally periodic dielectric layered structure with omnidirectional photonic band gap," *Appl. Phys. Lett.*, Vol. 77, pp. 3490-3492, 2000.
17. P. Markos and C.M. Soukoulis, "Numerical studies of left-handed materials and arrays of split ring resonators," *Physical Review E,*. Vol. 65, pp. 036622-1 to 036622-8, 2002.
18. N. Engheta, S.R. Nelatury, and A. Hoorfar, "Omega media as a metamaterial with negative permittivity and permeability," in *Dig. of USNC/URSI Meeting*, p. 47. San Antonio, TX, June 16-21, 2002.
19. J.B. Pendry, A.J. Holden, D.J. Robbins, and W.J. Stewart, "Extremely low frequency plasmons in thin-wire structures," *J. Phys.: Condens. Matter*, vol. 10, pp. 4785-4809, 1998.
20. D.A. Smith and N. Kroll, "Negative refractive index in left-handed materials," *Phys. Rev. Lett.*, vol. 85, pp. 2933-2936, 2000.
21. D.R. Smith, W.J. Padilla, D.C. Vier, S.C. Nemat-Nasser, and S. Schultz, "Composite medium with simultaneously negative permeability and permittivity," *Phys. Rev. Lett.*, vol. 84, pp. 4184-4186, 2000.
22. R. Marques, J. Martel, F. Mesa and F. Medina, "A new 2D isotropic left-handed metamaterial design: theory and experiment," *Micr. Opt. Technol. Lett.*, 35, no. 5, 2002, pp. 405-408.
23. C. L. Holloway, E. F. Kuester, J. Baker-Jarvis and P. Kabos, "A double negative (DNG) composite medium composed of magneto-dielectric spherical particles embedded in a matrix," *IEEE Trans. Ant. Prop.,* 51, no. 10, 2003, pp. 2596-2603.
24. E. F. Kuester, N. Memić, S. Shen, A. D. Scher, S. Kim, K. Kumley, and H. Loui, "A negative refractive index metamaterial based on a cube array of layered nonmagnetic sphereical particles," *Progress In Electromagnetics Research B*, vol. 33, pp. 175202, 2011
25. R.W. Ziolkowski and E. Heyman, "Wave propagation in media having negative permittivity and permeability," *Phys. Rev. E*, vol. 64, art. 056625, 2001.
26. R.A. Shelby, D.R. Smith, S.C. Nemat-Nasser, and S. Schultz, "Microwave transmission through a two-dimensional, isotropic left-handed material," *Appl. Phys. Lett.*, vol. 78, pp. 489-491, 2001.
27. C.L. Holloway, E.F. Kuester, J.A. Gordon, J. O'Hara, J. Booth and D. R. Smith, "An overview of the theory and applications of metasurfaces: The two-dimensional equivalents of metamaterials", *IEEE Antennas and Propagation Magazine*, vol. 54, no. 2, pp. 10-35, April 2012.
28. A.A. Maradudin, ed., *Structured Surfaces as Optical Metamaterials.* Cambridge, UK: Cambridge University Press, 2011.
29. E.F. Kuester, M.A. Mohamed, M. Piket-May and C.L. Holloway, "Averaged transition conditions for electromagnetic fields at a metafilm," *IEEE Trans. Antennas and Propagation*, vol. 51, pp. 2641-2651, 2003.
30. C.L. Holloway and E.F. Kuester, "A homogenization technique for obtaining generalized sheet transition conditions (GSTCs) for a metafilm embedded in a magneto-dielectric interface", *IEEE Trans. on Antenna and Propagation*, vo. 64, no. 11, pp. 4671-4686, 2016.
31. C.L. Holloway and E.F. Kuester, "Generalized Sheet Transition Conditions for a Metascreen–A Fishnet Maresurface", *IEEE Trans. on Antenna and Propagation*, vol. 66, no. 5, pp. 2414-2427, 2017.
32. C.L. Holloway, E.F. Kuester, and A. Dienstfrey, "A homogenization technique for obtaining generalized sheet transition conditions for an arbitrarily shaped coated-wire grating", *Radio Science*, vol. 49, no. 10, 813-850, 2014.
33. C.L. Holloway, A. Dienstfrey, E.F. Kuester, J.F. O'Hara, A.K. Azad and A.J. Taylor, "A discussion on the interpretation and characterization of metafilms-metasurfaces: The two-dimensional equivalent of metamaterials", *Metamaterials*, vol. 3, pp. 100-112, 2009.
34. C.L. Holloway, E.F. Kuester and A. Dienstfrey, "Characterizing metasurfaces/metafilms: The connection between surface susceptibilities and effective material properties", *IEEE Ant. Wireless Prop. Lett.*, vol. 10, pp. 1507-1511, 2011.
35. C.L. Holloway, M.A. Mohamed, and E.F. Kuester, "Reflection and Transmission Properties of a Metafilm: with an Application to a Controllable Surface Composed of Resonant Particles", *IEEE Transactions on Electromagnetic Compatibility,* vol. 47, no. 4, Nov. 2005, pp. 853-865.
36. C.L. Holloway, D.C. Love, E.F. Kuester, J.A. Gordon, and D.A. Hill, "Use of generalized sheet transition conditions to model guided waves on metasurfaces/metafilms,", *IEEE Trans. Ant. Prop.*, vol. 60, pp. 5173-5186, Nov. 2012.

37. C.L. Holloway, D.C. Love, E.F. Kuester, A. Salandrino, and N. Engheta, "Sub-Wavelength Resonators: On the use of Metafilms to Overcome the $\lambda/2$ size limit", *IET Microw. Antennas Propag.,* vol. 2, no. 2, pp. 120-129, March 2008.

38. C.L. Holloway and E.F. Kuester, "Reflection and Transmission Coefficients for a Metascreen: Retrieval Approach for Determining Effective Surface-Susceptibilities and Surface-Porosities", *IEEE Trans. on Antennas and Propag.,* 2017.

39. C.L. Holloway and E.F. Kuester, "Reflection and Transmission Coefficients for an Anisotropic Metascreen: Conversion Between TE and TM Modes", *Phys. Review B*, 2017.

40. C.L. Holloway, E.F. Kuester, and D. Novotny, "Waveguides Composed of Metafilms-Metasurface: The Two-Dimensional Equivalent of Metamaterials", *IEEE Antenna and Wireless Propagation Letters*, vol. 8, pp. 525-529, 2009.

41. C.L. Holloway, P. Kabos, M.A. Mohamed, E.F. Kuester, J. Gordon, M.D. Janezic, and J. Baker-Jarvis, "Realization of a Controllable Metafilm/metasurface Composed of Resonant Magnetodielectric Particles: Measurements and Theory", *IET Microwaves, Antennas, and Propagation, special issue on Microwave Metamaterials*, August 2010 – Volume 4, Issue 8, p.1111-1122 .

42. S. Kim, E.F. Kuester, C.L. Holloway, A.D. Scher, and J. Baker-Jarvis, "Boundary effects on the determination of the effective parameters of a metamaterials from normal incidence reflection and transmissions, *IEEE Trans. on Antenna and Propagation*,Vol. 59, No. 6, 2011.

43. S. Kim, E.F. Kuester, C.L. Holloway, A.D. Scher, and J. Baker-Jarvis, "Effective material property extraction of a metamaterial by taking boundary effects into account at TE/TM polarized incidence", *PIERS B*, , vol. 36, ISSN: 1937-6472, 2011.

44. J. Gordon, C.L. Holloway, J. Booth, "Fluid interactions with metafilms/metasurfaces for tuning, sensing, and microwave-assisted chemical processes", *Physical Review B*, 83, 205130, 2011.

45. J. Gordon, C. L. Holloway and A. Dienstfrey, "A physical explanation of angle-independent reflection and transmission properties of metafilms/metasurfaces," *IEEE Antennas Wireless Propag. Lett.*, 8, 2009, pp. 1127-1130.

46. S.A. Tretyakov and S. I. Maslovski, "Thin absorbing structure for all incident angles based on the use of a high-impedance surface," *Microwave and Optical Technology Letters,* 38, no. 3, 2003, pp. 175-178.

47. Y. Kotsuka, K. Murano, M. Amano and S. Sugiyama, "Novel right-handed metamaterial based on the concept of 'Autonomous control system of living cells, and its absorber applications," *IEEE Trans. Electromag. Compat.,* 52, no. 3, 2010, pp. 556-565.

48. Hu Tao, C.M. Bingham, A.C. Strikwerda, D. Pilon, C. Shrekenhamer, N.I. Landy, K. Fan, X. Zhang, W. J. Padilla and R.D. Averitt, "Highly flexible wide angle of incidence terahertz metamaterial absorber: Design, fabrication, and characterization," *Phys. Rev. B.*, 78, 2008, art. 241103.

49. N. I. Landy, S. Sajuyigbe, J. J. Mock, D. R. Smith and W. J. Padilla, "Perfect metamaterial absorber", *Phys. Rev. Lett.*, 100, 2008, art. 207402.

50. O. Luukkonen, F. Costa, C.R. Simovski, A. Monorchio and S.A. Tretyakov, "A thin electromagnetic absorber for wide incidence angles and both polarizations," *IEEE Trans. Ant. Prop.*, 57, no. 10, 2009, pp. 3119-3125.

51. F. Bilotti, A. Toscano, K. B. Alici, E. Ozbay, and L. Vegni, "Design of miniaturized narrowband absorber based on resonant-magnetic inclusions," *IEEE Trans. Electromag. Compat.,* 53, no. 1, 2011, pp. 63-72.

52. S. Sajuyigbe, M. Ross, P. Geren, S.A. Cummer, M.H. Tanielian and D.R. Smith, "Wide angle impedance matching metamaterials for waveguide-fed phased-array antenna", *IET Microwaves, Antennas, and Propagation*, 4, no. 8, 2010, pp.1063-1072.

53. H.-T. Chen, W. J. Padilla, J. M. O. Zide, S. R. Bank, A. C. Gossard, A. J. Taylor and R. D. Averitt, "Ultrafast optical switching of terahertz metamaterials fabricated on ErAs/GaAs nanoisland superlattices," *Opt. Lett.*, 32, no. 12, 2007, pp. 1620-1622.

54. H.-T. Chen, W.J. Padilla, J.M.O. Zide, A. C. Gossard, A. J. Taylor and R. D. Averitt, "Active terahertz metamaterial devices," *Nature,* 444, 2006, pp. 597-600.

55. H.-T. Chen, W. J. Padilla, M. J. Cich, A. K. Azad, R. D. Averitt and A. J. Taylor, "A metamaterial solid-state terahertz phase modulator" *Nature Photonics*, 3, 2009, pp. 148-151.

56. H.-T. Chen, J. F. OHara, A. K. Azad, A. J. Taylor, R. D. Averitt, D. B. Shrekenhamer and W. J. Padilla, "Experimental demonstration of frequency-agile terahertz metamaterials," *Nature Photonics*, 2, 2008, pp. 295-298.

57. W. L. Chan, H.-T. Chen, A. J. Taylor, I. Brener, M. J. Cich and D. M. Mittleman, "A spatial light modulator for terahertz beams," *Appl. Phys. Lett.*, 94, 2009, art. 213511.

58. X. G. Peralta, I. Brener, W. J. Padilla, E. W. Young, A. J. Hoffman, M. J. Cich, R. D. Averitt, M. C. Wanke, J. B. Wright, H.-T. Chen, J. F. OHara, A. J. Taylor, J. Waldman, W. D. Goodhue, J. Li and J. Reno, "External modulators for terahertz quantum-cascade lasers based on electrically-driven active metamaterials," *Metamaterials*, 4, 2, 2010, pp. 83-88.

59. H. Tao, A. C. Strikwerda, K. Fan, W. J. Padilla, X. Zhang and R. D. Averitt, "Reconfigurable terahertz metamaterials," *Phys. Rev. Lett.*, 103, 2009, art. 147401.

60. J. Han and A. Lakhtakia, "Semiconductor split-ring resonators for thermally tunable terahertz metamaterials," *J. Mod. Optics,* 56, 2009, pp. 554-557.

61. T. Driscoll, S. Palit, M. M. Qazilbash, M. Brehm, F. Keilmann, B.-G. Chae, S.-J. Yun, H.-T. Kim, S. Y. Cho, N. M. Jokerst, D. R. Smith and D. N. Basov, "Dynamic tuning of an infrared hybrid-metamaterial resonance using vanadium dioxide," *Appl. Phys. Lett.* 93, 2008, art. 024101.

62. T. Driscoll, H.-T. Kim, B.-G. Chae, B.-J. Kim, Y.-W. Lee, N. M. Jokerst, S. Palit, D. R. Smith, M. Di Ventra and D. N. Basov, "Memory metamaterials," *Science*, 325, 2009, pp. 1518-1521.

63. T. Driscoll, G. O. Andreev, D. N. Basov, S. Palit, S. Y. Cho, N. M. Jokerst and D. R. Smith, "Tuned permeability in terahertz split-ring resonators for devices and sensors," *Appl. Phys. Lett.,* 91, 2007, art. 062511.

64. T. A. Klar, A. V. Kildishev, V. P. Drachev and V. M. Shalaev, "Negative-index metamaterials: Going optical," *IEEE Journal of Selected Topics in Quantum Electronics*, 12, no. 6, 2006, pp. 1106-1115.

65. A. V. Kildishev, W. Cai, K. Chettiar, H. Yuan, A. K. Sarychev, V. P. Drachev and V. M. Shalaev, "Negative refractive index in optics of metal-dielectric composites," *J. Opt. Soc. Am. B,* 23, no. 3, 2006, pp. 423-433.

66. J. B. Pendry, "Negative refraction makes a perfect lens," *Phys. Rev. Lett.,* 85, 2000, pp. 3966-3969.

67. A. Al, A. Salandrino and N. Engheta, "Negative effective permeability and left-handed materials at optical frequencies" *Opt. Exp.* 14, no. 4, 2006, pp. 1557-1567.

68. G. Dolling, C. Enkrick, M. Wegener, C. M. Soukoulis and S. Linden, "Low-loss negative-index metamaterials at telecommunication wavelengths," *Opt. Lett.,* 31, no. 12, 2006, pp. 1800-1802.

69. T. J. Yen, W. J. Padilla, N. Fang, D. C. Vier, D. R. Smith, J. B. Pendry, D. N. Basov and X. Zhang, "Terahertz magnetic response from artificial materials," *Science*, 303, 2004, pp. 1494 1496.

70. J. A. Gordon and R. W. Ziolkowski, "The design and simulated performance of a coated nano-particle laser," *Optics Express*, 15, no. 5, 2007, pp. 2622-2653

71. M. I. Stockman, "Spasers explained," *Nature Photonics,* 2, 2008, pp. 327-329.

72. V. M. Shalaev, "Optical negative-index metamaterials," *Nature Photonics*, 1, 2007, pp. 41-48.

73. A. Alu and N. Engheta, "Theory of linear chains of metamaterials/plasmonic particles as subdiffraction optical nanotransmission lines," *Physical Review B*, 74, 2006, art. 205436.

74. C. Pfeiffer and A. Grbic, "Metamaterial Huygens Surfaces: Tailoring Wave Fronts with Reflectionless Sheets", *Phys. Review Lett.*, vol. 110, 197401, 2013.

75. C. Pfeiffer and A. Grbic, "Cascaded metasurfaces for complete phase and polarization control", *Applied Phys. Lett.*, vol. 102, no. 23, 231116, 2013.

76. N.M. Estakhri and A. Alu, "Wave-front Transformation with Gradient Metasurfaces", *Phys. Review X*, vol. 6, 041008, 2016.

77. A. Epstein and G.V. Eleftheriades, "Arbitrary Power-Conserving Field Transformations with Passive Lossless Omega-Type Bianisotropic Metasurfaces", *IEEE Transactions on Antennas and Propag.*, vol. 64, no. 9, 2017.

78. S. Hu, S. Yang, Z. Liu, J. Li, C Gu, "Broadband cross-polization conversion by symmtery-breaking ultrathin metasurfaces", *Applied Phy. Lett.*, vol. 111, 241108, 2017.

79. Y. Guo, M. Xiao, and S. Fan, "Topologically Protected Complete Polarization Conversion," *Phys. Rev. Lett.* vol. 119, 167401, 2017.

80. A.T. Pereda, F. Caminita, E. Martini, I. Ederra, J.C. Iriarte, R. Gonzalo, and S. Maci, "Dual Circularly Polarized Broadside Beam Metasurface Antenna", *IEEE Trans. on Antennas and Propag.*, vol. 64, no. 7, 2944-2953, 2016.

81. S.B. Glybovski, S.A. Tretyakov, P.A. Belov, Y.S. Kivshar, C.R. Simovski, "Metasurfaces: From microwaves to visible", *Physics Reports* vol. 634, 172, 2016.

82. D. Morits, M. Morits, V. Ovchinnikov, M. Omelyanovich, A. Tamminen, S. Tretyakov, C. Simovski, "Multifunctional stretchable metasurface for the THz range", *J. Opt.* vol. 16, no. 3, 032001, 2014.

83. J. Fang, "Generalized perfectly matched layers for the absorption of propagating and evanescent waves in lossless and lossy media," *IEEE Trans. Microwave Theory Tech.,* 44, 1996, pp. 2216-2222.

84. A. Alu and N. Engheta, "Three-dimensional nanotransmission lines at optical frequencies: A recipe for broadband negative-refraction optical metamaterials," *Physical Review B,* 75, 2007, art. 024304.

85. P. S. Neelakanta, *Handbook of Electromagnetic Materials*, New York: CRC Press, 1995.

86. A. H. Sihvola, *Electromagnetic mixing formulas and application.* London, Uni

87. E. F. Kuester and C. L Holloway, "Comparison of approximations for effective parameters of artificial dielectrics," *IEEE Trans. Microwave Theory Tech.*, vol. 38, pp. 1752–1755, 1990.

88. *Advances in Electromagnetics of Complex Media and Metamaterials* (S. Zouhdi, A. Sihvola, and M. Arsalane, eds.). Kluwer Academic Pub.: Boston, 2002.

89. T.K. Wu, *Frequency Selective Surface and Grid Array.* N.Y.: John Wiley & Sons, Inc., 1995.

90. S. Tretyakov, Analytical Modeling in Applied Electromagnetics, Boston-London, Artech House, 2003.

91. L. Brillouin, Wave Propagation in Periodic Structures. New York, Dover, 1953, chapter7.

92. A. Ishimaru, Electromagnetic Wave Propagation, Radiation, and Scattering. Englewood Cliffs, N.J., Prentice Hall, 1991, chapter 7.

93. J.A. Kong, Electromagnetic Wave Theory. New York, John Wiley & Sons, 1986, chapter 6.

94. B.A. Munk, *Frequency Sective Surfaces: Theory and Design.* Wiley, Inc., 2000.

95. C.M. Soukoulis, *Photonic Band Gap Materials*, Kluwer Academic Publishers, Dordrecht, 1996.

96. C.L. Holloway and E.F. Kuester, "Corrections to the classical continuity conditions at the interface of a composite medium", *Photonics and Nanostructures: Fundamentals and Applications*, vol. 11, no. 4, pp. 397422, November 2013.

97. A.M. Nicolson and G. Ross, "Measurement of the intrinsic properties of materials by time domain techniques", *IEEE Trans. Instrum. Meas.,* 19, 377-382, 1970.

98. W.B. Weir, "Automatic measurements of complex dielectric constant and permeability at microwave frequencies," *Proc. IEEE*, 62, 33-36, 1974.

99. D.R. Smith, S. Schultz, P. Markos, and C.M. Soukoulis, "Determination of effective permittivity and permeability of metamaterials from reflection and transmission coefficients", *Phys. Review B*, 65, 195104, 2002.

100. R.W. Ziolkowski, "Designs, fabrication, and testing of double negative metamaterials", *IEEE Trans. on Antennas and Propag.*, 51, 1516-1529, 2003.

101. S. Kim, E.F. Kuester, C.L. Holloway, A.D. Scher, and J. Baker-Jarvis, "Boundary effects on the determination of the effective parameters of a metamaterials from normal incidence reflection and transmissions, *IEEE Trans. on Antenna and Propagation*, vol. 59, no. 6, 2011.

102. S. Kim, E.F. Kuester, C.L. Holloway, A.D. Scher, and J. Baker-Jarvis, "Effective material property extraction of a metamaterial by taking boundary effects into account at TE/TM polarized incidence", *PIERS B*, , vol. 36, ISSN: 1937-6472, 2011.

103. X. Chen, T.M. Grezegorczyk, B.-I. Wu, J. Pacheco and J.A. Kong, "Robust method to retrieve the constitutive effective parameters of metamaterials", *Phys. Review E*, 70, 2004. 016608.

104. A.M. Saleh, K.R. Mahmoud, I.I. Ibrahim, and A.M. Attiya, "Analysis of anisotropic metasurfaces using generalized sheet transition condition", *J. of Electromagnetic Waves and Appl.* vol 30, no. 5, 661-675, 2016.

105. A.M. Saleh, K.R. Mahmoud, I.I. Ibrahim, and A.M. Attiya, "Generalized sheet transition condition (GSTC) for anisotropic metasurfaces", *33rd National Radio Science Conference (NRSC)* Aswan, Epypt, Feb 22-25, pp. 49-56, 2016.

106. Wainstein, L. A., "On the electrodynamic theory of grids" *Elektronika Bol'shikh Moshchnostei*, (2), (P. L. Kapitza and L. A. Wainstein, editors), 1963. Moscow: Nauka, pp. 26-74 [in Russian; Engl. transl. in *High-Power Electronics*, *2*. Oxford: Pergamon Press, 1966, chapter II, pp. 14-48].

107. Douglas, J.F., and Garboczi,E.J., "Intrinsic viscosity and the polarizability of particles having a wide range of shapes," in Prigogine, I., and Rice, S.A. (Eds.) Advances in Chemical Physics, vol. 91, (Wiley, New York, 1995), pp. 85153

108. E.F. Kuester and E. Liu, "Average transition conditions for electromagnetic fields at a metascreen of nonzero thickness", manuscript in preparation, 2017.

109. E.F. Kuester, E. Liu, and N.J. Krull "Average transition conditions for electromagnetic fields at a metascreen of vanishing thickness", manuscript in preparation, 2017.

110. C.L. Holloway and E.F. Kuester, "Equivalent boundary conditions for a perfectly conducting periodic surface with a cover layer," *Radio Sci.*, vol. 35, pp. 661-681, 2000.

111. T.B.A. Senior, and J.L. Volakis, *Approximate Boundary Conditions in Electromagnetics*. London: Institution of Electrical Engineers, p. 163, 1995.

112. R. W. Ziolkowski, P. Jin and C.-C. Lin, "Metamaterial-inspired engineering of antennas," *Proc. IEEE,* 99, no. 10, 2011, pp. 1720-1731.

113. P. Jin and R. W. Ziolkowski, "Metamaterial-inspired, electrically small, Huygens sources," *IEEE Antennas Wireless Propag. Lett.,* 9, 2010, pp. 501-505.

114. P. Jin and R. W. Ziolkowski, "Multiband extensions of the electrically small metamaterial-engineered Z antenna," *IET Microwaves, Antennas Propagation,* 4, no. 8, 2010, pp. 10161025.

115. C.-C. Lin and R. W. Ziolkowski, "Dual-band 3D magnetic EZ antenna," *Micr. Opt. Technol. Lett.*, 52, no. 4, 2010, pp. 971-975.

116. P. Jin and R. W. Ziolkowski, "Broadband, efficient, electrically small metamaterial-inspired antennas facilitated by active near-field resonant parasitic elements," *IEEE Trans. Antennas Propag.,* 58, no. 2, 2010, pp. 318-327.

117. P. Jin and R. W. Ziolkowski, "Low Q, electrically small, efficient near field resonant parasitic antennas," *IEEE Trans. Antennas Propag.,* 57, no. 9, 2009, pp. 2548-2563.

118. A. Erentok and R. W. Ziolkowski, "Metamaterial-inspired efficient electrically-small antennas," *IEEE Trans. Antennas Propag.*, 56, no. 3, 2008, pp. 691-707.

119. R. W. Ziolkowski and A. Erentok, "Metamaterial-based efficient electrically small antennas," *IEEE Trans. Antennas Propagat.,* 54, no. 7, 2006, pp. 2113-2130.

120. A. Alu and N. Engheta, "Tuning the Scattering Response of Optical Nanoantennas with Nanocircuit Loads", *Nature Photonics,* 2, May 2008, pp. 307-310.

121. I.A. Ibrahheem and M. Koch, "Coplanar waveguide metamaterials: The role of bandwidth modifying slots," *Appl. Phys. Lett.,* 91, 2007, art. 113517.

122. M. Quinten, A. Leitner, J. R. Krenn and F. R. Aussenegg, "Electromagnetic energy transport via linear chains of silver nanoparticles," *Opt. Lett.*, 23, no. 17, 1998, pp. 1331-1333.

123. S. A. Tretyakov and A. J. Viitanen, "Line of periodically arranged passive dipole scatterers," *Elec. Eng.,* 82, no. 6, 2000, pp. 353-361.

124. M. L. Brongersma, J. W. Hartman and H. A. Atwater, "Electromagnetic energy transfer and switching in nanoparticle chain arrays below the diffraction limit," *Phys. Rev. B,* 62, 2000, pp. 16356-16359.

125. W. H. Weber and G. W. Ford, "Propagation of optical excitations by dipolar interactions in metal nanoparticle chains," *Phys. Rev. B,* 70, 2004, art. 125429.

126. R. A. Shore and A. D. Yaghjian, "Traveling electromagnetic waves on linear periodic arrays of lossless spheres," *Electron. Lett.*, 41, no. 10, 2005, pp. 578-580.

127. R. A. Shore and A. D. Yaghjian, "Traveling electromagnetic waves on linear periodic arrays of lossless penetrable spheres," *IEICE Trans. Commun.*, E88-B, no. 6, 2005, pp. 2346-2352.

128. M. Guasoni and C. De Angelis, "Analytical approximations of the dispersion relation of a linear chain of nanoparticles," *Opt. Commun.*, 284, no. 7, 2011, pp. 1822-1827.

129. H. Lamb, "On group-velocity," *Proc. London Math. Soc.*, ser. 2, Vol. 1, pp. 473-479, 1904.

130. A. Schuster, *An Introduction to the Theory of Optics*. London: Edward Arnold, 1904, pp. 313-318.

131. H. C. Pocklington, "Growth of a wave-group when the group velocity is negative," *Nature*, Vol. 71, pp. 607-608, 1905.

132. V.G. Veselago, "The electrodynamics of substances with simultaneously negative values of and " [in Russian], *Usp. Fiz. Nauk*, 92, 1967, pp. 517-526 [Engl. transl. in *Sov. Phys. Uspekhi*, 10, 1968, pp. 509-514].

133. L. I. Mandel'shtam, "Lectures on certain problems of oscillation theory: Lecture 4," [Russian], in *Polnoe Sobraniye Trudov*, tom 5. Leningrad: Izdat. Akad. Nauk SSSR, 1950, pp. 461-467 [also in his *Lektsii po Optike, Teorii Otnositel'nosti i Kvantovoi Mekhanike*. Moscow: Nauka, 1972, pp. 431-437].

134. L. I. Mandel'shtam, "Group velocity in crystalline arrays," [Russian], *Zh. Eksp. Teor. Fiz.*, Vol. 15, pp. 475-478, 1945 [also in *Polnoe Sobraniye Trudov*, tom 2. Leningrad: Izdat. Akad. Nauk SSSR, 1947, pp. 334-338].

135. G. D. Malyuzhinets, "A note on the radiation principle," [Russian] *Zh. Tekh. Fiz.*, Vol. 21, pp. 940-942, 1951.

136. D. V. Sivukhin, "The energy of electromagnetic fields in dispersive media," [Russian] *Opt. Spektrosk.*, Vol. 3, pp. 308-312, 1957.

137. E. Shamonina and L. Solymar, "Metamaterials: How the subject started," *Metamaterials*, vol. 1, pp. 12-18, 2007.

138. E. Shamonina, "Slow waves in magnetic metamaterials: History, fundamentals and applications," *Phys. Stat. Sol. B*, vol. 245, pp. 1471-1482, 2008.

139. R. A. Silin, "On the history of backward electromagnetic waves in metamaterials," *Metamaterials*, vol. 6, pp. 1-7, 2012.

140. S. A. Tretyakov, "A personal view on the origins and developments of the metamaterial concept," *J. Optics*, vol. 19, art. 013002, 2017.

141. R. E. Collin and F. J. Zucker, **Antenna Theory: Part II**. NewYork: McGraw-Hill, 1969, ch. 20.

142. N. Engheta, "An idea for thin subwavelength cavity resonators using metamaterials with negative permittivity and permeability," *IEEE Antennas and Wireless Propagation Letters,* 1, 2002, pp. 10-13.

143. T. Hand, S. Cummer, and N. Engheta, "The Measured Electric Field Spatial Distribution within a Metamaterial Sub-Wavelength Cavity Resonator," *IEEE Trans. on Antennas and Propagation,* 55, no. 6, 207, pp. 1781-1788.

144. Caiazzo, S. Maci, and N. Engheta, "A metamaterial surface for compact cavity resonators," *IEEE Antennas and Wireless Propagation Letters,* 3, no. 1, pp. 261-264, 2004.

145. S. Tretyakov, **Analytical Modeling in Applied Electromagnetics**, Boston-London, Artech House, 2003.

146. M.I. Oksanen, S. A. Tretyakov and I. V. Lindell, "Vector circuit theory for isotropic and chiral slabs," *J. Electromag. Waves Appl.,* vol. 4, pp. 613-643, 1990.

147. S. A. Tretyakov, A. J. Viitanen, S. I. Maslovki and I. E. Saarela, "Impedance boundary conditions for regular dense arrays of dipole scatterers," *IEEE Trans. Ant. Prop.,* vol. 51, no. 8, pp. 2073-2078, 2003.

148. O. Luukkonen, C. Simovski, G. Granet, G. Goussetis, D. Lioubtchenko, A. V. Risnen and S. A. Tretyakov, "Simple and accurate analytical model of planar grids and high-impedance surfaces comprising metal strips or patches," *IEEE Trans. Ant. Prop.,* vol. 56, no. 6, 2008, pp. 1624-1632; correction, ibid., vol. 58, p. 2162, 2010.